Laboratoire *PhLAM*, L'Ecole Doctorale *SMRE*

Ordering effects in quantum optics

Effets d'ordonnement en optique quantique

Tobias Lipfert

Thèse préparée pour obtenir
le grade de Docteur en
Physique
Milieux dilués et optique fondamentale

Soutenue le 24 avril 2019 devant le jury composé de:

Prof.	Mikhail. I. KOLOBOV	Université de Lille	Directeur de thèse
Dr.	Giuseppe PATERA	Université de Lille	Co-Encadrant de thèse
Prof.	Daniel BRAUN	Universität Tübingen	Rapporteur
Prof.	Nicolas CERF	Université Libre de Bruxelles	Rapporteur et président du jury

Acknowledgements

The present contribution would not be possible without all the institutions and organizations involved. Namely, University of Lille directed by Jean-Christophe Camart; Laboratory PhLAM and its director Marc Douay; the Doctoral School SMRE with its coordinator Christophe Van Brussel and director Joël Cuguen, doctoral studies director Cristian Focsa and Majid Taki (former director). Hereby, I would like to thank them.

I would like to thank the members of the committee for their participation and contribution to the public defense of the present thesis: Prof. Nicolas Cerf from the Université Libre de Bruxelles and Prof. Daniel Braun from the Eberhard Karls Universität Tübingen. I feel very fortunate that my work has been approved by such a distinguished committee of theoreticians. I also want to thank Emiliano Pallecchi and Saliya Coulibaly for serving on my *comité de suivi de thèse*.

I want to thank my *directeur de thèse*, Prof. Mikhail I. Kolobov, for providing me with the opportunity to work in Lille and for teaching me the value of efficient scientific communication by means of focusing on ideas rather than technicalities; my *co-encadrant de thèse*, Giuseppe Patera, whose contagious enthusiasm, endless stream of ideas, moral support, and careful advice where key to the success of my work; visiting Professor in our group, Dimitri B. Horoshko, with his great eye for scientific relevance and from whom I learned a great deal about good scientific writing; fellow PhD student in our group, and fellow founding member of our very own "Sunday physics club", Junheng Shi, who became one of my greatest friends and with whom I shared many great discussions, not only about physics.

I also don't want to forget those responsible for the practical aspects of life at PhLAM: A big thank you to Walter Kolnierzak and the secretaries of our lab, Stéphanie Costeur, Marie-Therèse Ledee-Walasiak, Nathalie Damart for providing quick unbureaucratic advice on various administrative challenges; Benjamin Pfeuty (and before Saliya Coulibaly) for managing the coffee room coffee supply with a 50% discount for PhD students; all the cleaning staff – especially Sylvie Leceur – for keeping our offices clean.

Special thanks to Fabian Krumm for discussing his research with me, which provided a very interesting problem to solve, which then became part of the present contribution. The efficiency of our collaboration at a distance was a true joy. Special thanks to my former supervisor in Rostock, Jan Sperling, who despite no longer being directly responsible for me, continued to provide outstanding advice and comments and whose trust in my abilities has always been a great motivation. Both Fabian and Jan were part of Prof. Werner Vogel's group when I was doing my first scientific steps there. I want to thank Prof. Vogel for creating such a productive environment where opportunities where provided early on and for enabling me to present myself as a potential PhD student in Lille.

It should not remain unmentioned that my PhD position in Lille was funded by the QCUMbER project that received funding by the European Union's Horizon 2020 research and innovation programme under grant agreement No 665148. Among others, the QCUMbER project coordinator Prof. Brian Smith and project manager Paige Noyce were responsible for giving life to this project and for enabling the fruitful scientific exchange between the collaborators from Universities Rome, Oxford, Rostock, Sorbonne (Paris), Paderborn, and Lille at the various project meetings. I want to especially point out the outstandingly pleasant end-of-project conference in Oxford which was a full success and also gave some important impulses for this work.

Of course life is dull without friends. Their indirect moral contribution to my thesis can hardly be overstated. In Lille, I want to thank Alexey Tikan (whose full name I only mention here because I think he deserves every promotion as the great scientist I consider him to be), founding member of our "Sunday physics club" and simply the closest friend I had during my time in Lille; Cristina, who accompanied me for quite a while on this path and on many other journeys; Beatrice and Aurélien, my earliest friends in Lille who helped me with many obstacles of life in France; the, partially anarchistic, never boring, lunch/office/institute crew: Bastian, Sabine, Eva, Alexandre, Adrien, Katharina, Marin, Omar, Dana, Ramon, Darka, and many more; the "Brazilian" crew: Alan, Sasha, Melissa, Debora, and of course the incomparable Carolina; the Spanish connection: Elena, Carlos, and Javi. Apologies in advance for any omissions. Outside of Lille, I want to thank my friends from my time in Rostock: Lukas, Lucas, Charlotte, Thomas, Nis and of course Eric, Helge, and Anna Julia who invested 2×15 hours of train ride to attend my defense in Lille; my oldest friends from school: Joel, Dominik, and Latif – with whom, even after years of separation, every reunion feels as if we had never been apart.

The QCUMbER meetings and other conferences have led to some great exchanges (with, among others, Mattia, Thibault, Francesco, Tiphaine, Alex, Adrien, Benjamin, Luca, Martin, Syamsundar, Elizabeth, Stephan, etc.), be they scientific or private. Thank you for all the great times, that I often regretted to be so limited.

Last but not least, I would like to thank my parents for their unconditional and permanent support at my every step. And of course I should not let my brother and sister unmentioned. It is hard to think of anything that lifts my mood like a phone call with my family.

Contents

Introduction

When one quantizes the electromagnetic field, field variables are replaced by field operators; see, e.g., Refs. [1–4]. The quantum nature of light is reflected in the non-commutative algebra of these operators[1]. If explicitly time-dependent problems are considered, this gives rise to non-zero non-equal-time commutators of time-dependent operators. Thus, temporal correlations may arise that are not covered by Maxwells classical theory of light. A renowned phenomenon of this category is the quantum effect of photon antibunching [6,7], whose experimental verification in 1977 [8] may be considered as the final proof to Einsteins light quanta Hypothesis [9] (see also Refs. [10, 11]). Often, the dynamics of such non-stationary systems cannot be solved in terms of closed analytical expressions. In this case, one either has to revert to a purely numerical treatment or to time-dependent perturbation theory (cf. [12–14]).

Time-dependent perturbation theory is usually presented in the form of a Dyson series [15]. Approximations to the evolution operators of the systems are given in terms of truncation of such series. However, such approximations may violate certain symmetries of the underlying systems, as unitarity of the evolution operators is not preserved by such approximations. Alternatively, another type of approximative description is possible by neglecting the time ordering prescription of the Dyson series representation – the resulting approximated evolution operators will be unitary. Such an approximation is justified as long as non-equal-time commutators of the time-dependent Hamiltonians are not relevant for the dynamics of the system, i.e., it corresponds to neglecting these commutators. Consequently, we refer to all deviations – that are due to non-zero non-equal-time commutators – from neglected time ordering as (time) *ordering effects*. In Reference [16], such deviations were studied for the processes of sum frequency generation and parametric down conversion. Recently, in studies of ordering effects in dynamical systems, the Magnus expansion (ME) [17, 18] has been considered as a useful representation of the corresponding evolution operators, cf. [19–24].

Remarkably, the ME – which will play a central role in this contribution – provides for an alternative (exponential) representation of time-dependent perturbation theory [17, 18]. For time-dependent quantum systems, the ME is given by linear combinations of ordered time integrals over different orders of nested non-equal-time commutators of the time-dependent

[1] Let us note that, since non commutativity of quantum-mechanical operators is a pure quantum effect, it can be used for quantitative measure of nonclassicality of a quantum state of light, as very recently proposed in Ref. [5].

Hamiltonian. As such, the ME always remains within the Lie algebra that can be constructed from the time-dependent Hamiltonians. The exponent of the ME (and its truncations) corresponds to the (approximated) evolution operator of the system and, due to this exponential nature, important symmetries of the underlying system are usually not violated by approximations (cf. [18–21, 24]).

From a fundamental standpoint, another feature of the ME can be considered most striking: The lowest order of Magnus approximation (MA) corresponds exactly to the case of neglected time ordering. All other terms of the ME are due to (time) *ordering effects* and will, therefore, be referred to as (time) *ordering corrections*. Thus, the ME allows for a clear separation of (time) ordering effects from the effective Hamiltonian description with neglected time ordering.

However, the methods of ME are also subject to some limitations. When approximations of the evolution operator are formulated in terms of the ME, an increasing number of MA orders leads to a stepwise inclusion of ordering effects. That is, with higher orders of ordering correction, one moves closer to the correct dynamics of the system – i.e., the incorporation of all ordering effects. However, this is limited by two factors; (i) the expressions for higher order corrections can take quite complex forms (cf. [25]) which may make their evaluation quite tedious, and (ii) the ME generally only works within a finite radius of convergence, which means it may diverge at some point and the correct evolution of the system cannot be recovered in terms of increasing orders of corrections.

In the case of divergence, a comparison of the cases of neglected ordering effects with the approximations in terms of the ME will lead to misinterpretations. Admittedly, for small scales, where neglecting ordering effects is most appropriate, the ME does always converge. But significant deviations caused by the negligence of ordering effects may only arise after sufficiently long times. Thus, precise knowledge of the limits of convergence is indispensable in the study of (time) ordering effects in terms of the ME. Indeed, there exist sufficient upper bounds for evolution periods where convergence occurs, but exact upper bounds can generally only be found for generic cases [18].

In the present thesis we will analyze (time) ordering effects in the context of quantum optical systems. We consider two systems in particular, the process of single pass type-I parametric down-conversion (PDC) (cf. [26, 27]) and the classically driven Jaynes-Cummings dynamics of an ion in a Paul trap [or classically driven Jaynes-Cummings dynamics (CJCD) for short] (cf. [2, 23]). In the context of single pass type-I PDC[2], two scenarios will be considered in particular; the scenario of a monochromatic pump where continuous-wave (cw) squeezed light

[2] In this context we will adopt the nonlinear optics standard, where the evolution of light is usually described with respect to the distance covered rather than time. The perturbative formalism will be adjusted accordingly.

is generated and the scenario of a broad(-band) spectral pump where pulses that contain a multitude of squeezed field modes are generated.

The relevance of the PDC process stems from it being a main source of squeezed states of light (four wave mixing being another one, cf. [28]). These states of light are nonclassical states with unique features interesting from both fundamental and practical points of view [26, 29, 30] and they find numerous applications in laser interferometers, including gravitational wave detectors [31, 32], in quantum metrology [33], and in various protocols of quantum information, ranging from quantum teleportation to quantum computation [34, 35]. In the latter area of research, multimode squeezed states are recognized as a key resource for the measurement-based continuous-variable quantum computation [36–39], where they can be employed for one-way quantum computation protocols [40, 41].

The efficiency of employing squeezed states depends crucially on the degree of squeezing. As a consequence, there is a high demand for squeezed states with the highest possible degree of squeezing. The cw narrow-band squeezed light is perhaps the best-known realization of squeezing in optics and experiments in this direction have reached the record values of 15 dB squeezing in a band of about 100 MHz [42]. Broader bands (up to tens of THz) of squeezed light can be obtained in cw or quasi-cw regimes of PDC with the use of aperiodically poled quasi-phase-matched crystals [43–45]. On the other hand, PDC with pulsed broad spectral pumps opens the possibility to generate pulses that contain multiple spectrally broad modes of squeezed light at once. Such light, with quantum correlations between different parts of its frequency spectrum, can be generated both in single-pass [46–51] or cavity-enhanced configurations [52–55]. Tailoring the parametric interaction by pump shaping or crystal design allows for engineering of the quantum correlations of the generated light [56, 57]. In any case, the detection and implementation of squeezed states requires precise definition of the squeezing eigenmodes (and their corresponding degree of squeezing) in order to use the squeezing most efficiently. Analytical analysis of squeezing eigenmodes at high gain is complicated because of the nonstationarity of the problem. Several contributions have defined squeezing eigenmodes at high gain by neglecting (time) ordering effects [47, 48, 54]. Ordering effects in PDC with broad spectral pumps have been discussed in Refs. [19, 20], via higher orders of the MA. This thesis adds to this discussion by explicitly analyzing the impact of ordering effect on the squeezing eigenmodes via higher orders of MA in type-I PDC with a broad spectral pump. We also consider bispectral pulse generation as an exemplary scenario for a tailored parametric interaction. Before this, we perform a complete analysis of ordering effects in type-I PDC with a monochromatic pump, that is the limit case of the broad spectral pump model for vanishing pump widths and can be solved explicitly. We derive the corresponding eigenmodes of squeezing for this model, benchmark the MAs with respect to the explicit solution, and give further results and comparisons to Refs. [19, 20]. The presented work on type-I PDC with a monochromatic pump has undergone peer review and was published in Refs. [24, 58].

The classically driven Jaynes-Cummings dynamics model is an extension of the Jaynes-Cummings model. The latter describes an idealized scenario of the resonant interaction of a two-level system with only one radiation mode [60, 61]. Despite its simplicity, the Jaynes-Cummings model has proven to be applicable as a realistic model in experiments [62–65] and a vast field of physical effects, and states can and have been studied at hands of this model [65–80]. The Jaynes-Cummings model can also be adapted to describe the vibronic dynamics of ions in Paul traps (cf. Ref. [81, 82]) – for the case of weak coupling between the electronic two-level system of the atom and its motional states – by replacing the quantized mode of the electromagnetic field with the quantized center-of-mass-motion of the ion [83–85]. For the case of strong coupling, a nonlinear Jaynes-Cummings model was introduced [86], which describes the dynamics of a trapped ion [87, 88]. In Reference [23], the model was considered with a quantized pump field that is slightly detuned from resonance frequencies. If the motional degrees of freedom are coupled to the electronic states of the ion by a classical pump field, this yields the CJCD model. On the basis of this model, a plethora of motional quantum states (e.g., squeezed states, Fock states, etc.) can be realized [87, 89–97]. For the case where the pump field is slightly detuned from resonance frequencies, the system becomes non-stationary [23] and time ordering effects become relevant. In this thesis we give an explicit solution of the dynamics for this case and analyze how well time ordering effects are described by different orders of MA by comparing them to this exact solution. This work has been published in Ref. [59] and was not present in the literature before[3].

The goal of this thesis is to contribute to the establishment of the notion of (time) ordering effects as well as the methods of MA in the field of quantum optics. It is my hope that the present contribution can also serve as a helpful introduction to the methods of ME from the view point of quantum optics. To round of the discussion, we also give a extensive study of convergence limits of the ME in the context of the considered physical systems. We derive exact upper bounds of convergence that exceed known sufficient upper bounds for a wide range of configurations of the systems. This work on convergence limits has been included in Ref. [24] for the CJCD model, and in Ref. [58] for type-I PDC with a monochromatic pump and is, to my best knowledge, the first analysis of such exact limits in the context of quantum optical systems.

[3] Reference [59] also contains analysis (that are partially based on my explicit solution and and closed form MAs) of the impact of time ordering effects on the nonclassicality and non-Gaussianity of states via regularized quasi-probability distributions, which were performed by Fabian Krumm and which do thus not form part of the present thesis.

Chapter 1

Elements of quantum optics

Contents

Studying the quantum properties of radiation fields that cannot be described by classical electrodynamics is at the heart of quantum optics. The fundamental difference between the classical theory of electrodynamics and quantum electrodynamics is the canonical quantization of field variables. In the formalism of the description, this adds another layer of complexity as scalar, and vectorial quantities of electrodynamics do no longer commute. In this chapter, we recapitulate some well-established fundamentals of quantum optics (cf. [2]) that will lay the groundwork for all further discussions.

1.1 The quantized electromagnetic field

The classical electromagnetic field is described trough Maxwell's equations[1],

$$\nabla \mathbf{E}(\mathbf{r},t) = \frac{1}{\varepsilon_0}\rho(\mathbf{r},t), \tag{1.1}$$

$$\nabla \mathbf{B}(\mathbf{r},t) = 0, \tag{1.2}$$

$$\nabla \times \mathbf{E}(\mathbf{r},t) = -\dot{\mathbf{B}}(\mathbf{r},t), \tag{1.3}$$

$$\nabla \times \mathbf{B}(\mathbf{r},t) = \mu_0 \mathbf{j}(\mathbf{r},t) + \mu_0 \varepsilon_0 \dot{\mathbf{E}}(\mathbf{r},t). \tag{1.4}$$

Quantization is usually performed via the vector potential $\mathbf{A}$. Together with the scalar potential Φ, it can be used to define the electric and magnetic fields as

$$\mathbf{B}(\mathbf{r},t) = \nabla \times \mathbf{A}(\mathbf{r},t), \qquad \mathbf{E}(\mathbf{r},t) = -\dot{\mathbf{A}}(\mathbf{r},t) - \nabla\Phi(\mathbf{r},t). \tag{1.5}$$

These fields allows us to reformulate the eight scalar equations (1.1), (1.2), (1.3), and (1.4) in terms of the four scalar equations

$$\nabla \times \nabla \times \mathbf{A}(\mathbf{r},t) + \mu_0\epsilon_0 \ddot{\mathbf{A}}(\mathbf{r},t) + \mu_0\epsilon_0 \nabla\dot{\Phi}(\mathbf{r},t) = \mu_0 \mathbf{j}(\mathbf{r},t), \tag{1.6}$$

$$\Delta\Phi(\mathbf{r},t) + \nabla \mathbf{A}(\mathbf{r},t) = -\frac{1}{\epsilon_0}\rho(\mathbf{r},t). \tag{1.7}$$

Additionally, there is a gauge freedom as

$$\mathbf{A}(\mathbf{r},t) \mapsto \mathbf{A}(\mathbf{r},t) + \nabla f(\mathbf{r},t), \qquad \Phi(\mathbf{r},t) \mapsto \Phi(\mathbf{r},t) - \dot{f}(\mathbf{r},t) \tag{1.8}$$

fulfills the equations (1.6) and (1.7) identically. How the field is quantized can rely heavily on the considered scenarios. Most scenarios in quantum optics do not consider reference frames at relativistic speeds, and therefore the Coulomb gauge $\nabla \mathbf{A}(\mathbf{r},t) \equiv 0$ is usually chosen – this implies that $\mathbf{A}(\mathbf{r},t)$ is a transverse vector field.

The most straight forward scenario of field quantization is given when we consider the free electromagnetic field – i.e., where charges ρ and currents $\mathbf{j}$ are identical nil everywhere and at all times. For this case and under the above mentioned Coulomb gauge, Eqs. (1.6) and (1.7) reduce to the wave equation

$$\Delta \mathbf{A}(\mathbf{r},t) - \underbrace{\mu_0\epsilon_0}_{=c_0^{-2}} \ddot{\mathbf{A}}(\mathbf{r},t) = 0 \tag{1.9}$$

[1] Here and throughout this work , we denote the scalar product of two vectors as $\mathbf{ab}$, the vector product as $\mathbf{a} \times \mathbf{b}$ and the operator $\nabla = (\partial_x, \partial_y, \partial_z)^T$ is applied in the same manner, yielding divergence and curl respectively. Furthermore, ∇f denotes the gradient of the scalar quantity f.

and $\Phi(\mathrm{r},t) = 0$. The parameter c_0 is the speed of light in vacuum. Indeed, one may apply in this case the mechanism of canonical field quantization by finding the Lagrangian density for which the Euler-Lagrange equations yield (1.9), defining the canonical conjugate $\mathbf{\Pi}$ to $\mathbf{A}$, Legendre transforming the Lagrangian density to the Hamiltonian density, writing the Hamiltonian density in symmetric ordering of $\mathbf{A}$ and $\mathbf{\Pi}$, and finally replacing $\mathbf{A}$ and $\mathbf{\Pi}$ with field operators and their Poisson brackets by commutators divided by $(i\hbar)$ (cf. [2]).

The procedure of canonical field quantization will simply result in the quantized wave equation

$$\Delta\hat{\mathbf{A}}(\mathbf{r},t) - \frac{1}{c_0^2}\ddot{\hat{\mathbf{A}}}(\mathbf{r},t) = 0 \tag{1.10}$$

and the Hamiltonian of the free field

$$\hat{H}_0(t) = \frac{1}{2}\int_V \left[\epsilon_0\hat{\mathbf{E}}^2(\mathbf{r},t) + \mu_0^{-1}\hat{\mathbf{B}}^2(\mathbf{r},t)\right], \tag{1.11}$$

with the quantization Volume V and

$$\hat{\mathbf{E}}(\mathbf{r},t) = -\dot{\hat{\mathbf{A}}}(\mathbf{r},t), \qquad \hat{\mathbf{B}}(\mathbf{r},t) = \nabla\times\hat{\mathbf{A}}(\mathbf{r},t). \tag{1.12}$$

Equation (1.11) corresponds exactly to the classical expression for the energy of the free electromagnetic field. Through a separation of variables, $\hat{\mathbf{A}}(\mathbf{r},t) = \frac{1}{\sqrt{\varepsilon_0}}\sum_\lambda c_\lambda \mathbf{A}_\lambda(\mathbf{r})\hat{q}_\lambda(t)$, the operator,valued vector potential wave equation (1.10) can be separated into a time-dependent operator valued harmonic oscillator equation,

$$\ddot{\hat{q}}_\lambda(t) + \omega_\lambda^2\hat{q}_\lambda(t) = 0, \tag{1.13}$$

and a Helmholtz equation in the spatial components

$$\Delta\mathbf{A}_\lambda(\mathbf{r}) + \frac{\omega_\lambda^2}{c_0^2}\mathbf{A}_\lambda(\mathbf{r}) = 0. \tag{1.14}$$

In the box-quantization approach a cubic box with volume $V = L^3$ and side length L an periodic boundary conditions is considered. The Helmholtz equation (1.14) is then solved inside this box by plain waves. After defining annihilation and creation operators for the harmonic oscillator equation (1.13) one can take the infinite space limit $L\to\infty$ and obtains the vector potential operator in the Heisenberg picture as [2]

$$\hat{\mathbf{A}}(\mathbf{r},t) = \sum_\sigma\int d^3\mathbf{k}\sqrt{\frac{\hbar}{2\varepsilon_0\omega(\mathbf{k})(2\pi)^3}}\mathbf{e}_\sigma(\mathbf{k})e^{i[\mathbf{kr}-\omega(\mathbf{k})t]}\hat{a}_\sigma(\mathbf{k}) + \text{H.c.}. \tag{1.15}$$

Here $\mathbf{e}_\sigma(\mathbf{k})$ are polarization vectors such that $\mathbf{k}\mathbf{e}_\sigma(\mathbf{k}) = 0$ and $\omega(\mathbf{k}) = |\mathbf{k}|c_0$. The annihilation/creation operators fulfill bosonic commutator relations as

$$\left[\hat{a}_\sigma(\mathbf{k}), \hat{a}^\dagger_{\sigma'}(\mathbf{k}')\right] = \delta(\mathbf{k}-\mathbf{k}')\delta_{\sigma,\sigma'}, \qquad \left[\hat{a}_\sigma(\mathbf{k}), \hat{a}_{\sigma'}(\mathbf{k}')\right] = 0. \tag{1.16}$$

As the operator part after separation of variables in (1.10) fulfills the Harmonic oscillator equation (1.13), it is unsurprising that the Hamiltonian of this system takes the form

$$\hat{H}_0 = \sum_\sigma \int d^3\mathbf{k}\, \hbar\omega(\mathbf{k}) \left[\hat{a}^\dagger_\sigma(\mathbf{k})\hat{a}_\sigma(\mathbf{k}) + \frac{1}{2}\hat{1}\right], \tag{1.17}$$

i.e., it is a linear combination of harmonic oscillator Hamiltonians, $\hat{\mathcal{H}}_\sigma(\mathbf{k}) = \hbar\omega(\mathbf{k})[\hat{a}^\dagger_\sigma(\mathbf{k})\hat{a}_\sigma(\mathbf{k}) + \frac{1}{2}\hat{1}]$, for each monochromatic frequency/polarization mode of the field. The relation $\hat{\mathbf{E}}(\mathbf{r},t) = -\partial_t\hat{\mathbf{A}}(\mathbf{r},t)$ yields

$$\hat{\mathbf{E}}^{(+)}(\mathbf{r},t) = i\sum_\sigma \int \frac{d^3\mathbf{k}}{(2\pi)^{3/2}} \mathbf{e}_\sigma(\mathbf{k}) e^{i[\mathbf{k}\mathbf{r}-\omega(\mathbf{k})t]} \sqrt{\frac{\hbar\omega(\mathbf{k})}{2\varepsilon_0}}\hat{a}_\sigma(\mathbf{k}),$$

with

$$\hat{\mathbf{E}}^{(-)}(\mathbf{r},t) = \left(\hat{\mathbf{E}}^{(+)}(\mathbf{r},t)\right)^\dagger \text{ and } \hat{\mathbf{E}}(\mathbf{r},t) = \hat{\mathbf{E}}^{(+)}(\mathbf{r},t) + \hat{\mathbf{E}}^{(-)}(\mathbf{r},t). \tag{1.18}$$

1.2 Quantum states of bosonic systems

Naturally, we cannot discuss the quantum properties of light without referring to some fundamental states of the the electromagnetic field. As the process of quantization of the free field has revealed, each of the Hamiltonians of each field mode takes a representation resembling that of harmonic oscillators. Unsurprisingly, quantum states in quantum optics are thus formally identical with those of the the quantized harmonic oscillator [cf. (1.17)].

Among the plethora of states that have been considered in the field of quantum optics, the following four states will be of relevance for all below discussion; (i) the Fock state, which like no other state underlines the particle nature of light; (ii) the coherent state, which emulates the classical harmonic oscillator; (iii) the squeezed vacuum state, which for some linear combination of its quadratures has less quantum mechanical standard deviation then the vacuum state. The two latter states can be directly associated with unitary operators, i.e., the displacement and squeezing operators, respectively. The combination of displacement and squeezing operators results in squeezed coherent states.

For a start, we limit our discussion to single modes of the light field. Mode indices are thus omitted and we consider the Hamiltonian

$$\hat{H} = \hbar\omega \left(\hat{n} + \frac{1}{2} \right), \tag{1.19}$$

with the photon number operator $\hat{n} = \hat{a}^\dagger \hat{a}$ and the bosonic annihilation/creation operators, satisfying

$$[\hat{a}, \hat{a}^\dagger] = \hat{1}, \qquad [\hat{a}, \hat{a}] = [\hat{a}^\dagger, \hat{a}^\dagger] = \hat{0}. \tag{1.20}$$

As mentioned above, this is the Hamiltonian of the quantized Harmonic oscillator. The states discussed in the following thus apply also to other cases where a harmonic oscillator representation is valid, e.g., ions in a Paul trap or molecular vibrations. In the following, we list properties of these states. Derivations of these properties can be considered part of the standard canon of quantum optics and may be found in similar forms in (among others) Refs. [2, 4, 98, 99].

1.2.1 Fock states

Fock states fulfill the eigenvalue equation

$$\hat{n}|n\rangle = n|n\rangle \text{ for } n = 0, 1, 2, \ldots, \infty. \tag{1.21}$$

For $n = 0$, we get the vacuum state as $\hat{n}|0\rangle = 0$, and all subsequent Fock states can be generated from the vacuum state as

$$|n\rangle = \frac{\hat{a}^{\dagger n}}{\sqrt{n!}}|0\rangle. \tag{1.22}$$

Using the commutator relations and the condition $\hat{a}|0\rangle = 0$, one can show that they form an orthonormal complete system

$$\langle n|n'\rangle = \delta_{n,n'}, \qquad \hat{1} = \sum_{n=0}^{\infty} |n\rangle\langle n|. \tag{1.23}$$

The property that essentially motivates the nomenclature of the annihilation/creation operator is the effect of these operators on the Fock states,

$$\hat{a}|n\rangle = \sqrt{n}|n-1\rangle, \qquad \hat{a}^\dagger|n\rangle = \sqrt{n+1}|n+1\rangle. \tag{1.24}$$

1.2.2 Coherent states

Coherent states are the solutions to the eigenvalue equation

$$\hat{a}|\alpha\rangle = \alpha|\alpha\rangle. \tag{1.25}$$

They posses the Fock basis representation

$$|\alpha\rangle = e^{-|\alpha|^2/2} \sum_{n=0}^{\infty} \frac{\alpha^n}{\sqrt{n!}}|n\rangle \tag{1.26}$$

and are normalized to unity as $\langle\alpha|\alpha\rangle = 1$. However, they are not orthogonal

$$\langle\alpha|\beta\rangle = \exp\left(-\frac{1}{2}\left[|\alpha|^2 + |\beta|^2 - 2\alpha^*\beta\right]\right) \tag{1.27}$$

but complete

$$\hat{1} = \frac{1}{\pi}\int d^2\alpha\, |\alpha\rangle\langle\alpha|. \tag{1.28}$$

Indeed, this completeness also allows one to represent density operators of systems in terms of coherent states, i.e., in terms of the famous Glauber Sudarshan P quasiprobability [100, 101]. The coherent state can be generated by displacing the vacuum state

$$|\alpha\rangle = \hat{D}(\alpha)|0\rangle, \tag{1.29}$$

with the displacement operator

$$\hat{D}(\alpha) = e^{\alpha\hat{a}^\dagger - \alpha^*\hat{a}} = e^{-|\alpha|^2/2}e^{\alpha\hat{a}^\dagger}e^{-\alpha^*\hat{a}} = e^{|\alpha|^2/2}e^{-\alpha^*\hat{a}}e^{\alpha\hat{a}^\dagger}, \tag{1.30}$$

which imposes the linear shift

$$\hat{D}^\dagger(\alpha)\hat{a}\hat{D}(\alpha) = \hat{a} - \alpha. \tag{1.31}$$

1.2.3 Squeezed states

The squeezed vacuum state does not fulfill a straight forward eigenvalue equation [102] but may – similarly to the coherent state – be generated from vacuum by a unitary transformation

$$\hat{S}(\xi) = e^{\frac{1}{2}\left[\xi^*\hat{a}^2 - \xi\hat{a}^{\dagger 2}\right]} \tag{1.32}$$

as

$$|\xi\rangle = \hat{S}(\xi)|0\rangle. \tag{1.33}$$

This unitary operator goes by the name of squeezing operator. Its Fock basis representation reads as

$$|\xi\rangle = \frac{1}{\sqrt{\cosh(r)}} \sum_{n=0}^{\infty} \tanh^n(r) \frac{\sqrt{(2n)!}}{n!2^n} |2n\rangle, \tag{1.34}$$

where $\xi = re^{i\phi}$ is the polar representation of the complex squeezing parameter ξ – the radial component r is sometimes referred to as the gain exponent.

The maybe most astonishing property of squeezed vacuum states is the reduction of vacuum fluctuations in one quadrature. This is due to the fact, that the Squeezing operator causes a Bogoliubov transformation [103] of the annihilation/creation operators,

$$\begin{aligned} \hat{S}^\dagger(\xi)\hat{a}\hat{S}(\xi) &= \cosh(r)\hat{a} + e^{i\phi}\sinh(r)\hat{a}^\dagger, \\ \hat{S}^\dagger(\xi)\hat{a}^\dagger\hat{S}(\xi) &= \cosh(r)\hat{a}^\dagger + e^{-i\phi}\sinh(r)\hat{a}. \end{aligned} \tag{1.35}$$

We may write a generalized quadrature as

$$\hat{x}(\theta) = \frac{1}{\sqrt{2}} \left[e^{i\theta}\hat{a} + e^{-i\theta}\hat{a}^\dagger \right], \tag{1.36}$$

such that $\hat{x} = \hat{x}(\theta = 0)$ and $\hat{p} = \hat{x}(\theta = \pi/2)$. Furthermore, we have the Heisenberg uncertainty principle,

$$\langle \Delta\hat{x}^2(\theta)\rangle \langle \Delta\hat{x}^2(\theta + \pi/2)\rangle \geq |\frac{1}{2i}\langle [\hat{x}(\theta), \hat{x}(\theta + \pi/2)]\rangle|^2 = \frac{1}{4}, \tag{1.37}$$

where $\Delta\hat{x}(\theta) = \hat{x}(\theta) - \langle \hat{x}(\theta)\rangle$. With the transformations (1.35), one can show that

$$\begin{aligned} \langle \xi|\hat{x}(\theta)|\xi\rangle &= 0, \\ \langle \xi|\Delta\hat{x}^2(\theta)|\xi\rangle &= \frac{e^{-2r}}{2}\sin^2(\theta + \phi/2) + \frac{e^{2r}}{2}\cos^2(\theta + \phi/2). \end{aligned} \tag{1.38}$$

So whilst the noise is suppressed maximally by e^{-2r} in one quadrature, the uncertainty relation remains valid as it is compensated by the maximal noise increase of e^{2r}.

1.3 Gaussian unitary transformations and multimode squeezing

Above, we discussed some states of light in a single-mode context. This was motivated by the fact that we can represent the electric field in terms of monochromatic plane waves in vacuum[2]. However, in the framework of this work we will also be interested in wave packages of light, i.e., inherently non-monochromatic modes of light.

As seen above, monochromatic plane waves can serve as modal representations for the description of the electric field in vacuum and transparent dielectric media. Naturally, as the Fourier components form complete basis in the corresponding $\mathcal{L}^2(\mathbb{C})$ spaces, we can equally decompose the field into any other $\mathcal{L}^2(\mathbb{C})$ basis, e.g., Hermite-Gauss functions. Thus, for a component $\hat{E}(\mathbf{r},t)$ of the electric field $\hat{\mathbf{E}}(\mathbf{r},t)$, we can always find a representation in terms of a complete set of orthogonal $\mathcal{L}^2(\mathbb{C})$ modal functions $\{f_k(\mathbf{r},t)\}$ as (cf. [2, 3, 104])

$$\hat{E}(\mathbf{r},t) = \sum_k \hat{a}_k f_k^*(\mathbf{r},t) + \text{H.c.}, \tag{1.39}$$

where $a_k(a_k^\dagger)$ are the annihilation(creation) operators for the mode with index k. To simplify the following discussion, it is convenient to consider that the modal functions are normalized to unity.

If we consider a finite number of n of optical modes $k = 1, \ldots, n$, we can introduce a column vector of annihilation and creation operators $\hat{\boldsymbol{\xi}} = (\hat{a}_1, \ldots, \hat{a}_n, \hat{a}_1, \ldots, \hat{a}_n)^T$[3]. The bosonic commutator relations are then recovered as

$$\hat{\boldsymbol{\xi}}\hat{\boldsymbol{\xi}}^\dagger - \hat{\boldsymbol{\xi}}^{\dagger T}\hat{\boldsymbol{\xi}}^T = \mathbf{K} = \begin{pmatrix} I & 0 \\ 0 & -I \end{pmatrix}, \tag{1.40}$$

where I is the $n\times n$ identity matrix. Correspondingly, a vector of modal functions $\mathbf{f}(\mathbf{r},t) = (f_1(\mathbf{r},t), \ldots, f_n(\mathbf{r},t), f_1^*(\mathbf{r},t), \ldots, f_n^*(\mathbf{r},t))^T$ may be defined, which allows us to write $\hat{E}(\mathbf{r},t) = \mathbf{f}^\dagger(\mathbf{r},t)\hat{\boldsymbol{\xi}}$. In the remainder of this section, we adopt this notation of boldface variables for $2n\times 2n$ matrices and roman for $n\times n$ matrices.

[2] A similar representation is possible for dielectric media, i.e., in the absence of isolated sources [105–107]. However, its derivation requires a lot more effort.

[3] Note, that this notation has to be used with care as it includes transpositions (which act on vectors and matrices) and adjungations (which additionally act on operators).

1.3.1 General Gaussian operations on multimode fields

Unitary transformations of $\hat{\boldsymbol{\xi}}$ that preserve Gaussianity in the Wigner representation are called a Gaussian unitary transformations and have the form

$$\hat{\boldsymbol{\xi}}' = \hat{\mathcal{U}}^\dagger \hat{\boldsymbol{\xi}} \hat{\mathcal{U}}, \qquad \hat{\mathcal{U}} = \exp\left(-i\hat{\mathcal{H}}\right), \tag{1.41}$$

where the generator $\hat{\mathcal{H}}$ of the transformation is a second-order polynomial of annihilation and creation operators. For the sake of simplicity, we omit the linear part of this polynomial which describes displacements, i.e., we only consider generators of quadratic order which take form

$$\hat{\mathcal{H}} = \hat{\boldsymbol{\xi}}^\dagger \mathbf{H} \hat{\boldsymbol{\xi}}, \tag{1.42}$$

with the Hermitian matrix $\mathbf{H}$ that can be structured as

$$\mathbf{H} = \begin{pmatrix} H_0 & H_I \\ H_I^* & H_0^* \end{pmatrix}, \tag{1.43}$$

where H_0 is Hermitian and H_I is complex symmetric (i.e. $H_I \in \mathbb{C}^{n\times n}$ and $H_I^T = H_I$). This implies symmetric ordering of $\hat{\mathcal{H}}$. Note that despite our matrix notation, $\hat{\mathcal{H}}$ is a scalar operator valued quantity

$$\hat{\mathcal{H}} = \sum_{n,m=1}^{N} \left\{ (H_0)_{m,n} \hat{a}_m^\dagger \hat{a}_n + (H_I)_{m,n} \hat{a}_m^\dagger \hat{a}_n^\dagger + (H_I^*)_{m,n} \hat{a}_m \hat{a}_n + (H_0^*)_{m,n} \hat{a}_m \hat{a}_n^\dagger \right\}. \tag{1.44}$$

In this notation, it is straightforward to show that

$$[i\hat{\mathcal{H}}, \hat{a}_k] = -2i \sum_{n=1}^{N} \left\{ (H_0)_{k,n} \hat{a}_n + (H_I)_{k,n} \hat{a}_n^\dagger \right\}, \tag{1.45}$$

which, by conjugation, also yields $[i\hat{\mathcal{H}}, \hat{a}_k^\dagger] = 2i \sum_{n=1}^{N} \{ (H_0^*)_{k,n} \hat{a}_n + (H_I^*)_{k,n} \hat{a}_n^\dagger \}$. In the matrix notation, this implies (cf. [108])

$$[i\hat{\mathcal{H}}, \hat{\boldsymbol{\xi}}] = -2i \mathbf{K} \mathbf{H} \hat{\boldsymbol{\xi}}. \tag{1.46}$$

With the Hadamard Lemma,

$$e^{\hat{X}} \hat{Y} e^{-\hat{X}} = \sum_{p=0}^{\infty} \frac{1}{p!} \mathrm{ad}_{\hat{X}}^p \hat{Y}, \tag{1.47}$$

where we denote nested commutators by the adjoint ad as

$$\mathrm{ad}^{p+1}_{\hat{X}}\hat{Y} = [\hat{X}, \mathrm{ad}^{p}_{\hat{X}}\hat{Y}], \qquad \mathrm{ad}^{0}_{\hat{X}}\hat{Y} = \hat{Y}, \tag{1.48}$$

and $\mathrm{ad}^{p}_{i\hat{\mathcal{H}}}\hat{\boldsymbol{\xi}} = (-2i\mathbf{KH})^p\,\hat{\boldsymbol{\xi}}$, we get (cf. [108])

$$\hat{\mathcal{U}}^\dagger\hat{\boldsymbol{\xi}}\hat{\mathcal{U}} = e^{i\mathcal{H}}\hat{\boldsymbol{\xi}}e^{-i\hat{\mathcal{H}}} = \sum_{p=0}^{\infty}\frac{1}{p!}\,(-2i\mathbf{KH})^p\,\hat{\boldsymbol{\xi}} = e^{-2i\mathbf{KH}}\hat{\boldsymbol{\xi}}. \tag{1.49}$$

The notation in terms of ad emphasizes that applying the nested commutators $\mathrm{ad}_{\hat{X}}$ is itself a linear operation/map and is frequently used in Lie theory (see, e.g., the proof of Magnus theorem in Ref. [18]). Thus, the transformation is equally representable in terms of a linear matrix transform,

$$\hat{\boldsymbol{\xi}}' = \mathbf{S}\hat{\boldsymbol{\xi}}, \tag{1.50}$$

with $\mathbf{S} = e^{-2i\mathbf{KH}}$. Consequently, the matrix and operator formalism are homomorph (cf. [108]):

$$\hat{\mathcal{U}} = e^{-i\hat{\boldsymbol{\xi}}^\dagger\mathbf{H}\hat{\boldsymbol{\xi}}} \leftrightarrow \mathbf{S} = e^{-2i\mathbf{KH}}. \tag{1.51}$$

In order to fulfill bosonic commutator relations, $\mathbf{S}$ is required to fulfill the relation

$$\mathbf{SKS}^\dagger = \mathbf{K}. \tag{1.52}$$

Matrices that are connected to purely quadratic Hamiltonians by the homomorphism (1.51) fulfill this relation and will be referred to as *complex symplectic* and can be represented as [108, 109]

$$\mathbf{S} = \begin{pmatrix} A & B \\ B^* & A^* \end{pmatrix}, \tag{1.53}$$

where the complex matrices A and B satisfy the relation $AA^\dagger - BB^\dagger = I$ and the matrix AB^T is complex symmetric, i.e., $AB^T \in \mathbb{C}^{n\times n}$ and $(AB^T) = AB^T$.

1.3.2 Passive Gaussian unitary transformation

The Gaussian unitary transformations can be categorized in some important subclasses. One such subclass are the transformations for which the total number of photons remains preserved, i.e., $\hat{\boldsymbol{\xi}}^\dagger\hat{\boldsymbol{\xi}} = \hat{\boldsymbol{\xi}}'^\dagger\hat{\boldsymbol{\xi}}'$. Such transformations are known as passive Gaussian unitary transformations [108, 109] and correspond physically to mixing different modes on a multiport interferometer. In Eqs. (1.53) and (1.44), total photon-number conservation implies $B = H_I = 0$

and A takes unitary form with $A = \exp(-2iH_0)$. Thus, the complex symplectic transform reads

$$\mathbf{S} = \begin{pmatrix} e^{-2iH_0} & 0 \\ 0 & e^{2iH_0^*} \end{pmatrix} \tag{1.54}$$

and is in itself also unitary. Consequently, this subgroup has the same dimension, n^2, as the unitary group $\mathrm{U}(n)$.

Another important point is that the passive Gaussian transformations correspond to a change of mode basis. This is because a unitary transformation preserves the field,

$$\hat{E}(\mathbf{r},t)(\mathbf{r},t) = \mathbf{f}^\dagger(\mathbf{r},t)\hat{\boldsymbol{\xi}} = \mathbf{f}'^\dagger(\mathbf{r},t)\hat{\boldsymbol{\xi}}', \text{ where } \mathbf{f}'(\mathbf{r},t) = \begin{pmatrix} e^{-2iH_0} & 0 \\ 0 & e^{2iH_0} \end{pmatrix} \mathbf{f}(\mathbf{r},t). \tag{1.55}$$

Such a change of basis is possible, as the passive transformation preserves the orthogonality of field modes as

$$\int d^3\mathbf{r}\, \mathbf{f}'(\mathbf{r},t)\mathbf{f}'^\dagger(\mathbf{r},t) = \int d^3\mathbf{r}\, \mathbf{f}(\mathbf{r},t)\mathbf{f}^\dagger(\mathbf{r},t) = \mathbf{I}, \tag{1.56}$$

where $\mathbf{I}$ is the $2n\times 2n$ identity matrix.

1.3.3 Mode-wise squeezing

Another class of Gaussian unitary transformations is given by the transformations where $H_0 = 0$ and $H_I = \frac{1}{2i}R$ with the diagonal matrix $R = \mathrm{diag}\{r_1, ..., r_n\}$, where $r_1, ..., r_n \in \mathbb{R}$ are squeezing parameters[4]. This type of transformation is called mode-wise squeezing as each of the field modes, described by the operators $\hat{\boldsymbol{\xi}}$, is squeezed according to the squeezing parameters $r_1, \dots r_n$ contained in R. The complex symplectic matrix for this class of transformations consequently reads as

$$\mathbf{S} = \exp\begin{pmatrix} 0 & R \\ R & 0 \end{pmatrix} = \begin{pmatrix} \cosh(R) & \sinh(R) \\ \sinh(R) & \cosh(R) \end{pmatrix}. \tag{1.57}$$

[4]We note here that if we would consider complex parameters $\xi_1, \dots \xi_n$, with $\xi_k = r_k e^{i\phi_k}$, this would also correspond to mode-wise squeezing in terms of the complex squeezing parameters ξ_k. However, the phase $e^{i\phi_k}$ in terms of the argument ϕ_k of the complex parameter ξ_k acts as a passive Gaussian unitary transformation. For the sake of distinguishing the two classes of transformations, it is thus convenient to consider real squeezing parameters r_k only to define the class of mode-wise squeezing. Furthermore, note that the sign of r_k can also be absorbed into the argument ϕ_k – i.e., into a passive Gaussian unitary transformation – and we will mostly consider $r_1, \dots, r_n \geq 0$ – i.e., R is positive semi-definite.

The corresponding unitary operator can be written as

$$\hat{\mathcal{U}} = \exp\left\{\hat{\boldsymbol{\xi}}^{\dagger}\begin{pmatrix} 0 & -\frac{1}{2}R \\ \frac{1}{2}R & 0 \end{pmatrix}\hat{\boldsymbol{\xi}}\right\} = e^{-\frac{r_1}{2}\left(a_1^{\dagger 2}-a_1^2\right)}e^{-\frac{r_2}{2}\left(a_2^{\dagger 2}-a_2^2\right)}\cdots e^{-\frac{r_n}{2}\left(a_n^{\dagger 2}-a_n^2\right)}, \tag{1.58}$$

i.e., it can be decomposed in terms of mode-wise single-mode squeezing. Naturally, this subclass has dimensionality of n.

1.3.4 Bloch-Messiah decomposition

The central mathematical procedure for defining the modes of squeezing of a multimode optical field is the decomposition of an arbitrary Gaussian unitary transformation into two passive transformations and one mode-wise squeezing transformation:

$$\mathbf{S} = \begin{pmatrix} V & 0 \\ 0 & V^* \end{pmatrix}\exp\left\{\begin{pmatrix} 0 & R \\ R & 0 \end{pmatrix}\right\}\begin{pmatrix} W & 0 \\ 0 & W^* \end{pmatrix}^{\dagger}, \tag{1.59}$$

where the matrices V and W are unitary and the diagonal matrix R is positive semi-definite. This decomposition is known as Bloch-Messiah reduction/decomposition. It was introduced by Bloch and Messiah for fermions [110] and later generalized to bosons [111]. The physical meaning of this procedure is the possibility of realizing any Gaussian unitary transformation by means of two multiport interferometers and a number of single-mode squeezers [112]. A schematic illustration of this concept is given in Fig. 1.1.

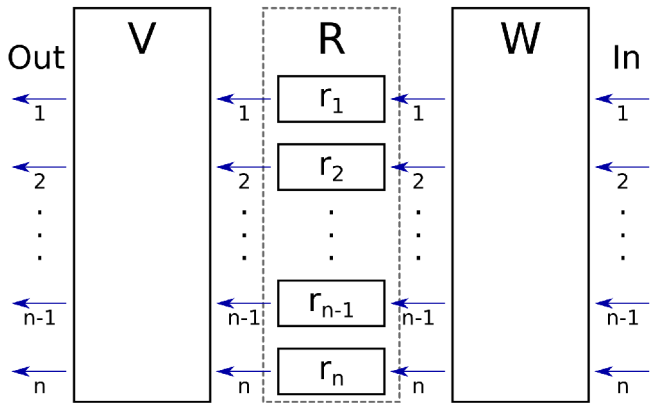

Figure 1.1: Illustration of the Bloch-Messiah decomposition. The input-output relation of a general Gaussian unitary transformation can always be realized in terms of three separate transformations; firstly, a unitary transform W that mixes modes of light; secondly, mode-wise single-mode squeezing R; thirdly, another unitary transform V that again mixes modes of light.

The decomposition Eq. (1.59) can be written in the following form, used by Braunstein [112]:

$$A = V\cosh(R)W^\dagger, \qquad B = V\sinh(R)W^T. \tag{1.60}$$

Consequently, the full dimensionality of the symplectic group is that of the two passive transforms plus the dimensionality of the mode-wise squeezing, i.e., $2n^2 + n$.

The Bloch-Messiah decomposition can be reduced to a Takagi decomposition (cf. [113, 114]). The Takagi decomposition is a symmetric singular-value decomposition of a complex symmetric matrix $M = M^T \in \mathbb{C}^{n\times n}$ as [115]

$$M = P\Xi P^T \tag{1.61}$$

where Ξ is diagonal semi-definite and P is unitary. Indeed, if one, e.g., sets $M = AB^T$, the Takagi decomposition (1.61) yields the Bloch-Messiah decomposition as

$$\begin{aligned} R &= \frac{1}{2}\mathrm{arcsinh}\left(2\Xi\right), \\ V &= P, \\ W &= A^\dagger P f(\Xi), \end{aligned} \tag{1.62}$$

where the function $f(z) = 1/\cosh(\mathrm{arcsinh}(2\mathrm{z})/2)$ is applied to the diagonal elements of Ξ. This allows us to use a simple implementation for this decomposition; see appendix B.

1.3.5 Multimode squeezing

We are now equipped with the necessary tools to describe multimode squeezing in the context of the symplectic matrix formalism. For the case of multimode squeezing $H_0 = 0$ and $H_I = \frac{1}{2i}Z$ with a complex symmetric matrix $Z = Z^T$ which is not required to be diagonal, the Gaussian unitary operator takes the form [116]

$$\hat{\mathcal{U}} = \exp\left\{\frac{\hat{\vec{a}}^T Z^* \hat{\vec{a}}}{2} - \frac{\hat{\vec{a}}^\dagger Z \hat{\vec{a}}^{\dagger T}}{2}\right\}, \tag{1.63}$$

where $\hat{\vec{a}} = (\hat{a}_1, \ldots, \hat{a}_n)^T$. Note the formal similarity of of the operator (1.63) to (1.32). Naturally, if Z contains only diagonal elements, (1.63) describes mode wise squeezing (cf. Sec. 1.3.3). However, when Z is a non-diagonal matrix, one can always recover a mode-wise squeezing perspective with an appropriate choice of mode basis. This follows as the Bloch-

Messiah decomposition for this class of operators is symmetric in the sense that

$$\mathbf{S} = \begin{pmatrix} Q & 0 \\ 0 & Q^* \end{pmatrix} \exp\left\{ \begin{pmatrix} 0 & R \\ R & 0 \end{pmatrix} \right\} \begin{pmatrix} Q & 0 \\ 0 & Q^* \end{pmatrix}^\dagger, \tag{1.64}$$

with the Takagi decomposition of Z,

$$Z = QRQ^T, \tag{1.65}$$

in terms of the unitary matrix Q.

A simple and illustrative example for multimode squeezing is the case of the two-mode-squeezed vacuum state. To this end, we consider a field that can be described in terms of two modes,

$$\hat{E}(\mathbf{r},t) = \sum_{k=1,2} \hat{a}_k f_k^*(\mathbf{r},t) + \text{H.c.}. \tag{1.66}$$

Applying the operator

$$\hat{S}_{1,2}(\xi) = e^{\xi^* \hat{a}_1 \hat{a}_2 - \xi \hat{a}_1^\dagger \hat{a}_2^\dagger}, \tag{1.67}$$

which corresponds to

$$Z = \frac{\xi}{2i} \begin{pmatrix} 0 & 1 \\ 1 & 0 \end{pmatrix} \tag{1.68}$$

in Eq. (1.63), to vacuum yields the two-mode-squeezed vacuum state

$$\hat{S}_{1,2}(\xi)|0,0\rangle = \frac{1}{\cosh(|\xi|)} \sum_{n=0}^{\infty} \left(-e^{i\arg(\xi)}\tanh(|\xi|)\right)^n |n,n\rangle. \tag{1.69}$$

It is of course possible to represent the two-mode field (1.66) in another mode basis,

$$\hat{E}(\mathbf{r},t) = \sum_{k=1,2} \hat{b}_k g_k^*(\mathbf{r},t) + \text{H.c.}, \tag{1.70}$$

where

$$g_1(\mathbf{r},t) = \frac{1}{\sqrt{2}}\left[f_1(\mathbf{r},t) + f_2(\mathbf{r},t)\right], \qquad \hat{b}_1 = \frac{1}{\sqrt{2}}\left[\hat{a}_1 + \hat{a}_2\right], \tag{1.71}$$

$$g_1(\mathbf{r},t) = \frac{1}{i\sqrt{2}}\left[f_1(\mathbf{r},t) - f_2(\mathbf{r},t)\right], \qquad \hat{b}_2 = \frac{1}{i\sqrt{2}}\left[\hat{a}_1 - \hat{a}_2\right]. \tag{1.72}$$

This corresponds to a passive Gaussian unitary transformation (cf. Sec. 1.3.2). In this basis, the operator (1.69) is factorized in terms of single-mode squeezing operators, i.e.,

$$\hat{S}_{1,2}(\xi) = \underbrace{e^{\frac{1}{2}[\xi^* \hat{b}_1^2 - \xi \hat{b}_1^{\dagger 2}]}}_{=\hat{S}_1(\xi)} \underbrace{e^{\frac{1}{2}[\xi^* \hat{b}_2^2 - \xi \hat{b}_2^{\dagger 2}]}}_{=\hat{S}_2(\xi)}. \tag{1.73}$$

Applying them to vacuum yields two squeezed states

$$\hat{S}_1(\xi)\hat{S}_2(\xi)|0,0\rangle = |\xi,\xi\rangle, \tag{1.74}$$

where the squeezing parameter has multiplicity of two. So clearly there are quantum correlations present in the two-mode squeezed vacuum state (1.69).

Let us now illustrate what would happen if an ill-suited mode basis is chosen in measurements at hands of our two-mode squeezed vacuum state example (1.69). If a measurement solely performed in one mode (without loss of generality, we consider f_1), all measurement outcomes are determined in terms of the reduced density operator

$$\hat{\rho}_1 = \mathrm{Tr}_2\left\{\hat{S}(\xi)|0,0\rangle\langle 0,0|\hat{S}^\dagger(\xi)\right\} = \frac{1}{\cosh^2(|\xi|)} \sum_{k=0}^{\infty} \left(\tanh^2(|\xi|)\right)^k |k\rangle\langle k|, \tag{1.75}$$

where the mode f_2 has been traced out. Note that (1.75) is a thermal state with $\hbar\beta\omega = -2\ln(\tanh|\xi|)$. Thus, with this choice of measurement basis, only thermal noise can be recovered, i.e., all quantum correlations are destroyed. We can take this as an illustration for the importance of choice of proper measurement basis when one aims at measuring quantum correlations of multimode squeezed states.

Note that, whilst we can always reduce multimode squeezing to mode-wise squeezing by choosing appropriate modes, such a choice of modes might not always be the most convenient. Consider, e.g., the photon-pair generation in a type-II PDC process with a monochromatic pump where one generates pairwise photons of different polarization. Using a polarizing beam splitter, two beams of different polarization can be spatially separated. In such a case, the description in terms of the separate beam modes that are two-mode squeezing entangled can be considered more intuitive than to consider single-mode squeezing eigenmodes in terms of mixtures of beam modes (see. Ref. [117] for a thorough discussion of the connection between representations in terms of two-mode squeezing and in terms of single-mode squeezing. Therein generalizations to more than two modes are also considered.).

1.3.6 Displacement and seeding

In the above discussion, we have neglected displacement. This is simply because generators of the form

$$\hat{\mathcal{H}} = \hat{\boldsymbol{\xi}}^\dagger \mathbf{H} \hat{\boldsymbol{\xi}} - i\boldsymbol{\beta}^\dagger \mathbf{K} \hat{\boldsymbol{\xi}}, \tag{1.76}$$

where $\boldsymbol{\beta} = (\beta_1, \ldots, \beta_n, \beta_1^*, \ldots, \beta_n^*)^T \in \mathbb{C}^{2n}$, will not play a role in this manuscript. However in the context of PDC that we will encounter below, one might be interested also in coherently seeded PDC processes. Thus, it might be interesting to consider

$$|\boldsymbol{\beta}\rangle = \hat{D}(\boldsymbol{\beta})|\text{Vac.}\rangle, \qquad \hat{D}(\boldsymbol{\beta}) = e^{-\boldsymbol{\beta}^\dagger \mathbf{K} \hat{\boldsymbol{\xi}}}. \tag{1.77}$$

As there appear no quadratic terms, the mode-wise factorization of the displacement operator is always trivial as

$$\hat{D}(\boldsymbol{\beta}) = \hat{D}(\beta_1)\hat{D}(\beta_2)\cdots\hat{D}(\beta_n), \tag{1.78}$$

i.e., in terms of single-mode displacement operators. Moreover, it's impact is simply linear in the sense , that

$$\hat{D}^\dagger(\boldsymbol{\beta})\hat{\boldsymbol{\xi}}\hat{D}(\boldsymbol{\beta}) = \hat{\boldsymbol{\xi}} - \boldsymbol{\beta}. \tag{1.79}$$

Thus, when a Gaussian transformation $\hat{\mathcal{U}}$ (corresponding to the symplectic transform $\mathbf{S}$) is seeded, this can be expressed in terms of a modification of annihilation-creation operators as

$$\hat{D}^\dagger(\boldsymbol{\beta})\hat{\mathcal{U}}^\dagger\hat{\boldsymbol{\xi}}\hat{\mathcal{U}}\hat{D}^\dagger(\boldsymbol{\beta}) = \hat{D}^\dagger(\boldsymbol{\beta})\mathbf{S}\hat{\boldsymbol{\xi}}\hat{D}^\dagger(\boldsymbol{\beta}) = \mathbf{S}\hat{\boldsymbol{\xi}} + \mathbf{S}\boldsymbol{\beta}. \tag{1.80}$$

We take this as a justification to neglect seeding in various parts of this contribution as the seeded case can easily be constructed from the non-seeded case by linear transformations.

1.4 Time-dependent perturbation theory

Time-dependent perturbation theory in quantum mechanics may be applied when explicitly time-dependent Hamiltonians are considered. In this section, we recall some fundamentals of time-dependent perturbation theory. All content of this section may be found in introductions to quantum mechanics, e.g., Refs. [12–14].

For explicitly time-dependent Hamiltonians, it is often not possible to find analytical solutions for a state $|\Psi(t)\rangle$ that fulfills the Schrödinger equation

$$i\hbar\partial_t|\Psi(t)\rangle = \hat{H}(t)|\Psi(t)\rangle, \tag{1.81}$$

or an operator $\hat{A}(t)$ that fulfills the Heisenberg equation

$$i\hbar\partial_t\hat{A}(t) = [\hat{A}(t), \hat{H}(t)], \tag{1.82}$$

with initial conditions $|\Psi(t = t_0)\rangle$ and $\hat{A}(t = t_0)$, respectively. Formally, solutions can be formulated in terms of a evolution operators

$$|\Psi(t)\rangle = \hat{\mathcal{U}}(t, t_0)|\Psi(t_0)\rangle, \qquad \hat{A}(t) = \hat{\mathcal{U}}^\dagger(t, t_0)\hat{A}(t_0)\hat{\mathcal{U}}(t, t_0), \tag{1.83}$$

which fulfill the Schrödinger equation

$$i\hbar\partial_t\hat{\mathcal{U}}(t, t_0) = \hat{H}(t)\hat{\mathcal{U}}(t, t_0), \tag{1.84}$$

with the initial condition $\hat{\mathcal{U}}(t = t_0, t_0) = \hat{1}$. To discuss orders of perturbation, it is convenient to adopt an alternative notation as $\hat{H}(t) = \gamma\hbar\hat{\mathcal{H}}(t)$ with a expansion parameter $\gamma > 0$. The evolution equation then rewrites as

$$\partial_t\hat{\mathcal{U}}(t, t_0) = -i\gamma\hat{\mathcal{H}}(t)\hat{\mathcal{U}}(t, t_0). \tag{1.85}$$

1.4.1 Dyson series and time-ordered exponential

In what can be considered the standard approach to time-dependent perturbation theory, a direct integration of (1.85) leads to the operator-valued integral equation

$$\hat{\mathcal{U}}(t, t_0) = \hat{1} - i\gamma\int_{t_0}^{t} dt'\,\hat{\mathcal{H}}(t')\hat{U}(t', t_0) \tag{1.86}$$

which has form of a Fredholm integral equation of the second kind (cf. [118]). By repeated substitution of this equation into itself (i.e., fixpoint iteration) one obtains the Dyson series representation of the evolution operator [15]

$$\begin{aligned}\hat{\mathcal{U}}(t, t_0) = \hat{1} + (-i\gamma)\int_{t_0}^{t} dt_1\,\hat{\mathcal{H}}(t_1) + (-i\gamma)^2\int_{t_0}^{t} dt_1\int_{t_0}^{t_1} dt_2\,\hat{\mathcal{H}}(t_1)\hat{\mathcal{H}}(t_2)\\ + (-i\gamma)^3\int_{t_0}^{t} dt_1\int_{t_0}^{t_1} dt_2\int_{t_0}^{t_2} dt_3\,\hat{\mathcal{H}}(t_1)\hat{\mathcal{H}}(t_2)\hat{\mathcal{H}}(t_3) + \dots.\end{aligned} \tag{1.87}$$

Reformulating the Dyson series in terms of the time ordering operator $\mathcal{T}$ that orders $\hat{\mathcal{H}}(t)$ with larger t to the right yields the time-ordered exponential representation of the evolution operator

$$\begin{aligned}\hat{\mathcal{U}}(t,t_0) &= \hat{1} + \frac{(-i\gamma)}{1!}\int_{t_0}^{t} dt_1\, \hat{\mathcal{H}}(t_1) + \frac{(-i\gamma)^2}{2!}\int_{t_0}^{t} dt_1 \int_{t_0}^{t} dt_2\, \mathcal{T}\hat{\mathcal{H}}(t_1)\hat{\mathcal{H}}(t_2) \\ &+ \frac{(-i\gamma)^3}{3!}\int_{t_0}^{t} dt_1 \int_{t_0}^{t} dt_2 \int_{t_0}^{t} dt_3\, \mathcal{T}\hat{\mathcal{H}}(t_1)\hat{\mathcal{H}}(t_2)\hat{\mathcal{H}}(t_3) + \dots \\ &= \mathcal{T} e^{-i\gamma \int_{t_0}^{t} dt' \hat{\mathcal{H}}(t')} = \mathcal{T} e^{-\frac{i}{\hbar}\int_{t_0}^{t} dt' \hat{H}(t')}. \end{aligned} \tag{1.88}$$

Note that for constant Hamiltonians $\hat{H}_{\text{const.}}$ – such that $\forall t : \partial_t \hat{H}_{\text{const.}} = 0$ – the familiar expression $\hat{\mathcal{U}}(t,t_0) = e^{-\frac{i}{\hbar}H_{\text{const.}}(t-t_0)}$ for the evolution operator is recovered.

The solution of (1.85) in terms of the Dyson series and time-ordered exponential is, however, of a very formal nature and evaluation of these expressions is usually as hard as solving the original problem directly. However, the series representations can be used to obtain approximations to the evolution operator by truncating the series in some order in terms of the expansion parameter γ. The first three orders of Dyson series approximation do thus, e.g., read as

$$\begin{aligned}\hat{\mathcal{U}}_1(t,t_0) &= \hat{1} + \frac{(-i\gamma)}{1!}\int_{t_0}^{t} dt_1\, \hat{\mathcal{H}}(t_1) \\ \hat{\mathcal{U}}_2(t,t_0) &= \hat{\mathcal{U}}_1(t,t_0) + \frac{(-i\gamma)^2}{2!}\int_{t_0}^{t} dt_1 \int_{t_0}^{t} dt_2\, \mathcal{T}\hat{\mathcal{H}}(t_1)\hat{\mathcal{H}}(t_2) \\ \hat{\mathcal{U}}_3(t,t_0) &= \hat{\mathcal{U}}_2(t,t_0) + \frac{(-i\gamma)^3}{3!}\int_{t_0}^{t} dt_1 \int_{t_0}^{t} dt_2 \int_{t_0}^{t} dt_3\, \mathcal{T}\hat{\mathcal{H}}(t_1)\hat{\mathcal{H}}(t_2)\hat{\mathcal{H}}(t_3). \end{aligned} \tag{1.89}$$

Thus, as this does not have exponential form, we can see that unitarity of evolution operators is not preserved by this approximation method.

1.4.2 Magnus series expansion

The Magnus expansion is an alternative representation of the time evolution operator. It is essentially an exponential representation of the evolution operator as

$$\hat{\mathcal{U}}(t,t_0) = \exp\left(-i\hat{\mathcal{M}}(t,t_0)\right). \tag{1.90}$$

It can be shown that the operator $\hat{\mathcal{M}}(t,t_0)$ fulfills the differential equation [17]

$$\partial_t \hat{\mathcal{M}}(t,t_0) = \gamma \sum_{\ell=0}^{\infty} \frac{B_\ell}{\ell!} (-i)^\ell \mathrm{ad}^\ell_{\hat{\mathcal{M}}(t,t_0)} \hat{\mathcal{H}}(t), \tag{1.91}$$

where B_ℓ are the Bernoulli numbers $B_0 = 1$, $B_1 = -1/2$, $B_2 = 1/6$,etc. The Magnus expansion is the expansion of the exponent $\hat{\mathcal{M}}(t,t_0)$ in terms of the expansion parameter γ,

$$-i\hat{\mathcal{M}}(t,t_0) = \sum_{k=1}^{\infty} (-i\gamma)^k \, \hat{\mathcal{M}}_k(t,t_0). \tag{1.92}$$

Substituting the expansion into the Magnus differential equation (1.91), iteratively equating powers of γ and integrating, yields expressions for the $\hat{\mathcal{M}}_k(t,t_0)$ [18]. The first three orders read, e.g., as [18]

$$\begin{aligned}
\hat{\mathcal{M}}_1(t,t_0) &= \int_{t_0}^{t} dt_1 \, \hat{\mathcal{H}}(t_1), \\
\hat{\mathcal{M}}_2(t,t_0) &= \frac{1}{2} \int_{t_0}^{t} dt_1 \int_{t_0}^{t_1} dt_2 \, [\hat{\mathcal{H}}(t_1), \hat{\mathcal{H}}(t_2)], \\
\hat{\mathcal{M}}_3(t,t_0) &= \frac{1}{6} \int_{t_0}^{t} dt_1 \int_{t_0}^{t_1} dt_2 \int_{t_0}^{t_2} dt_3 \, \Big\{ [\hat{\mathcal{H}}(t_1), [\hat{\mathcal{H}}(t_2), \hat{\mathcal{H}}(t_3)]] + [\hat{\mathcal{H}}(t_3), [\hat{\mathcal{H}}(t_2), \hat{\mathcal{H}}(t_1)]] \Big\}.
\end{aligned} \tag{1.93}$$

Likewise, higher order terms are equally given in terms of linear combinations of time-ordered integrals of nested commutators in terms of the Hamiltonians $\hat{\mathcal{H}}$.

The first order approximation in terms of the ME – i.e., the first order MA – is given by the first term of the series (1.92) as

$$\hat{\mathcal{U}}_1(t,t_0) = e^{-i\gamma \int_{t_0}^{t} d\tilde{t} \, \hat{\mathcal{H}}(\tilde{t})}. \tag{1.94}$$

This expression corresponds to (1.88) with neglected time ordering, cf. [16, 23, 24]. All other terms, $k > 1$, of the ME are corrections in terms of time ordering and, therefore, account for (time) ordering effects [16, 19–24].

It should be mentioned that the ME is not guaranteed to converge. However, one can find a sufficient criterion for the convergence: The Magnus expansion (1.92) converges if [18]

$$|\gamma| \int_{t_0}^{t} d\tilde{t} \, \|\hat{\mathcal{H}}(\tilde{t})\|_2 < \pi. \tag{1.95}$$

Here, $\|\cdots\|_2$ stands for the spectral norm. This norm can be calculated as the maximal singular value of $\hat{\mathcal{H}}$, which for Hermitian Hamiltonians is given in terms of their maximum absolute value eigenvalue. Let us emphasize that is a solely sufficient criterion and that for the physical systems considered in the present manuscript, one may achieve convergence of the ME well above this sufficient bound.

1.4.3 Quadratic Hamiltonians

For the annihilation creation operators, as represented in Sec. 1.3.1, the evolution is governed as

$$\partial_t \hat{\boldsymbol{\xi}}(t) = \frac{\gamma}{i}[\hat{\boldsymbol{\xi}}(t), \hat{\mathcal{H}}(t)]. \tag{1.96}$$

Thus, if we consider quadratic Hamiltonians only [cf. (1.42)] this leads to

$$\partial_t \hat{\boldsymbol{\xi}}(t) = -i\gamma \mathbf{F}(t)\hat{\boldsymbol{\xi}}(t). \tag{1.97}$$

where $\mathbf{F}(t) = 2\mathbf{KH}(t)$, cf. (1.46). The evolution in time can thus again be described in terms of a symplectic linear transformation [cf. (1.41)] as $\hat{\boldsymbol{\xi}}(t) = \mathbf{S}(t, t_0)\hat{\boldsymbol{\xi}}(t_0)$ such that

$$\partial_t \mathbf{S}(t, t_0) = -i\gamma \mathbf{F}(t)\mathbf{S}(t, t_0). \tag{1.98}$$

Due to the similarity of the matrix differential equation (1.98) to the evolution operator equation (1.85), the Dyson series and MAs can be equally reformulated in terms of matrices. In the case of the MAs, equal orders of approximation in matrix and operator formulation yield exactly the same results; see Appendix A. The corresponding sufficient convergence bound for the ME,

$$-i\mathbf{M}(t, t_0) = \sum_{k=1}^{\infty} (-i\gamma)^k \, \mathbf{M}_k(t, t_0). \tag{1.99}$$

with, e.g.,

$$\mathbf{M}_1(t, t_0) = \int_{t_0}^{t} dt_1 \, \mathbf{F}(t_1) \tag{1.100}$$

is again given in terms of

$$\int_{t_0}^{t_{\max}} dt \, \|\mathbf{F}(t)\|_2 < \pi. \tag{1.101}$$

As $\mathbf{F}$ is matrix-valued, the spectral norm can be evaluated in terms of matrix singular value decomposition.

Chapter 2

Parametric down-conversion with a monochromatic pump

Contents

This chapter will concern our first application of the methods of ME and MA to a physical system. To this end we will consider the process of collinear type-I PDC in a nonlinear $\chi^{(2)}$ crystal with a plane-wave monochromatic pump of frequency ω_p [26]. Due to the $\chi^{(2)}$ nonlinearity in the crystal a three-wave interaction takes place, in which a incoming pump photon of frequency ω_p is converted into two secondary photons, usually referred to as *signal* and *idler* photons with frequencies ω_s and ω_i, respectively. Energy is conserved in this process such that

$$\omega_p = \omega_s + \omega_i. \tag{2.1}$$

Furthermore, momentum conservation holds such that

$$\mathbf{k}_p = \mathbf{k}_s + \mathbf{k}_i, \tag{2.2}$$

where $\mathbf{k}_p$, $\mathbf{k}_s$, and $\mathbf{k}_i$ are the wave vectors of the pump, signal, and idler mode, respectively. It is often convenient to describe frequencies in terms of sideband frequencies as $\omega_s = \omega_0 + \Omega$, $\omega_i = \omega_0 - \Omega$ around the carrier frequency $\omega_0 = \omega_p/2$ – a schematic illustration of the PDC process with these sideband frequencies is given in Fig. 2.1. In the type-I configuration the signal and

idler photons have the same polarization, i.e., they have ordinary polarization whilst the pump has extraordinary polarization in the crystal. For simplicity, we will consider the collinear case only, where all wave vectors are parallel and signal and idler photons are in the same mode. We consider a coordinate system with the z-axis in the direction of the pump wave propagation – i.e., $\mathbf{k}_p = k_p \mathbf{e}_z$ – and the origin at the front edge of the crystal. The pump is considered to be a classical monochromatic wave, $E_p^{(+)}(t,z) = E_p e^{i(k_p z - \omega_p t)}$, with strong coherent amplitude $E_p \in \mathbb{C}$ (such that quantum fluctuations of the pump field can be neglected). Momentum conservation then implies that the wave vector of the down-converted light, $k(\Omega)$, of frequency $\omega_0 + \Omega$ matches the wave vector at the pump frequency as $k_0 = k(0) = k_p/2$.

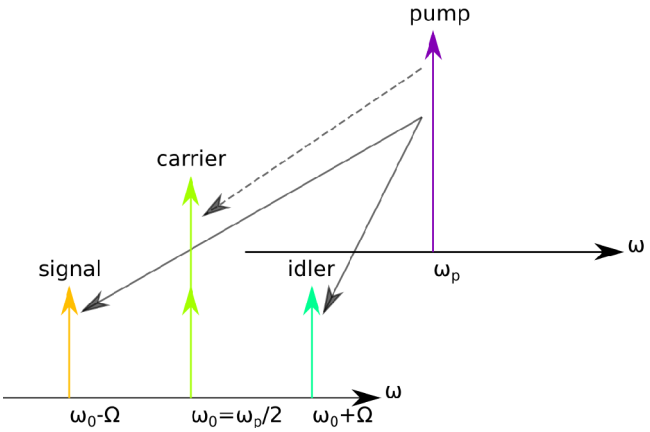

Figure 2.1: Schematic illustration of the type-I PDC process. The pump photon is down-converted into signal and idler photons (solid arrows) of opposed radio-frequencies Ω and $-\Omega$. In the degenerate case both photons have carrier frequency (dashed arrow). Vertical arrows indicate photons.

It is often convenient to describe the evolution of the fields in nonlinear optics with respect to the distance covered rather than time [26, 48, 119]. Such a description can be obtained in the following representation: The down-converted wave is described by the positive-frequency operator $\hat{E}^{(+)}(t,z)$ normalized to photon-flux units, which can be decomposed into Fourier components as [27]

$$\hat{E}^{(+)}(t,z) = \int \frac{d\Omega}{\sqrt{2\pi}} e^{i[k_0 z - (\omega_0+\Omega)t]} \hat{a}(\Omega, z), \tag{2.3}$$

where $\hat{a}(\Omega, z)$ is the photon annihilation operator with the frequency $\omega_0 + \Omega$ and the longitudinal coordinate z – also referred to as sideband operator below. It fulfills the bosonic commutator relations [27]

$$[\hat{a}(\Omega,z), \hat{a}^\dagger(\Omega',z)] = \delta(\Omega - \Omega'), \qquad [\hat{a}(\Omega,z), \hat{a}(\Omega',z)] = 0. \tag{2.4}$$

The nonlinear interaction inside the $\chi^{(2)}$ crystal leads to the following evolution equation for the down converted light [26, 27]

$$\partial_z \hat{a}(\Omega, z) = i[k(\Omega) - k_0]\hat{a}(\Omega, z) + \sigma \hat{a}^\dagger(-\Omega, z), \tag{2.5}$$

where $|\sigma|$ is proportional to the length L of the crystal the $\chi^{(2)}$ non linearity and the strength of the pump. The argument $\arg(\sigma)$ of the coupling constant σ is determined via the phase of the pump.

Note that the evolution equation (2.5) is formulated in terms of z rather than t. Indeed, $\hat{a}(\Omega, z)$ can be considered to be in the Heisenberg picture with respect to z as its spatial evolution can be obtained from a Heisenberg equation of motion as (cf. [48])

$$\partial_z \hat{a}(\Omega, z) = i[\hat{H}, \hat{a}(\Omega, z)], \tag{2.6}$$

with the Hamiltonian (in the Schrödinger picture) $\hat{H} = \hat{H}_0 + \hat{H}_{\text{int}}$, where

$$\begin{aligned} \hat{H}_0 &= \frac{1}{2} \int d\Omega \; [k(\Omega) - k_0] \left\{ \hat{a}^\dagger(\Omega)\hat{a}(\Omega) + \hat{a}(\Omega)\hat{a}^\dagger(\Omega) \right\}, \\ \hat{H}_{\text{int}} &= \frac{\sigma}{2i} \int d\Omega \, \hat{a}^\dagger(\Omega)\hat{a}^\dagger(-\Omega) + \text{H.c.}. \end{aligned} \tag{2.7}$$

Here, H_0 describes propagation, whilst $\hat{H}_{\text{int}}$ describes the effect of nonlinear interaction inside the crystal. Thus, the roles of time t and distance covered z can be considered reversed in the quantum description and we will apply the methods of ME as discussed in Sec. 1.4 to study ordering effects in terms of z rather than t.

We shall use another operator, $\hat{\epsilon}(\Omega, z)$, defined by the relation [26]

$$\hat{a}(\Omega, z) = \hat{\epsilon}(\Omega, z) e^{i(k(\Omega) - k_0)z}, \tag{2.8}$$

The operator $\hat{\epsilon}(\Omega, z)$ is convenient for the description of the nonlinear interaction inside the crystal and is a quantum-mechanical analog of the classical slowly-varying amplitude (cf. [120]). The evolution of the down-converted wave in the crystal is described by the equation [26, 120]

$$\partial_z \hat{\epsilon}(\Omega, z) = \sigma e^{i\Delta(\Omega)z} \hat{\epsilon}^\dagger(-\Omega, z), \tag{2.9}$$

with the initial condition $\hat{\epsilon}(\Omega, 0)$. Here,

$$\Delta(\Omega) = k_p - k(\Omega) - k(-\Omega) \tag{2.10}$$

is the phase-mismatch function such that $\Delta(\Omega = 0) = 0$. The passage from $\hat{a}(\Omega, z)$ to $\hat{\epsilon}(\Omega, z)$ can be considered a passage to the interaction picture as

$$\partial_z \hat{\epsilon}(\Omega, z) = i[\hat{\epsilon}(\Omega, z), \hat{\tilde{H}}_{\text{int}}(z)], \tag{2.11}$$

where

$$\hat{\tilde{H}}_{\text{int}}(z) = \frac{\sigma}{2i} \int d\Omega \, e^{i\Delta(\Omega)z} \hat{\epsilon}^\dagger(\Omega)\hat{\epsilon}^\dagger(-\Omega) + \text{H.c.}. \tag{2.12}$$

Equation (2.9) describes a process of conversion of a pump photon with the frequency ω_p into signal and idler photons with opposite sideband frequencies Ω and $-\Omega$. Note, that for $\Omega = 0$ Eq. (2.9) becomes z-independent and is degenerate in terms of frequencies, as both operators in the equation describe the same frequency mode – this case is also depicted in Fig. 2.1.

Indeed, closed form exact solutions to the above evolution equations are already known [26]. However, for the PDC process with non-monochromatic pumps – which we will treat in the subsequent chapter – no analytical solutions are known and one is bound to revert to perturbative approximations. Thus, we consider here the application of the ME and MAs for the case of a monochromatic pump. This allows us to compare ordering effects obtained by MA with the analytical solutions. The following analysis can thus be considered a benchmark of the utility of the methods of ME in the context of PDC. The work we present in this chapter, for the application of the Magnus expansion and Bloch Messiah decomposition to the PDC process with a monochromatic pump, has also been published in Refs. [24, 58].

2.1 Explicit solution of the dynamics

The solution of Eq. (2.9) has the form of a Bogoliubov transformation [26],

$$\hat{\epsilon}(\Omega, L) = A(\Omega)\hat{\epsilon}(\Omega, 0) + B(\Omega)\hat{\epsilon}^\dagger(-\Omega, 0), \tag{2.13}$$

with the complex coefficients $A(\Omega)$ and $B(\Omega)$ given by [26]

$$\begin{aligned} A(\Omega) &= e^{i\Delta L/2}\left[\cosh(\Gamma L) - i\frac{\Delta}{2\Gamma}\sinh(\Gamma L)\right], \\ B(\Omega) &= e^{i\Delta L/2}\frac{\sigma}{\Gamma}\sinh(\Gamma L), \end{aligned} \tag{2.14}$$

where $\Gamma = \sqrt{|\sigma|^2 - (\Delta/2)^2}$. At perfect phase-matching, where $\Delta(\Omega) = 0$, and in the band of frequencies around this frequency, Γ is real. Outside this band Γ is purely imaginary and the hyperbolic functions in Eq. (2.14) become trigonometric. Thus, outside of this band of real Γ we expect oscillatory behavior. Note, that the frequency detuning Ω enters Eq. (2.14) only

through $\Delta(\Omega)$ which is an even function. Therefore, the functions $A(\Omega)$ and $B(\Omega)$ are also even.

The sideband operator undergoes a similar Bogoliubov transformation

$$\hat{a}(\Omega, L) = U(\Omega)\hat{a}(\Omega, 0) + V(\Omega)\hat{a}^{\dagger}(-\Omega, 0), \tag{2.15}$$

where

$$U(\Omega) = A(\Omega)e^{i(k(\Omega)-k_0)L}, \qquad V(\Omega) = B(\Omega)e^{i(k(\Omega)-k_0)L}. \tag{2.16}$$

The Bogoliubov transformation(2.15) is fully characterized by four real parameters. Indeed, Eq. (2.15) together with its Hermite conjugate with opposite detuning $-\Omega$ is described by four complex numbers $U(\pm\Omega)$, $V(\pm\Omega)$. The unitarity of the Bogoliubov transformation imposes four real conditions $|U(\pm\Omega)|^2 - |V(\pm\Omega)|^2 = 1$, and $U(\Omega)/V(\Omega) = U(-\Omega)/V(-\Omega)$ (the last complex equation provides two real conditions), so that only four real parameters remain. These four real parameters can be defined through the squeezing parameter, and three characteristic angles [26]

$$r(\Omega) = \ln\left(|U(\Omega)| + |V(\Omega)|\right), \tag{2.17}$$

$$\psi_L(\Omega) = \frac{1}{2}\arg\left[U(\Omega)V(-\Omega)\right], \tag{2.18}$$

$$\psi_0(\Omega) = \frac{1}{2}\arg\left[U^{-1}(\Omega)V(\Omega)\right], \tag{2.19}$$

$$\kappa(\Omega) = \frac{1}{2}\arg\left[U(\Omega)U^{-1}(-\Omega)\right], \tag{2.20}$$

where the first three parameters are even functions of Ω, while the fourth one is odd.

To understand the physical meaning of these parameters we consider the eigenquadrature operators for each pair of modes with opposite detunings [26]

$$\begin{aligned}\hat{X}_1(\Omega, z) &= \hat{a}(\Omega, z)e^{-i\psi_z(\Omega)} + \hat{a}^{\dagger}(-\Omega, z)e^{i\psi_z(\Omega)},\\ \hat{X}_2(\Omega, z) &= -i\left[\hat{a}(\Omega, z)e^{-i\psi_z(\Omega)} - \hat{a}^{\dagger}(-\Omega, z)e^{i\psi_z(\Omega)}\right].\end{aligned} \tag{2.21}$$

For $z = 0$, Eq. (2.21) defines the eigenquadrature operators $\hat{X}_j(\Omega, 0), j = 1, 2$ at the input of the crystal, and for $z = L$ it defines the eigenquadrature operators $\hat{X}_j(\Omega, L), j = 1, 2$ at its output. In terms of these eigenquadratures the transformation (2.15) can be rewritten in the form

$$\hat{X}_j(\Omega, L) = e^{\pm r(\Omega)+i\kappa(\Omega)}\hat{X}_j(\Omega, 0), \tag{2.22}$$

where the upper(lower) sign corresponds to $j = 1(j = 2)$. It follows from Eq. (2.22) that the quadrature $\hat{X}_2(\Omega, L)$ is squeezed below the standard quantum limit, while the conjugate quadrature $\hat{X}_1(\Omega, L)$ is stretched above that limit. The squeezing parameter $r(\Omega)$ determines the degree of squeezing at the output of the crystal. The angle of squeezing $\psi_L(\Omega)$ and the seeding angle $\psi_0(\Omega)$ are due to the nonlinear interaction and determine the choice of the coordinate axes on the complex plane for the eigenquadrature components at the output and input of the nonlinear crystal, respectively.

The last parameter $\kappa(\Omega)$ in our case of even $A(\Omega)$ and $B(\Omega)$ is independent of the nonlinear properties of the crystal and is given by

$$\kappa(\Omega) = \frac{1}{2}\left[k(\Omega) - k(-\Omega)\right] L \approx \tau_g \Omega, \tag{2.23}$$

where $\tau_g = L/v_g$ is the characteristic time during which the down-converted wave travels through the crystal at the group velocity $v_g = 1/k'(0)$. Thus, the angle $\kappa(\Omega)$ describes the effect of the group delay due to crystal dispersion. Substituting Eq. (2.14) into Eqs. (2.16), (2.18), and (2.19), and denoting $\varphi = \arg\sigma$, we obtain

$$\begin{aligned}\psi_L(\Omega) &= \varphi - \psi_0(\Omega) \\ &= \frac{\varphi}{2} + \frac{1}{2}\arg\left[\cosh(\Gamma L) - \frac{i\Delta}{2\Gamma}\sinh(\Gamma L)\right] + \frac{1}{2}\arg\left[\frac{1}{\Gamma}\sinh(\Gamma L)\right].\end{aligned} \tag{2.24}$$

This equation indicates that due to the symmetry of our system, two angles $\psi_L(\Omega)$ and $\psi_0(\Omega)$ are not independent. Therefore, in what follows we shall provide results only for the angle $\psi_L(\Omega)$ at the output of the crystal. It is worth noting that this symmetry manifests itself due to particular choice of our PDC scheme, and is not necessarily present in all PDC processes. For example, for PDC in aperiodically poled quasi-phase-matched crystals this additional symmetry is lifted, and the angles $\psi_L(\Omega)$ and $\psi_0(\Omega)$ become independent [43, 44].

In the case of vacuum input the correlation function of the squeezed quadrature component $X_2(\Omega, L)$ at the output of the crystal can be evaluated using Eqs. (2.15)-(2.22) and is given by

$$\langle \hat{X}_2(\Omega, L)\hat{X}_2(\Omega', L)\rangle = s(\Omega)\delta(\Omega + \Omega'), \tag{2.25}$$

where

$$s(\Omega) = \exp[-2r(\Omega)] \tag{2.26}$$

is known as the spectrum of squeezing. The spectrum of squeezing together with the angle of squeezing are shown in Fig. 2.2 as functions of the phase-mismatch angle $\theta(\Omega) = \Delta(\Omega)L/2$. The amplitude of the pump is characterized by the parametric gain exponent $g = |\sigma|L$.

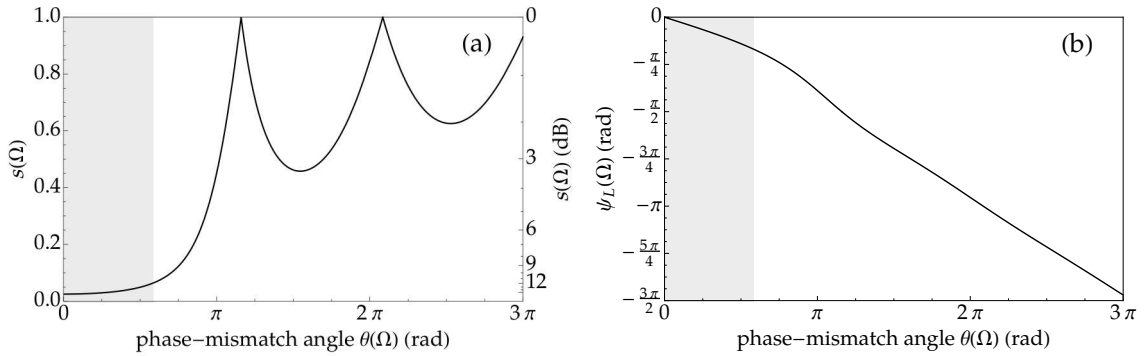

Figure 2.2: Graphs of (a) the spectrum of squeezing $s(\Omega)$ and (b) the angle of squeezing $\psi_L(\Omega)$ as functions of the phase mismatch angle $\theta(\Omega)$ for the exact solution. The gain exponent is $g = 1.84$. The phase of the pump is chosen so that $\varphi = 0$. The gray area indicates the band, where Γ is real. Figure as presented in Ref. [24] with a modified plotrange.

The angle in Fig. 2.2b – and in all subsequent Figures of this chapter – is the continuous version of the angle of squeezing $\psi_L(\Omega)$. The original angle of squeezing $\psi_L(\Omega)$ in Eq. (2.18) experiences a jump of $\pi/2$ at the frequencies Ω where $r(\Omega) = 0$. In Fig. 2.2b we have corrected for this jump in order to make the $\psi_L(\Omega)$ a continuous function. In other words, the continuous version of $\psi_L(\Omega)$ corresponds to the stretched quadrature between the odd and the even zeros of $r(\Omega)$.

From Fig. 2.2a, we see that squeezing is maximal for perfect phase matching when the phase-mismatch angle is zero, $\theta(\Omega) = 0$. For increasing mismatch it shows oscillations, decreasing in magnitude until disappearing completely for very large values of $\theta(\Omega)$ (not shown in Fig. 2.2a). The angle of squeezing decreases monotonously with $\theta(\Omega)$ approaching its asymptotic value $\psi_L(\Omega) \to -\theta(\Omega)/2$.

2.2 Matrix formulation

The theory of PDC, as recapitulated in the previous section, can be formulated in a compact matrix form which will allow us to perform the Bloch-Messiah decomposition and the ME. We collect the slowly-varying operators $\hat{\epsilon}(\Omega)$ and $\hat{\epsilon}(-\Omega)$ as well as the sideband operators $\hat{a}(\Omega, z)$ and $\hat{a}(-\Omega, z)$ in a column vector as

$$\hat{\mathbf{a}}(z) = \begin{pmatrix} \hat{a}(\Omega, z) \\ \hat{a}(-\Omega, z) \\ \hat{a}^\dagger(\Omega, z) \\ \hat{a}^\dagger(-\Omega, z) \end{pmatrix}, \qquad \hat{\boldsymbol{\xi}}(z) = \begin{pmatrix} \hat{\epsilon}(\Omega, z) \\ \hat{\epsilon}(-\Omega, z) \\ \hat{\epsilon}^\dagger(\Omega, z) \\ \hat{\epsilon}^\dagger(-\Omega, z) \end{pmatrix}, \tag{2.27}$$

which are connected according (2.8) to $\boldsymbol{a}(z) = \boldsymbol{\Phi}_z \boldsymbol{\xi}(z)$, where the unitary matrix $\boldsymbol{\Phi}_z$ is defined as follows

$$\boldsymbol{\Phi}_z = \mathrm{diag}\{e^{i\delta k(\Omega)z}, e^{i\delta k(-\Omega)z}, e^{-i\delta k(\Omega)z}, e^{-i\delta k(-\Omega)z}\}, \tag{2.28}$$

with $\delta k(\Omega) = k(\Omega) - k_0$. Here and below, when it does not lead to ambiguity, we shall omit the arguments Ω and $-\Omega$ in order to simplify the notations. This vector notation allows us to rewrite Eq. (2.9) in a matrix form

$$\partial_z \hat{\boldsymbol{\xi}}(z) = -i\mathbf{F}(z)\hat{\boldsymbol{\xi}}(z). \tag{2.29}$$

The coupling matrix $\mathbf{F}$ is given by

$$\mathbf{F}(z) = \begin{pmatrix} 0 & i\sigma e^{i\Delta z} P \\ i\sigma^* e^{-i\Delta z} P & 0 \end{pmatrix}, \tag{2.30}$$

where

$$P = \begin{pmatrix} 0 & 1 \\ 1 & 0 \end{pmatrix}. \tag{2.31}$$

The operators $\hat{\boldsymbol{\xi}}^{\mathrm{out}}$ at the output of the crystal, $z = L$, are related with the operators $\hat{\boldsymbol{\xi}}^{\mathrm{in}}$ at its input, $z = 0$, by a linear matrix transformation, $\hat{\boldsymbol{\xi}}^{\mathrm{out}} = \mathbf{S}\hat{\boldsymbol{\xi}}^{\mathrm{in}}$, with the matrix $\mathbf{S}$ given by

$$\mathbf{S} = \begin{pmatrix} A(\Omega)I & B(\Omega)P \\ B(\Omega)^* P & A(\Omega)^* I \end{pmatrix}. \tag{2.32}$$

This linear transformation preserves the commutator relations of the operators $\hat{\boldsymbol{\xi}}^{\mathrm{in}}$ and, therefore, the matrix $\mathbf{S}$ is a complex symplectic matrix [109], satisfying the relation $\mathbf{SKS}^\dagger = \mathbf{K}$ [see also (1.52)], with

$$\mathbf{K} = \begin{pmatrix} I & 0 \\ 0 & -I \end{pmatrix}. \tag{2.33}$$

In terms of the sideband operators the exact solution is written as $\hat{\mathbf{a}}^{\mathrm{out}} = \tilde{\mathbf{S}}\hat{\mathbf{a}}^{\mathrm{in}}$, where the complex symplectic matrix $\tilde{\mathbf{S}} = \boldsymbol{\Phi}_L \mathbf{S}$ is expressed through the four real parameters given by

Eqs. (2.17)-(2.20) as

$$\tilde{\mathbf{S}} = \begin{pmatrix} e^{i(\psi_L-\psi_0)}\cosh(r)\Lambda & e^{i(\psi_L+\psi_0)}\sinh(r)\Lambda P \\ e^{-i(\psi_L+\psi_0)}\sinh(r)\Lambda^* P & e^{i(\psi_0-\psi_L)}\cosh(r)\Lambda^* \end{pmatrix}, \tag{2.34}$$

where

$$\Lambda = \begin{pmatrix} e^{i\kappa} & 0 \\ 0 & e^{-i\kappa} \end{pmatrix}. \tag{2.35}$$

Equation (2.34) is the complex symplectic representation of the Bogoliubov transformation Eq. (2.15).

2.2.1 Bloch-Messiah decomposition

The Bloch-Messiah decomposition in our case consists in factorization of the symplectic matrix $\tilde{\mathbf{S}}$ in a product of three matrices [112],

$$\tilde{\mathbf{S}} = \mathbf{V}\mathbf{D}(r)\mathbf{W}^\dagger, \tag{2.36}$$

with the unitary 4×4 matrices $\mathbf{V}$ and $\mathbf{W}$ that have the following structure

$$\mathbf{V} = \begin{pmatrix} V & 0 \\ 0 & V^* \end{pmatrix}, \qquad \mathbf{W} = \begin{pmatrix} W & 0 \\ 0 & W^* \end{pmatrix}, \tag{2.37}$$

where the 2×2 matrix blocks V and W are defined as

$$V = \frac{e^{i\psi_L}}{\sqrt{2}} \begin{pmatrix} e^{i\kappa} & 0 \\ 0 & e^{-i\kappa} \end{pmatrix} \begin{pmatrix} 1 & i \\ 1 & -i \end{pmatrix}, \qquad W = \frac{e^{i\psi_0}}{\sqrt{2}} \begin{pmatrix} 1 & i \\ 1 & -i \end{pmatrix}. \tag{2.38}$$

The three characteristic angles are taken at the detuning Ω. The real 4×4 matrix $\mathbf{D}(r)$ is given by

$$\mathbf{D}(r) = \begin{pmatrix} \cosh(r)\, I & \sinh(r)\, I \\ \sinh(r)\, I & \cosh(r)\, I \end{pmatrix} = \exp\begin{pmatrix} 0 & rI \\ rI & 0 \end{pmatrix}, \tag{2.39}$$

where again r is taken at detuning Ω.

2.2.2 Squeezing eigenmodes

The Bloch-Messiah decomposition allows us to define the squeezing eigenmodes for the output field by the relation[1],

$$\begin{pmatrix} \hat{b}_c(\Omega) \\ \hat{b}_s(\Omega) \end{pmatrix} = V^\dagger \begin{pmatrix} \hat{a}(\Omega, L) \\ \hat{a}(-\Omega, L) \end{pmatrix} = \frac{e^{-i\psi_L}}{\sqrt{2}} \begin{pmatrix} \hat{a}(\Omega, L)e^{-i\kappa} + \hat{a}(-\Omega, L)e^{i\kappa} \\ -i\hat{a}(\Omega, L)e^{-i\kappa} + i\hat{a}(-\Omega, L)e^{i\kappa} \end{pmatrix}. \tag{2.40}$$

According to Eq. (2.36) the annihilation operators of these modes are expressed as

$$\begin{aligned} \hat{b}_c(\Omega) &= \cosh(r)\hat{b}_{in;c}(\Omega) + \sinh(r)\hat{b}^\dagger_{in;c}(\Omega), \\ \hat{b}_s(\Omega) &= \cosh(r)\hat{b}_{in;s}(\Omega) + \sinh(r)\hat{b}^\dagger_{in;s}(\Omega), \end{aligned} \tag{2.41}$$

via the input seed modes $\hat{b}_{in;c}(\Omega)$ and $\hat{b}_{in;s}(\Omega)$, defined as

$$\begin{pmatrix} \hat{b}_{in;c}(\Omega) \\ \hat{b}_{in;s}(\Omega) \end{pmatrix} = W^\dagger \begin{pmatrix} \hat{a}(\Omega, 0) \\ \hat{a}(-\Omega, 0) \end{pmatrix} = \frac{e^{-i\psi_0}}{\sqrt{2}} \begin{pmatrix} \hat{a}(\Omega, 0) + \hat{a}(-\Omega, 0) \\ -i\hat{a}(\Omega, 0) + i\hat{a}(-\Omega, 0) \end{pmatrix}. \tag{2.42}$$

We can see from Eq. (2.41), that the eigenmodes described by $\hat{b}_{c,s}(\Omega)$ are squeezed along the same direction in phase space with the same degree of squeezing $r(\Omega)$.

We can define the Hermitian operators for the generalized "position" and "momentum" of the squeezing eigenmodes

$$\begin{aligned} \hat{q}_{c,s}(\Omega) &= \hat{b}_{c,s}(\Omega) + \hat{b}^\dagger_{c,s}(\Omega), & \hat{p}_{c,s}(\Omega) &= -i\hat{b}_{c,s}(\Omega) + i\hat{b}^\dagger_{c,s}(\Omega), \\ \hat{q}_{in;c,s}(\Omega) &= \hat{b}_{in;c,s}(\Omega) + \hat{b}^\dagger_{in;c,s}(\Omega), & \hat{p}_{in;c,s}(\Omega) &= -i\hat{b}_{in;c,s}(\Omega) + i\hat{b}^\dagger_{in;c,s}(\Omega). \end{aligned} \tag{2.43}$$

The transformation of the operators, defined by Eq. (2.41) in the nonlinear crystal, corresponds to single-mode squeezing

$$\hat{q}_{c,s}(\Omega) = e^{r(\Omega)}\hat{q}_{in;c,s}(\Omega), \qquad \hat{p}_{c,s}(\Omega) = e^{-r(\Omega)}\hat{p}_{in;c,s}(\Omega). \tag{2.44}$$

Thus, the transformation of the operators, defined by Eq. (2.43) in the nonlinear crystal can be interpreted as modulation of quantum fluctuations in the nonlinear interaction [26]. Using the Hermitian operators (2.43) we can express the non-Hermitian quadrature operators in

[1] Note that $\hat{b}_{c,s}(\Omega)$ is defined for positive Ω only. Negative $\Omega < 0$ should not be considered for these operators as $\hat{b}_c(\Omega) = \hat{b}_c(-\Omega)$ and $\hat{b}_s(\Omega) = -\hat{b}_s(-\Omega)$, i.e., this would lead to a double coverage of the phase space. This should be kept in mind in all following calculations

Eq. (2.21) as

$$\hat{X}_1(\Omega, L) = e^{i\kappa}\frac{\hat{q}_c(\Omega) + i\hat{q}_s(\Omega)}{\sqrt{2}}, \qquad \hat{X}_2(\Omega, L) = e^{i\kappa}\frac{\hat{p}_c(\Omega) + i\hat{p}_s(\Omega)}{\sqrt{2}},$$
$$\hat{X}_1(\Omega, 0) = \frac{\hat{q}_{in;c}(\Omega) + i\hat{q}_{in;s}(\Omega)}{\sqrt{2}}, \qquad \hat{X}_2(\Omega, 0) = \frac{\hat{p}_{in;c}(\Omega) + i\hat{p}_{in;s}(\Omega)}{\sqrt{2}}. \tag{2.45}$$

We see that the quadrature operator $\hat{X}_1(\Omega, L)$ combines the position operators of two squeezing eigenmodes, while the quadrature operator $\hat{X}_2(\Omega, L)$ combines their momentum operators. If we consider a vacuum input we obtain[2]

$$\langle \Delta\hat{p}_{c,s}(\Omega)\Delta\hat{p}_{c,s}(\Omega')\rangle = \langle \hat{p}_{c,s}(\Omega)\hat{p}_{c,s}(\Omega')\rangle = s(\Omega)\delta(\Omega - \Omega'),$$
$$\langle \Delta\hat{q}_{c,s}(\Omega)\Delta\hat{q}_{c,s}(\Omega')\rangle = \langle \hat{q}_{c,s}(\Omega)\hat{q}_{c,s}(\Omega')\rangle = \frac{1}{s(\Omega)}\delta(\Omega - \Omega'). \tag{2.46}$$

Let us stress the difference between the modes described by the operators $\hat{a}(\Omega, L)$ and $\hat{a}(-\Omega, L)$ from the eigenmodes described by the operators $\hat{b}_c(\Omega)$ and $\hat{b}_s(\Omega)$: The first ones are in a *two-mode squeezed state* and, therefore, entangled, while the second ones are each in a *single-mode squeezed state* and therefore statistically independent (see also the discussion of two-mode squeezing in Sec. 1.3.5). This is the reason why we call these modes *squeezing eigenmodes*. The modal functions of the electric field operator corresponding to these squeezing eigenmodes, $f_c(t, z|\Omega)$ and $f_s(t, z|\Omega)$, are given by

$$\begin{pmatrix} f_c(t, z|\Omega) \\ f_s(t, z|\Omega) \end{pmatrix} = V^\dagger \begin{pmatrix} e^{i\Omega t} \\ e^{-i\Omega t} \end{pmatrix} \frac{e^{-i(k_0 z - \omega_0 t)}}{\sqrt{2\pi}} = \frac{e^{-i(k_0 z - \omega_0 t + \psi_L)}}{\sqrt{\pi}} \begin{pmatrix} \cos\left[(\Omega - \kappa)t\right] \\ \sin\left[(\Omega - \kappa)t\right] \end{pmatrix}. \tag{2.47}$$

The spectral profiles of these modes include two delta-functions at the frequencies $\omega_0 - \Omega$ and $\omega_0 + \Omega$. Thus, the squeezing eigenmodes are bichromatic. We note that the modal functions, Eq. (2.47), are the functions of time t and the longitudinal coordinate z, while the frequency Ω and the indices c, s serve as the mode markers, equivalent to an integer index in the case of discrete modes.

In conclusion, we have defined the squeezing eigenmodes and demonstrated that the group delay dispersion parameter $\kappa(\Omega)$ and the squeezing angle $\psi_L(\Omega)$ define the modal functions in which single mode squeezing is present, while the squeezing parameter $r(\Omega)$ determines the degree of squeezing. The last parameter $\psi_0(\Omega)$ defines the modal functions of the input seed modes

$$\begin{pmatrix} f_{in;c}(t, z|\Omega) \\ f_{in;s}(t, z|\Omega) \end{pmatrix} = W^\dagger \begin{pmatrix} e^{i\Omega t} \\ e^{-i\Omega t} \end{pmatrix} \frac{e^{-i(k_0 z - \omega_0 t)}}{\sqrt{2\pi}} = \frac{e^{-i(k_0 z - \omega_0 t + \psi_0)}}{\sqrt{\pi}} \begin{pmatrix} \cos\left(\Omega t\right) \\ \sin\left(\Omega t\right) \end{pmatrix}. \tag{2.48}$$

[2]Here, we use the standard notation $\Delta\hat{q}_{c,s}(\Omega) = \hat{q}_{c,s}(\Omega) - \langle\hat{q}_{c,s}(\Omega)\rangle$ and $\Delta\hat{p}_{c,s}(\Omega) = \hat{p}_{c,s}(\Omega) - \langle\hat{p}_{c,s}(\Omega)\rangle$.

Seeding the PDC process with a quantum state in the $f_{in;c}(t,z|\Omega)(f_{in;s}(t,z|\Omega))$ field mode will yield the corresponding squeezed sate in the $f_c(t,z|\Omega)(f_s(t,z|\Omega))$ field mode at the output of the nonlinear crystal. Thus, knowledge of the modal functions of the input seed modes (2.48) provides for the deliberate preparation of quantum states that are squeezed at the output of the nonlinear crystal. In the following we will analyze how these parameters are affected by ordering effects in different order of MA.

2.3 Approximations in terms of the Magnus expansion

The monochromatic pump case is the only case of pump configuration in PDC where we have access to an analytical solution. Thus, it can serve as an important case to benchmark the quality of approximation in PDC in terms of the ME. In analogy to (1.99) we can represent the solution of (2.29) as

$$\mathbf{S} = \exp\left(-i\mathbf{M}\right), \qquad -i\mathbf{M} = \sum_{\ell=1}^{\infty} (-i)^{\ell}\, \mathbf{M}_{\ell}, \tag{2.49}$$

where the longitudinal coordinate z takes the role of the time parameter in the perturbative expansion (cf. Sec.1.4.3). As the crystal length is usually a fixed parameter we also omit the length L as a parameter. The first three terms in Eq. (2.49) are

$$\mathbf{M}_1 = \int_0^L dz\, \mathbf{F}(z), \tag{2.50}$$

$$\mathbf{M}_2 = \frac{1}{2}\int_0^L dz_1 \int_0^{z_1} dz_2\, [\mathbf{F}(z_1), \mathbf{F}(z_2)], \tag{2.51}$$

$$\mathbf{M}_3 = \frac{1}{6}\int_0^L dz_1 \int_0^{z_1} dz_2 \int_0^{z_2} dz_3\, \left\{[\mathbf{F}(z_1), [\mathbf{F}(z_2), \mathbf{F}(z_3)]] + [\mathbf{F}(z_3), [\mathbf{F}(z_2), \mathbf{F}(z_1)]]\right\}. \tag{2.52}$$

By keeping the first k terms in the ME given by (2.49), we obtain an approximation, i.e., the MA of the kth order

$$\mathbf{S}_k = \exp\left\{\sum_{\ell=1}^{k} (-i)^{\ell}\, \mathbf{M}_{\ell}\right\}. \tag{2.53}$$

A remarkable property of this approximation in the context of PDC is the symplectic structure of the approximate transformation matrix $\mathbf{S}_k$ for any k. That the symplectic structure remains preserved follows from the Lie algebra structure of operators quadratic in annihilation creation operators. This property of $\mathbf{S}_k$ implies conservation of the commutation relations

for the creation and annihilation operators of the field for each order k. This feature of the MA represents a great advantage as compared to other approximate methods such as, e.g., the Dyson expansion (see also Sec. 1.4.1). In particular, it will guarantee that for a coherent input state to the PDC process the output state for each order k of the MA will be a squeezed coherent state with the respective four real parameters defined above.

Therefore, for each order k of the MA we shall define a respective symplectic matrix $\tilde{\mathbf{S}}_k = \mathbf{\Phi}_L \mathbf{S}_k$, for the transformation of the sideband operators, which can be parameterized by four real parameters $\{r_k(\Omega), \psi_{L,k}(\Omega), \psi_{0,k}(\Omega), \kappa_k(\Omega)\}$, similarly to the parametrization of the exact solution in Eq. (2.34).

By the sufficient criterion (1.101) in terms of the spectral norm $\|\cdots\|_2$ we can guarantee convergence as long as

$$\int_0^L dz \|\mathbf{F}(z)\|_2 < \pi. \tag{2.54}$$

From Eq. (2.30), we find that the maximal eigenvalue of $\mathbf{F}(z)^\dagger \mathbf{F}(z)$ is $|\sigma|^2$ and, therefore, $\|\mathbf{F}(z)\|_2 = |\sigma|$. This value provides the upper bound of Eq. (2.54) as $g = \pi$, corresponding to 27 dB of maximum squeezing. In reality, such a degree of squeezing would require the exceedingly high pump intensity and would invalidate the undepleted-pump approximation of our model. The record value of squeezing in the cw regime at present is 15 dB [42]. Even if the limit of 27 dB for squeezing does not seem to be attainable experimentally in the near future, the theory allows us to use this value as the limit of convergence of the ME.

The first-order MA is obtained by keeping only the term $\mathbf{M}_1$ in Eq. (2.49), which is equivalent to neglecting the z-ordering in the z-ordered exponent $\mathbf{S} = \mathcal{T} \exp\left(-i \int_0^L dz\, \mathbf{F}(z)\right)$. Substituting Eq. (2.30) into Eq. (2.50), and performing the integration we obtain

$$-i\mathbf{M}_1 = \begin{pmatrix} 0 & b_1 e^{i(\varphi+\theta)} P \\ b_1 e^{-i(\varphi+\theta)} P & 0 \end{pmatrix}, \tag{2.55}$$

where $b_1 = g\,\mathrm{sinc}(\theta)$. Evaluating the exponent of Eq. (2.55) in terms of its power series and summing up even and odd powers separately, we arrive at

$$\mathbf{S}_1 = e^{-i\mathbf{M}_1} = \begin{pmatrix} I\cosh(b_1) & P e^{i(\varphi+\theta)} \sinh(b_1) \\ P e^{-i(\varphi+\theta)} \sinh(b_1) & I\cosh(b_1) \end{pmatrix}. \tag{2.56}$$

The symplectic matrix $\mathbf{S}_1$ determines the transformation of the slowly-varying amplitudes $\hat{\boldsymbol{\xi}}(z)$. Passing to the symplectic matrix $\tilde{\mathbf{S}}_1$ for the sideband operators $\hat{\mathbf{a}}(z)$ yields

$$\tilde{\mathbf{S}}_1 = \begin{pmatrix} e^{-i\theta}\Lambda\cosh(b_1) & \Lambda P e^{i\varphi}\sinh(b_1) \\ \Lambda^* P e^{-i\varphi}\sinh(b_1) & e^{i\theta}\Lambda^*\cosh(b_1) \end{pmatrix}. \tag{2.57}$$

Comparing Eq. (2.57) with Eq. (2.34), we conclude that in the first-order MA the parameter $\kappa(\Omega)$ is the same as in the exact solution and that the relation $\psi_{0,1}(\Omega) = \varphi - \psi_{L,1}(\Omega)$ holds as well. As for the other two parameters, characterizing the Bogoliubov transformation, they are different,

$$r_1(\Omega) = g|\mathrm{sinc}(\theta)|, \tag{2.58}$$

$$\psi_{L,1}(\Omega) = \frac{1}{2}(\varphi - \theta) + \frac{1}{2}\arg[\mathrm{sinc}(\theta)]. \tag{2.59}$$

We remind that the phase-mismatch angle $\theta(\Omega)$ is a function of the frequency Ω, as defined in Sec. 2.1.

In the second-order MA we keep the two first terms $\mathbf{M}_1$ and $\mathbf{M}_2$ in Eq. (2.49). For calculating the second term $\mathbf{M}_2$ we evaluate the commutator

$$[\mathbf{F}(z_1), \mathbf{F}(z_2)] = 2i|\sigma|^2 \sin\left(\Delta(\Omega)(z_2 - z_1)\right)\mathbf{K}. \tag{2.60}$$

Subsequently integrating the commutator according to Eq. (2.51), we obtain

$$\mathbf{M}_2 = \frac{g^2}{2i}\left[j_0(\theta)\sin(\theta) - j_1(\theta)\cos(\theta)\right]\mathbf{K}. \tag{2.61}$$

Here, $j_m(\theta)$ are the spherical Bessel functions, i.e., $j_0(\theta) = \mathrm{sinc}(\theta)$, $j_1(\theta) = [\mathrm{sinc}(\theta) - \cos(\theta)]/\theta$, etc.

Evaluating the exponent of $-i\mathbf{M}_1 - \mathbf{M}_2$ and multiplying the result by $\mathbf{\Phi}_L$ we obtain the second-order approximation of the symplectic matrix

$$\tilde{\mathbf{S}}_2 = \begin{pmatrix} U_2 & V_2 \\ V_2^* & U_2^* \end{pmatrix}, \tag{2.62}$$

where the 2×2 matrix blocks U_2 and V_2 are defined as

$$U_2 = \Lambda e^{-i\theta}\left(\cosh(\gamma_2) + \frac{ia_2}{\gamma_2}\sinh(\gamma_2)\right), \qquad V_2 = \Lambda P e^{i\varphi}\frac{b_2}{\gamma_2}\sinh(\gamma_2), \tag{2.63}$$

with Λ as defined in Eq. (2.35) and

$$a_2 = \frac{g^2}{2}\left[j_0(\theta)\sin(\theta) - j_1(\theta)\cos(\theta)\right], \qquad b_2 = g j_0(\theta),$$
$$\gamma_2 = \sqrt{b_2^2 - a_2^2}. \tag{2.64}$$

We observe from Eq. (2.63) that the phase of V_2 is equal to φ and that γ_2 may become imaginary if $|a_2| > |b_2|$, but $\sinh(\gamma_2)/\gamma_2$ is always real. Therefore, the relation $\psi_{0,2}(\Omega) = \varphi - \psi_{L,2}(\Omega)$ holds in the second-order approximation as well. Comparing Eq. (2.62) with Eq. (2.34), we also conclude that the parameter κ in the second-order approximation is that of the exact solution, $\kappa_2(\Omega) = \kappa(\Omega)$. The two remaining parameters read as

$$r_2(\Omega) = \ln\left\{\left|\cosh(\gamma_2) + \frac{i a_2}{\gamma_2}\sinh(\gamma_2)\right| + \left|\frac{b_2}{\gamma_2}\sinh(\gamma_2)\right|\right\},$$
$$\psi_{L,2}(\Omega) = \frac{\varphi}{2} - \frac{\theta}{2} + \frac{1}{2}\arg\left[\cosh(\gamma_2) + \frac{i a_2}{\gamma_2}\sinh(\gamma_2)\right] + \frac{1}{2}\arg(b_2) + \frac{1}{2}\arg\left[\frac{\sinh(\gamma_2)}{\gamma_2}\right]. \tag{2.65}$$

In the third-order MA we keep the first three terms $\mathbf{M}_1$, $\mathbf{M}_2$, and $\mathbf{M}_3$ in Eq. (2.49). After evaluating the corresponding commutators and performing the integration, we obtain

$$\mathbf{M}_3 = \frac{g^3}{6i}\left[j_0(\theta) + j_2(\theta) - j_0^3(\theta)\right]\begin{pmatrix} 0 & e^{i(\varphi+\theta)}P \\ e^{-i(\varphi+\theta)}P & 0 \end{pmatrix}, \tag{2.66}$$

and

$$\tilde{\mathbf{S}}_3 = \begin{pmatrix} U_3 & V_3 \\ V_3^* & U_3^* \end{pmatrix}, \tag{2.67}$$

with the 2×2 matrix blocks U_3 and V_3 defined as

$$U_3 = \Lambda e^{-i\theta}\left(\cosh(\gamma_3) + \frac{i a_3}{\gamma_3}\sinh(\gamma_3)\right), \qquad V_3 = \Lambda P e^{i\varphi}\frac{b_3}{\gamma_3}\sinh(\gamma_3), \tag{2.68}$$

where

$$a_3 = \frac{g^2}{2}\left[j_0(\theta)\sin(\theta) - j_1(\theta)\cos(\theta)\right], \qquad b_3 = g j_0(\theta) + \frac{g^3}{6}\left[j_0(\theta) + j_2(\theta) - j_0^3(\theta)\right],$$
$$\gamma_3 = \sqrt{b_3^2 - a_3^2}. \tag{2.69}$$

We observe that the relations $\psi_{0,3}(\Omega) = \varphi - \psi_{L,3}(\Omega)$, $\kappa_3(\Omega) = \kappa(\Omega)$ hold in the third-order approximation as well, and that the other two parameters are given by equations, similar to Eqs. (2.65). We remind that the corrections of the MA higher than the first-order are due to

non-zero commutators of the matrix $\mathbf{F}(z)$ with itself at different points z. Thus, deviations from the first-order MA are the manifestations of this non-commutativity, i.e., ordering effects.

2.3.1 Comparison of Magnus approximations

With the closed form expressions for the MAs above, we can benchmark the quality of approximation with respect to the exact solution. This is of particular interest with respect to the analysis in the subsequent chapter, where we allow for non-monochromatic pumps and no such exact solution exists. The monochromatic pump model can be obtained as a limit case of the broad spectral (i.e., non-monochromatic) pump model, in the limit of vanishing pump widths. It can thus be expected, that observations made on the quality of approximation remain qualitatively valid for the case of broadband pumps. Moreover, as we have shown above, do ordering effects manifest themselves in modifications of the spectrum of squeezing $s(\Omega)$ and the angle of squeezing $\psi_L(\Omega)$. This allows for a convenient visualization of the quality of MAs in terms of these two parameters.

In Fig. 2.3 we compare the frequency dependence of the spectrum of squeezing $s(\Omega)$ and the angle of squeezing $\psi_L(\Omega)$ for the exact solution, obtained in Sec. 2.1, and the three first orders of MA at three different orders of gain $g = 0.7, 1.8, 3$, corresponding to 6, 16, and 26 dB of maximum squeezing obtained for perfect phase matching, respectively. Since frequency enters only via the phase-mismatch angle $\theta(\Omega)$, we use this angle as abscissa for the figures. We assume that the phase of the pump is chosen so that $\varphi = 0$. We remind the reader that the angle in Figs. 2.3b, 2.3d, and 2.3f is the continuous version of the angle of squeezing, as discussed in Sec. 2.1.

At the lowest considered gain ($g = 0.7$ =6 dB) in Fig. 2.3a and Fig. 2.3b all three approximations coincide and reproduce the exact behavior. Thus, here a first-order MA would suffice and one can consider this a low-gain regime. However, note that with a maximum squeezing of 6 dB we are already in a regime that exceeds a single photon interpretation .

Figure 2.3c illustrates that the first-order MA for the considered gain ($g = 1.8$ =16 dB) gives rather poor approximation for the exact solution. Moreover, the second-order approximation does not improve this difference, and only in the third-order the approximate solution approaches the exact one. With the angle of squeezing, shown in Fig. 2.3d, the situation is different: it is also rather far from the exact solution in the first approximation, but becomes much closer to the exact one already in the second-order approximation. Thus, for a monochromatic pump the even orders of the ME mainly correct the angle of squeezing, while the odd orders mainly correct the degree of squeezing. We may conjecture that this behavior is applicable for higher orders as well and generally for the non-monochromatic pump.

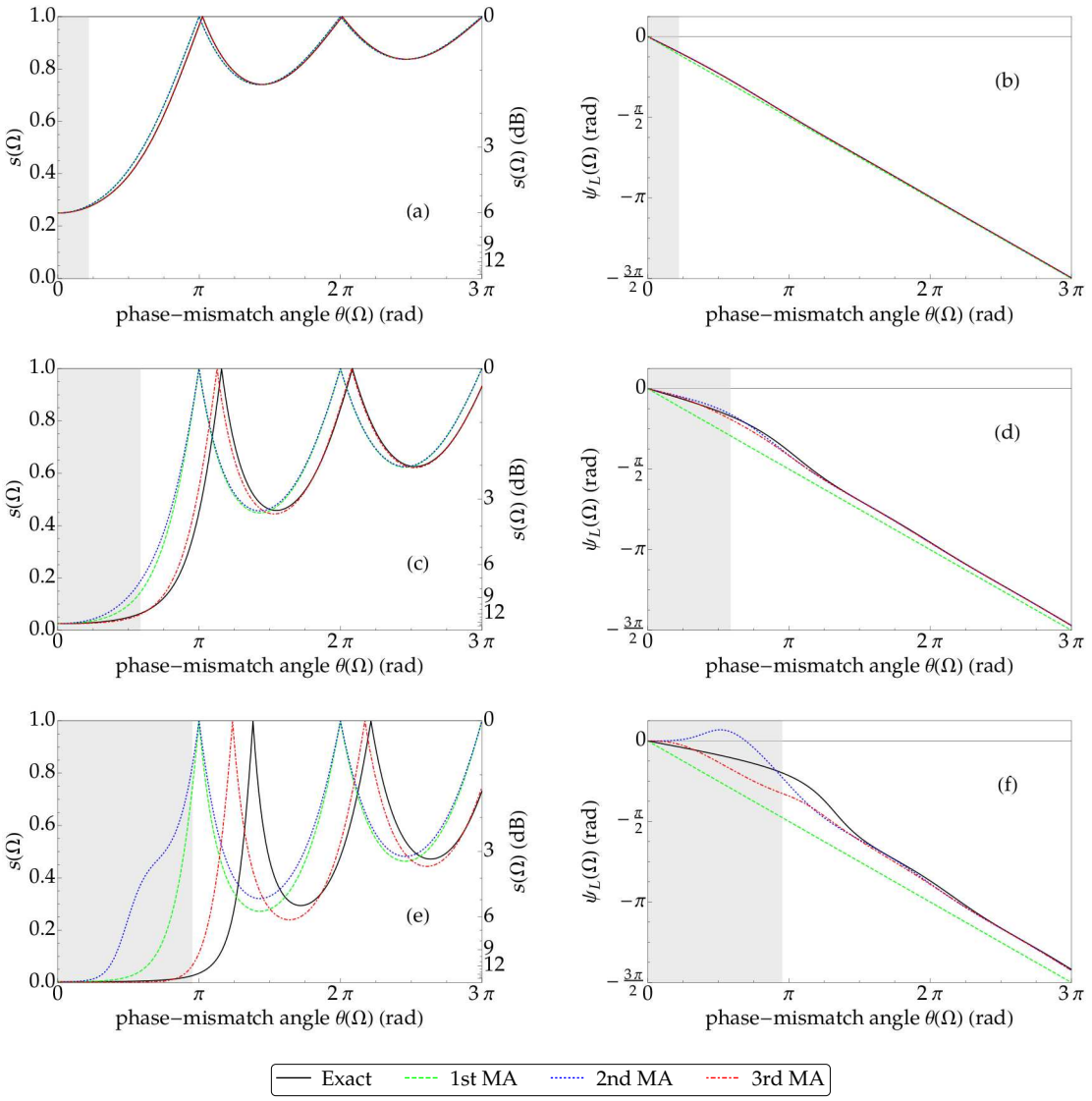

Figure 2.3: The squeezing spectrum s_k (a,c,e) and the squeezing angle $\psi_{L,k}$ (b,d,f) for the first order $k = 1$ (green, dashed), second order $k = 2$ (blue, dotted), and third order $k = 3$ (red, dot-dashed) MA compared to the exact solution $k = 0$ (black, solid) at $g = 0.7 = 6\,\mathrm{dB}$ (a&b), $g = 1.8 = 16\,\mathrm{dB}$ (c&d), and $g = 3 = 26\,\mathrm{dB}$ (e&f). Figure as presented in Ref. [58]; here we have additionally illustrated the band where Γ by a gray area.

Lastly, we may turn our attention to the highest considered gain ($g = 3$ =26 dB) in Fig. 2.3e and 2.3f. Here we can see that the first three orders of MA fail to reproduce the exact behavior. However, the approximation seems to improve for larger phase-mismatch angles. Indeed, for frequencies Ω where $\Delta(\Omega) \to \pm\infty$, we can easily find $r, r_k \to 0$, $\psi_L, \psi_{L,k} \to \psi_{L,1}$, i.e., these parameters coincide with those of the exact solution at $\Delta(\Omega) \to \pm\infty$. Correspondingly, for the frequencies Ω of the perfect phase matching, where $\Delta(\Omega) = 0$, one can easily find $r_k = g = r$ and $\psi_{L,k} = \psi_L$. This asymptotic behavior at $\Omega = 0$ and $\Omega \to \pm\infty$ is illustrated in Fig. 2.4. Thus, for PDC any order of approximation will yield the correct limiting behavior [24], which can be considered an advantage of this approximation method.

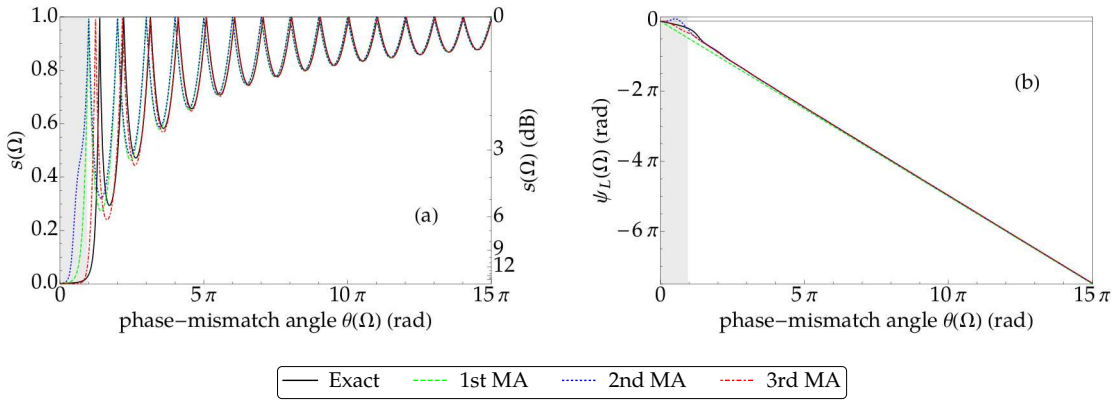

Figure 2.4: The squeezing spectrum s_k (a) and the squeezing angle $\psi_{L,k}$ at $g = 3 = 26\,\mathrm{dB}$ (b) for the first order $k = 1$ (green, dashed), second order $k = 2$ (blue, dotted), and third order $k = 3$ (red, dot-dashed) MA compared to the exact solution $k = 0$ (black, solid) for a wide range of the phase mismatch-angles θ. Figure as presented in Ref. [58]; here we have additionally illustrated the band where Γ is real by a gray area.

2.3.2 Generic estimate for the applicability of the first-order approximation

It should be noted that a significant difference between the exact solution and the first-order MA appears only for rather high values of the gain exponent g. For $g < 1.15$, corresponding to squeezing below 10 dB, this difference is hardly visible. Thus, the first-order MA can be effectively used in the regimes of the high-gain PDC where the maximal degree of squeezing is below a certain value. Above this limit the first-order approximation is not valid, and the higher orders of MA should be taken into account. We shall call a regime of PDC above this limit of squeezing *ultra-high-gain* PDC. The boundary for this regime depends on the acceptable error in the degree of squeezing. One possibility for giving such a definition is related to the distance between the first zeros of the degree of squeezing in the exact solution $r(\Omega)$ and its first-order approximation $r_1(\Omega)$, corresponding to the points $s(\Omega) = 1$ in Fig. 2.3. It follows from Eq. (2.17) that the first zero of $r(\Omega)$ corresponds to the frequency where $B(\Omega) = 0$. From Eq. (2.14), we find that this is the frequency where $\Gamma L = i\pi$ or $\theta = \sqrt{g^2 + \pi^2} = \theta_0$. From Eq. (2.58), we obtain the first zero of $r_1(\Omega)$ as $\theta_1 = \pi$. The relative distance can be defined as $d = (\theta_0 - \theta_1)/\theta_1 = \sqrt{(g/\pi)^2 + 1} - 1$. For tolerable relative distance of 10% we have $g \leq 1.44$, which corresponds to 12.5 dB of maximal squeezing. Thus, for PDC with a monochromatic pump we can accept the value of 12.5 dB of maximal squeezing as the boundary between the high-gain and the ultra-high-gain regimes. The numerical study of Ref. [16] shows that for pulsed PDC this boundary is about 12 dB of squeezing, which is compatible with our analytical result. In Chapter. 5 we will take a more detailed look at the convergence of the MA.

2.3.3 Homodyne detection of down-converted light

To see the impact of time ordering corrections in a measurement context let us consider the scenario in which broadband squeezed light from PDC is usually observed: Balanced homodyne detection (cf. [2]). In this measurement scheme a strong local oscillator field $E_{\mathrm{LO}}^{(+)}(t,z)$ is is mixed on a $50{:}50$ beam splitter with the measured field $\hat{E}^{(+)}(t,z)$. The corresponding beam splitter transformation can be written as

$$\begin{pmatrix}\hat{E}_1^{(+)}(t)\\ \hat{E}_2^{(+)}(t)\end{pmatrix} = \frac{1}{\sqrt{2}}\begin{pmatrix}1 & 1\\ -1 & 1\end{pmatrix}\begin{pmatrix}\hat{E}^{(+)}(t,L)\\ E_{\mathrm{LO}}^{(+)}(t,L)\end{pmatrix}. \tag{2.70}$$

The intensity of the two output beams are detected by photodetectors of equal quantum efficiency, η, and the observed quantity is the difference photocurrent collected from two photodetectors, which we simply call *photocurrent* and denote $\hat{i}(t)$. For simplicity we limit all our studies to vacuum input, i.e., the measured state is a squeezed vacuum. In that case the mean value $\langle\hat{i}(t)\rangle$ is zero [26] and we write the experimentally observed quantity of photocurrent fluctuation $\delta\hat{i}(t) = \hat{i}(t) - \langle\hat{i}(t)\rangle$ as

$$\delta\hat{i}(t) = \eta\left[\hat{E}_1^{(-)}(t)\hat{E}_1^{(+)}(t) - \hat{E}_2^{(-)}(t)\hat{E}_2^{(+)}(t)\right] = \eta E_{\mathrm{LO}}^{(-)}(t,L)\hat{E}^{(+)}(t,L) + \text{H.c.}. \tag{2.71}$$

If we consider the local oscillator as as a monochromatic field at the carrier frequency of the down-converted light $E_{\mathrm{LO}}^{(+)}(t,z) = \mathcal{E}_0 e^{i[k_0 z - \omega_0 t]}$, with $\mathcal{E}_0 = |\mathcal{E}_0|e^{i\beta}$, the autocorrelation function of photocurrent fluctuation for vacuum input reads as

$$\frac{1}{\eta^2}\langle\delta\hat{i}(t)\delta\hat{i}(t-\tau)\rangle = |\mathcal{E}_0|^2\delta(t-t') + |\mathcal{E}_0|^2\int\frac{d\Omega}{\sqrt{2\pi}}e^{-i\Omega t}\int\frac{d\Omega'}{\sqrt{2\pi}}e^{-i\Omega' t')\tau}\langle{:}\hat{X}(\Omega,L)\hat{X}(\Omega',L){:}\rangle, \tag{2.72}$$

where colons $:\cdots:$ denote the normal ordering prescription and

$$\begin{aligned}\hat{X}(\Omega,L) &= e^{-i\beta}\hat{a}(\Omega,L) + e^{i\beta}\hat{a}^\dagger(-\Omega,L)\\ &= \hat{X}_1(\Omega,L)\cos[\psi_L(\Omega)-\beta] - \hat{X}_2(\Omega,L)\cos[\psi_L(\Omega)-\beta].\end{aligned} \tag{2.73}$$

is the Fourier transform of the measured field quadrature. The first term on the right-hand side of Eq. (2.72) represents the shot noise, while the second one is proportional to the autocorrelation function of the normally ordered measured field quadrature.

Note, that the down-converted field is stationary in time and thus the autocorrelation function $\langle\delta\hat{i}(t)\hat{i}(t')\rangle$ only depends of the difference of times $\tau = t - t'$. The Fourier transform over

this time-difference τ defines the the photocurrent spectral density [98]

$$(\delta i)^2_\Omega = \int d\tau e^{i\Omega\tau} \langle \delta\hat{i}(t)\delta\hat{i}(t')\rangle, \tag{2.74}$$

which for the considered case of vacuum input evaluates to [24]

$$(\delta i)^2_\Omega = \eta^2|\mathcal{E}_0|^2 \left[e^{2r(\Omega)}\cos^2(\psi_L(\Omega)-\beta) + e^{-2r(\Omega)}\sin^2(\psi_L(\Omega)-\beta)\right], \tag{2.75}$$

where $\beta = \arg(\mathcal{E}_0)$ is the phase of the local oscillator. The effect of squeezing manifests itself as reduction of the fluctuations of photocurrent below the shot-noise level $|\mathcal{E}_0|^2$ for particular choice of the phase of the local oscillator. The photon flux of the strong local oscillator is accepted to be much higher than that of the measured field, $|\mathcal{E}_0|^2 \ll \langle \hat{E}^{(-)}(t,L)\hat{E}^{(+)}(t,L)\rangle$ such that for unit quantum efficiency the shot noise level can be obtained from the mean sum of photocurrents of the two detectors $\langle i_+\rangle = \eta|\mathcal{E}_0|^2$.

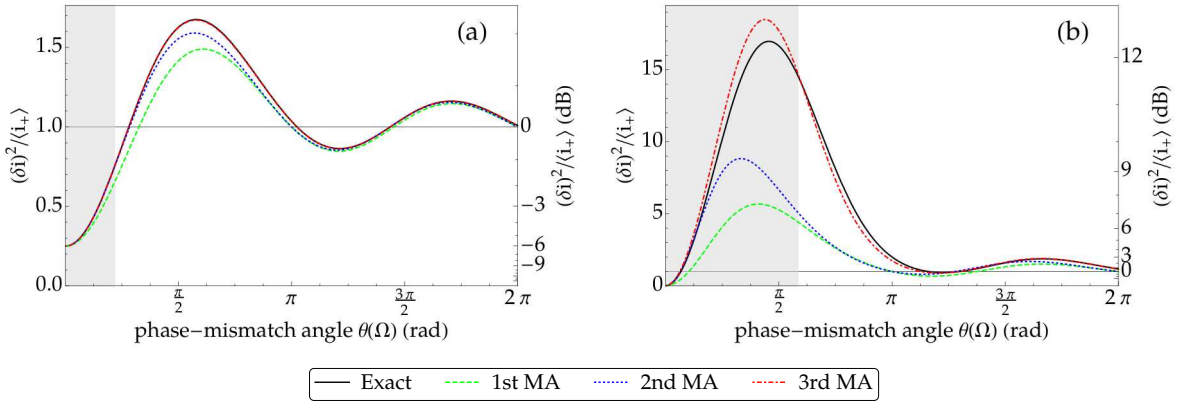

Figure 2.5: The normalized photocurrent noise spectrum for balanced homodyne detection of the down-converted light obtained from exact solution and three first orders of the MA. The gain exponents are chosen as (a) $g = 0.7$, corresponding to 6 dB of the maximal squeezing and (b) $g = 1.84$, corresponding to 16 dB of the maximal squeezing. The gray area indicates the band, where Γ is real. Perfect quantum efficiency, $\eta = 1$, is considered. Figure as presented in Ref. [24].

It is, very interesting to see the effect of different orders of the MA on the experimentally observable quantity (2.75). We assume perfect quantum efficiency, such that $\langle i_+\rangle = |\mathcal{E}_0|^2$. Then, assuming that β can be chosen such that $\psi_L(\Omega) - \beta = \pi/2$ for the frequency Ω of perfect phase matching, where $\theta(\Omega) = 0$ and squeezing is maximal, we can obtain the normalized photocurrent noise spectrum,

$$(\delta i)^2_\Omega/\langle i_+\rangle = \left[e^{2r(\Omega)}\sin^2[\psi_L(\Omega)] + e^{-2r(\Omega)}\cos^2[\psi_L(\Omega)]\right]. \tag{2.76}$$

In Fig. 2.5 we present the normalized photocurrent noise spectrum for two different values of g, corresponding to moderate and high degree of squeezing. We can observe that for moderate levels of squeezing shown in Fig. 2.5a the deviation of all three orders of MA from the exact solution remains tolerable, while for the high level of squeezing in Fig. 2.5b only the third-

order MA gives a tolerable approximation for the exact solution. The physical origin of this effect can be explained as follows: For high level of squeezing the photocurrent noise spectrum becomes much more sensitive to the errors in the squeezing angle in the corresponding order of the MA. This errors are responsible for the contribution into the photocurrent noise from the stretched component of the broadband squeezed state.

2.3.4 Dependence on the gain exponent

In the previous subsections we have considered the dependence of the degree of squeezing $r(\Omega)$, the angle of squeezing $\psi_L(\Omega)$, and the photocurrent noise spectrum on the frequency Ω for fixed gain exponent g. In this subsection we use a complementary approach and consider the dependence of the degree of squeezing against the gain exponent g, $r(g)$, for a fixed frequency Ω. The simplest case is for the frequency of the perfect phase matching, $\Delta(\Omega) = 0$, where we have for the exact solution and for all orders of MA, $r(g) = g$, i. e. a linear dependence on g and, therefore, on the pump amplitude. It is remarkable, that this linearity is preserved in the first-order MA, as follows from from Eq. (2.58).

In Fig. 2.6 we present the gain dependence of the degree of squeezing for non-zero phase mismatch, $\Delta(\Omega) \neq 0$. One can observe a nonlinear dependence of $r(g)$ against g in the exact solution and a linear one in the first-order MA. Since the difference between the first-order MA and the exact solution is negligible for g below the boundary of the ultra-high-gain, we conclude that deviations from linearity in the dependence of $r(g)$ can serve as a signature of the ultra-high-gain regime. One can also appreciate that the third-order MA improves the conversion towards the exact solution as compared with the the second-order MA in the gray area. Above the value of $g = \pi$ the convergence of the ME is not guaranteed by the sufficient criterion (2.54).

The dependence of the degree of squeezing on g shown in Fig. 2.6 can be easily measured experimentally, since the gain exponent g is proportional to the amplitude of the pump wave. A deviation from the linear dependence can be observed as difference of the parametric gain for non-zero phase mismatch from the behavior given by $\mu \sinh(\nu E_p)$, where E_p is the pump amplitude, and μ and ν are some fitting parameters. Let us mention here that for aperiodically poled crystals this dependence is different even below the ultra-high-gain regime, and has been recently observed in the experiment [45].

For better understanding the dependence of the degree of squeezing $r(\Omega)$ and its respective ℓth order MAs $r_\ell(\Omega)$ on g, we perform the Taylor expansions of $r_\ell(\Omega)$ in g,

$$r_\ell(\Omega) = \sum_{k=1}^{\infty} r_\ell^{[k]}(\Omega) \frac{g^k}{k!}. \tag{2.77}$$

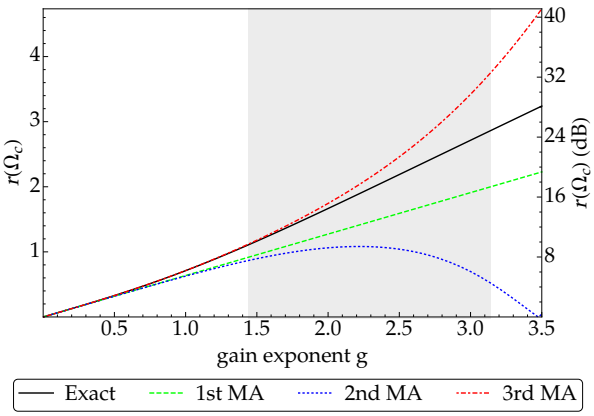

Figure 2.6: The degree of squeezing $r(\Omega_c)$ as function of gain exponent g for $\Delta(\Omega) \neq 0$. The frequency Ω_c is chosen so that $\Delta(\Omega_c)L = \pi$. Four curves correspond to the exact solution r (black, solid), the first-order MA r_1 (green, solid), the second-order MA r_2 (blue, dashed), and the third-order MA r_3 (red, dotted). The gray area indicates the region of the ultra-high gain, from $g = 1.44$ to $g = \pi$ (12.5 to 27 dB of squeezing). Above $g = \pi$ the convergence of the ME is not guaranteed. Figure as presented in Ref. [24].

The analytical expressions for the Taylor coefficients in Eq. (2.77) up to the 4-th order are given in Tab. 2.1. As follows from this Table, the correct value of the first-order Taylor coefficient

k	$r^{[k]}(\Omega)$	$r_1^{[k]}(\Omega)$	$r_2^{[k]}(\Omega)$	$r_3^{[k]}(\Omega)$
1	$j_0(\theta)$	$j_0(\theta)$	$j_0(\theta)$	$j_0(\theta)$
2	0	0	0	0
3	$j_0(\theta) - j_0^3(\theta) + j_2(\theta)$	0	0	$j_0(\theta) - j_0^3(\theta) + j_2(\theta)$
4	0	0	0	0

Table 2.1: The Taylor coefficients for the degree of squeezing $r(\Omega)$ and its MAs up to 4th order in the gain exponent g. We remind that $\theta(\Omega) = \Delta(\Omega)L/2$.

$r_1^{[1]}(\Omega) = r^{[1]}(\Omega)$ appears in the first-order MA. The second-order Taylor coefficient for $r(\Omega)$ vanishes, since the latter is an odd function of g. As a result, the second-order MA makes no correction to the degree of squeezing in the second order of g. This observation corroborates the result of Ref. [19], where the authors have predicted that for PDC with vacuum input the second-order MA provides no correction in the second order in g. The third-order MA gives the correct value of the third-order Taylor coefficient $r_3^{[3]}(\Omega) = r^{[3]}(\Omega)$. It can be speculated that the correct value for the kth Taylor coefficient appears in the kth order of the ME.

A similar decomposition can be written for the angle of squeezing $\psi_L(\Omega)$,

$$\psi_{L,\ell}(\Omega) = \sum_{k=0}^{\infty} \psi_{L,\ell}^{[k]}(\Omega) \frac{g^k}{k!}, \tag{2.78}$$

with the corresponding coefficients shown in Tab. 2.2.

k	$\psi_L^{[k]}(\Omega)$	$\psi_{L,1}^{[k]}(\Omega)$	$\psi_{L,2}^{[k]}(\Omega)$	$\psi_{L,3}^{[k]}(\Omega)$
0	$\frac{1}{2}(\varphi-\theta)$	$\frac{1}{2}(\varphi-\theta)$	$\frac{1}{2}(\varphi-\theta)$	$\frac{1}{2}(\varphi-\theta)$
1	0	0	0	0
2	$\zeta(\theta)$	0	$\zeta(\theta)$	$\zeta(\theta)$
3	0	0	0	0

Table 2.2: The Taylor coefficients for the angle of squeezing $\psi_L(\Omega)$ and its approximations up to 3-rd order in the gain exponent g. We have introduced a shortcut $\zeta(\theta)=\frac{1}{2}(\sin(\theta)j_0(\theta)-\cos(\theta)j_1(\theta))$.

From Table 2.2, we conclude that for the angle of squeezing the correct value of the kth Taylor coefficient is given by the kth and above orders of the MA, at least for the first 4 orders. It can be speculated that this dependence holds as well for the higher orders of the ME.

Chapter 3

Parametric down-conversion with a non-monochromatic pump

Contents

We now turn our attention to scenario of increased complexity compared to that of type-I PDC with a monochromatic pump as discussed in chapter 2: The process of type-I PDC with a broad spectral pump. As we will see, in the case where one considers a broad spectral (i.e., non-monochromatic) pump, we are no longer able to find analytical solutions to the evolution equation within the $\chi^{(2)}$ crystal. Thus, the ME becomes itself a tool for the description of the system. For broad spectral pumps a multitude of frequencies couple in the interaction and thus, eigenmodes of squeezing attain complex spectral structures, i.e., frequency eigenmodes [112]. The most exciting application of such pulses containing a multitude of squeezing eigenmodes may be one-way quantum computation protocols (cf. [37]).

Here the ME can yield useful intuition on how the scenario changes at high gain. In Ref. [16] it has been shown that for the process of broad spectral PDC ordering effect become relevant at high pump gain and impact the shape of squeezing eigenmodes. In this reference the first-order MA – in the form of a Dyson series with neglected ordering – has been compared to numerical solutions of the evolution equations and ordering corrections have not been considered explicitly. In Ref. [19] the methods of MA have been applied to the type-II PDC process.

However, the Bloch-Messiah decomposition and the resulting eigenmodes of squeezing where not considered explicitly therein.

3.1 The model

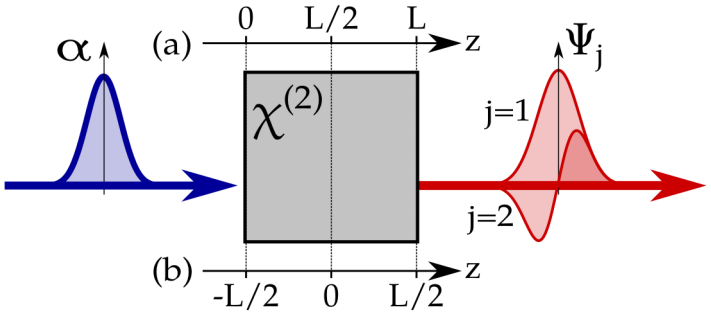

Figure 3.1: Illustration of the PDC process with broad spectral pumps. The pump pulse (blue) enters the crystal and the down converted light (red) is generated in a multitude of pulse modes Ψ_j. The spatial coordinates are chosen such that the z-axis is taken along the propagation direction of the pump in the crystal. Two different coordinate systems are considered, one where the input surface lays at $z = 0$ (a) and one where the input surface lays at $z = -L/2$ (b).

We consider the scenario of the type-I PDC process with a non-monochromatic plane-wave pump in a crystal of length L as illustrated in Fig. 3.1. As in the case of monochromatic PDC, the positive-frequency operator $\hat{E}^{(+)}(t,z)$ of the down converted light normalized to photon-flux units can be decomposed into Fourier components as

$$\hat{E}^{(+)}(t,z) = \int \frac{d\Omega}{\sqrt{2\pi}} e^{i[k_0 z - (\omega_0+\Omega)t]} \hat{a}(\Omega,z), \tag{3.1}$$

where again $\omega_0 = \omega_p/2$ is the central carrier frequency, k_0 is the corresponding wave vector, Ω is the radio frequency, and $\hat{a}(\Omega,z)$ is the photon annihilation operator with the frequency $\omega_0 + \Omega$ at position z in the crystal. We will also again make use of the operators [26]

$$\hat{\epsilon}(\Omega,z) = e^{-i[k(\Omega)-k_0]z} \hat{a}(\Omega,z). \tag{3.2}$$

We consider a coordinate system such that the input(output) face of the crystal lays at $z = 0 (z = L)$. The evolution of the bosonic operators – of the light collinear to the pump propagation direction in the ordinary mode – is then governed by the equation [27]

$$\partial_z \hat{\epsilon}(\Omega,z) = \frac{g}{L} \int d\Omega'\, e^{i\Delta(\Omega,\Omega')z} \alpha(\Omega+\Omega') \hat{\epsilon}^\dagger(\Omega',z), \tag{3.3}$$

where $\alpha(\Omega)$ is the frequency envelope function of the pump wave,

$$E_p^{(+)}(t,z) = \frac{1}{\sqrt{2\pi}} \int d\Omega\, e^{ik_p(\Omega)z - i(\omega_p+\Omega)t} \alpha(\Omega), \tag{3.4}$$

that is considered undepleted during the propagation though the crystal [i.e., $\forall z : \partial_z \alpha(\Omega) = 0$]. The dimensionless gain parameter g depends on pump strength, crystal length, and nonlinear susceptibility [27]. The pump envelope function α is normalized as

$$\int d\Omega |\alpha(\Omega)|^2 = \mathcal{N}_p^2 = \text{const.}\,, \tag{3.5}$$

such that the pump strength only enters the evolution equation (3.3) though the gain parameter g. However, in the context of our analysis it will be beneficial to adjust the constant pump normalization to the first-order MA – this will be specified further below. The spectral shape of the pump can be engineered in order to modify the generated squeezing eigenmodes and the degrees of squeezing – see, e.g., Refs. [56, 57]. Pump shape engineering exceeds the scope of this contribution and we will limit our studies to Gaussian pump shapes.

The phase-mismatch function

$$\Delta(\Omega, \Omega') = k_p(\Omega + \Omega') - k(\Omega) - k(\Omega'), \tag{3.6}$$

determines the efficiency of the parametric process that is described by the integral kernel

$$f(\Omega, \Omega', z) = \frac{1}{L} e^{i\Delta(\Omega,\Omega')z} \alpha(\Omega + \Omega'). \tag{3.7}$$

Note, that the pump-wave-vector dispersion relation depends on the angle θ of the extraordinary pump wave to the optical axis of the crystal and that Δ is symmetric in its arguments as $\Delta(\Omega, \Omega') = \Delta(\Omega', \Omega)$. Furthermore note that, for $\alpha(\Omega) = \delta(\Omega) L\sigma/g$ the evolution equation for the monochromatic case, described in the preceding chapter, is recovered.

We now consider a change of coordinate system that will simplify later expressions. When we perform the ME, e.g., in the first order we would perform the integral over the length of the crystal of the coupling kernel $f(\Omega, \Omega', z)$ such that

$$\int_0^L dz\, f(\Omega, \Omega', z) = \alpha(\Omega + \Omega') e^{i\Delta(\Omega,\Omega')L/2} \text{sinc}(\Delta(\Omega, \Omega')L/2) \tag{3.8}$$

where a phase of $e^{i\Delta(\Omega,\Omega')L/2}$ in terms of the phase-mismatch function Δ appears. However, if instead we could integrate symmetrically from $-L/2$ to $L/2$ this phase does not appear as

$$\int_{-L/2}^{L/2} dz\, f(\Omega, \Omega', z) = \alpha(\Omega + \Omega') \text{sinc}(\Delta(\Omega, \Omega')L/2), \tag{3.9}$$

which would simplify the description. We can achieve such a description simply by noting that we may perform the linear transform $z \mapsto z + L/2$ in Eq. (3.3) such that

$$\partial_z \hat{\epsilon}(\Omega, z + L/2) = \frac{g}{L} \int d\Omega' \, e^{i\Delta(\Omega,\Omega')(z+L/2)} \alpha(\Omega + \Omega') \hat{\epsilon}^\dagger(\Omega', z + L/2) \tag{3.10}$$

and then introducing the new, phase modulated operators $\hat{b}(\Omega, z) = e^{ik(\Omega)L/2} \epsilon(\Omega, z + L/2)$ and consider the pump envelope α to be obtained by phase modulation of another envelope β as $\alpha(\Omega) = e^{-ik_p(\Omega)L/2} \beta(\Omega)$, which then leads to

$$\partial_z \hat{b}(\Omega, z) = \frac{g}{L} \int d\Omega' \, e^{i\Delta(\Omega,\Omega')z} \beta(\Omega + \Omega') \hat{b}^\dagger(\Omega', z). \tag{3.11}$$

The substitution $\hat{b}(\Omega, z) = e^{ik(\Omega)L/2} \epsilon(\Omega, z + L/2)$ assigns a change of coordinates such that initial conditions at the input of the crystal and final transformations at the output are transformed accordingly as $\hat{b}(\Omega, -L/2) = e^{ik(\Omega)L/2} \epsilon(\Omega, z)$ and $\hat{b}(\Omega, L/2) = e^{ik(\Omega)L/2} \epsilon(\Omega, L)$. The two different coordinate systems are displayed in Fig. 3.1. Thus, by considering phase modulated fields at the input and output faces of the crystal, symmetric integration from $-L/2$ to $L/2$ in the ME is achieved – this simplification has been considered by several authors (see, e.g., Refs. [16, 121, 122]). As this avoids the aforementioned phase-factors all further discussion will center around the evolution equation (3.11).

3.1.1 Coarse graining and modes

Let us point out that Eq. (3.11) possesses no general analytical solution. In order to achieve a more efficient description of the Eq. (3.11) – in particular with regards to numerical applications – a coarse grained description with discretized frequencies is considered. Such a description is often also interesting for a practical description in measurements, e.g., in multi-pixel homodyne detection [123, 124]. The real line – on which the frequencies Ω are defined – is divided into pixel intervals $\mathbb{F}_k = [(k - 1/2)\delta\Omega, (k + 1/2)\delta\Omega)$. Such a basis is well suited if the pixel width $\delta\Omega$ is much smaller than the characteristic structures of the kernel, i.e., if the kernel function $f(\Omega, \Omega', z) = \frac{1}{L} e^{i\Delta(\Omega,\Omega')z} \beta(\Omega + \Omega')$ is well approximated by a step function

$$f(\Omega, \Omega', z) \cong \sum_{k,k'=-k_{\max}}^{k_{\max}} f(k\delta\Omega, k'\delta\Omega, z) \mathbf{1}_{\mathbb{F}_k}(\Omega) \mathbf{1}_{\mathbb{F}_{k'}}(\Omega'), \tag{3.12}$$

with the indicator function

$$\mathbf{1}_{\mathbb{F}_k}(\Omega) = \begin{cases} 1 & \Omega \in \mathbb{F}_k \\ 0 & \text{else} \end{cases}. \tag{3.13}$$

The cutoff at k_{max} is motivated by the fact that very fast oscillations (i.e., where the phase-mismatch function is very large) cancel to zero, this essentially corresponds to a rotating wave approximation. Applying (3.12) in (3.11) and collecting bosonic operators

$$\hat{b}_k(z) = \frac{1}{\sqrt{\delta\Omega}} \int\limits_{\mathbb{F}_k} d\Omega\, \hat{b}(\Omega, z), \tag{3.14}$$

then yields the discretized differential equation

$$\partial_z \hat{b}_k(z) = g \sum_{k'=-k_{\text{max}}}^{k_{\text{max}}} f_{k,k'}(z) \hat{b}^\dagger_{k'}(z), \tag{3.15}$$

where $f_{k,k'}(z) = \delta\Omega f(k\delta\Omega, k'\delta\Omega, z)$ are the coefficients of the symmetric matrix $f(z) = f^T(z)$. Naturally the $\hat{b}_k$ fulfill bosonic commutator relations

$$[\hat{b}_k(z), \hat{b}^\dagger_{k'}(z)] = \delta_{k,k'}, \qquad [\hat{b}_k(z), \hat{b}_{k'}(z)] = 0. \tag{3.16}$$

Note that a transition from (3.15) to (3.11) is possible by the Riemann integral limit $\delta\Omega \to 0^+$ where the full frequency dependent operators are recovered by

$$\hat{b}(\Omega, z) \cong \frac{1}{\sqrt{\delta\Omega}} \sum_{k=-k_{\text{max}}}^{k_{\text{max}}} \mathbf{1}_{\mathbb{F}_k}(\Omega) \hat{b}_k(z). \tag{3.17}$$

In the context of PDC with broad spectral pumps, considering (coarse grained) monochromatic modes may not be the most efficient of descriptions. Thus, let us consider the transformation to an alternative set of modes. We consider a orthonormal base of frequency envelope functions $\Psi_\ell(\Omega)$ with $\ell = 0, 1, \dots$ that fulfill the completeness relation

$$\delta(\Omega - \Omega') = \sum_{\ell=0}^{\infty} \Psi_\ell(\Omega) \Psi^*_\ell(\Omega') \tag{3.18}$$

and are well approximated in the coarse grained representation with resolution $\delta\Omega$ as

$$\Psi_{\ell,k} = \frac{1}{\sqrt{\delta\Omega}} \int\limits_{\mathbb{F}_k} d\Omega\, \Psi_\ell(\Omega) \approx \sqrt{\delta\Omega} \Psi_\ell(k\delta\Omega), \qquad \Psi_\ell(\Omega) \cong \frac{1}{\sqrt{\delta\Omega}} \sum_{k=-k_{\text{max}}}^{k_{\text{max}}} \Psi_{\ell,k} \mathbf{1}_{\mathbb{F}_k}(\Omega), \tag{3.19}$$

such that orthonormality,

$$\delta_{\ell,\ell'} = \int d\Omega\, \Psi^*_\ell(\Omega) \Psi^*_{\ell'}(\Omega) \cong \sum_{k,k'=-k_{\text{max}}}^{k_{\text{max}}} \Psi^*_{\ell,k} \Psi_{\ell',k} \underbrace{\frac{1}{\delta\Omega} \int d\Omega\, \mathbf{1}_{\mathbb{F}_k}(\Omega) \mathbf{1}_{\mathbb{F}_{k'}}(\Omega)}_{=\delta_{k,k'}} = \sum_{k=-k_{\text{max}}}^{k_{\text{max}}} \Psi^*_{\ell,k} \Psi_{\ell',k}, \tag{3.20}$$

remains preserved. Then the bosonic operators that govern excitations of these field modes can be obtained as

$$\hat{c}_\ell(z) = \int d\Omega\, \Psi_\ell^*(\Omega)\hat{b}(\Omega, z) \tag{3.21}$$

and the inversion of this transform reads as

$$\hat{b}(\Omega, z) = \sum_\ell \Psi_\ell(\Omega)\hat{c}_\ell(z). \tag{3.22}$$

By inserting the expression (3.17) into (3.21) we obtain

$$\hat{c}_\ell(z) = \sum_{k=-k_{\text{max}}}^{k_{\text{max}}} \underbrace{\left[\frac{1}{\sqrt{\delta\Omega}} \int d\Omega\, \Psi_\ell^*(\Omega)\mathbf{1}_{\mathbb{F}_k}(\Omega)\right]}_{=\Psi_{\ell,k}} \hat{b}_k(z). \tag{3.23}$$

For $n = 2k_{\text{max}} + 1$ the orthogonality (3.20) implies that the $n\times n$ matrix $V_{k,\ell} = \Psi_{\ell,k}$ with $k = -k_{\text{max}} \dots k_{\text{max}}$ and $\ell = 0, 1, \dots, 2k_{\text{max}}$ is unitary and thus follows that (3.23) is a unitary transform

$$\hat{c}_\ell(z) = \sum_{k=-k_{\text{max}}}^{k_{\text{max}}} V_{\ell,k}^\dagger \hat{b}_k(z), \tag{3.24}$$

which contains information about the field modes Ψ_ℓ corresponding to the operators $\hat{c}_\ell$ as

$$V = \sqrt{\delta\Omega} \begin{pmatrix} \Psi_0(-k_{\text{max}}\delta\Omega) & \Psi_1(-k_{\text{max}}\delta\Omega) & \dots & \Psi_{2k_{\text{max}}}(-k_{\text{max}}\delta\Omega) \\ \vdots & \vdots & \vdots & \vdots \\ \Psi_0(-\delta\Omega) & \Psi_1(-\delta\Omega) & \dots & \Psi_{2k_{\text{max}}}(-\delta\Omega) \\ \Psi_0(0) & \Psi_1(0) & \dots & \Psi_{2k_{\text{max}}}(0) \\ \Psi_0(\delta\Omega) & \Psi_1(\delta\Omega) & \dots & \Psi_{2k_{\text{max}}}(\delta\Omega) \\ \vdots & \vdots & \vdots & \vdots \\ \Psi_0(k_{\text{max}}\delta\Omega) & \Psi_1(k_{\text{max}}\delta\Omega) & \dots & \Psi_{2k_{\text{max}}}(k_{\text{max}}\delta\Omega) \end{pmatrix}. \tag{3.25}$$

This allows us to connect passive Gaussian unitary transformations V in the coarse grained representation to frequency modes Ψ_ℓ of the field [57]. Note however, that the number of field modes described by invertible unitary matrix transformations of field operators is limited by $n = 2k_{\text{max}} + 1$ which is a consequence of the coarse graining cutoff at k_{max}. The corresponding modal functions of the electric field are then given as

$$f_\ell(t, z) = \int \frac{d\Omega}{\sqrt{2\pi}} e^{-i\{k(\Omega)[z-L/2]-[\omega_0+\Omega]t\}} \Psi_\ell^*(\Omega). \tag{3.26}$$

Naturally, a coarse grained description is only viable if the it approximates the continuous modes well. Thus, we will use the two notations interchangeably in the following.

3.1.2 Matrix formulation

In order to further facilitate notation, we collect the bosonic operators as

$$\hat{\boldsymbol{\xi}}(z) = (\hat{b}_{-k_{\max}}(z), \dots, \hat{b}_{k_{\max}}(z), \hat{b}^\dagger_{-k_{\max}}(z), \dots, \hat{b}^\dagger_{k_{\max}}(z))^T. \tag{3.27}$$

In this notation Eq. (3.15) can be written as

$$\partial_z \hat{\boldsymbol{\xi}}(z) = -ig\mathbf{F}(z)\hat{\boldsymbol{\xi}}(z), \tag{3.28}$$

with

$$\mathbf{F}(z) = \begin{pmatrix} 0 & F(z) \\ -F^*(z) & 0 \end{pmatrix}, \qquad [F(z)]^{k_{\max}}_{k,k'=-k_{\max}} = if_{k,k'}(z). \tag{3.29}$$

This evolution equation can equally be obtained as

$$\partial_z \hat{\boldsymbol{\xi}}(z) = -i\gamma[\hat{\mathcal{H}}(z), \hat{\boldsymbol{\xi}}(z)] \tag{3.30}$$

in terms of the quadratic Hamiltonian

$$\hat{\mathcal{H}}(z) = \hat{\boldsymbol{\xi}}^\dagger(z) \begin{pmatrix} 0 & \frac{1}{2}F(z) \\ \frac{1}{2}F^*(z) & 0 \end{pmatrix} \hat{\boldsymbol{\xi}}(z). \tag{3.31}$$

As pointed out in Sec. 1.4.3: The description of ordering effects in terms of the ME in the matrix formalism is completely analogous to the operator formalism for quadratic Hamiltonians. Thus, throughout the following we will focus on the matrix description (3.28) and only make use of the operator formalism when it is more convenient.

Now let us consider a formal solution of (3.28) in terms of the symplectic transform $\mathbf{S}$ from the input of the crystal at $z = -L/2$ to the output at $z = L/2$ as

$$\hat{\boldsymbol{\xi}}(L/2) = \mathbf{S}\hat{\boldsymbol{\xi}}(-L/2). \tag{3.32}$$

The Bloch-Messiah decomposition of the symplectic transform $\mathbf{S}$ may be written as

$$\mathbf{S} = \begin{pmatrix} V & 0 \\ 0 & V^* \end{pmatrix} \begin{pmatrix} \cosh(R) & \sinh(R) \\ \sinh(R) & \cosh(R) \end{pmatrix} \begin{pmatrix} W & 0 \\ 0 & W^* \end{pmatrix}^\dagger, \tag{3.33}$$

where V and W describe passive Gaussian unitary transformations and the diagonal matrix R contains the squeezing parameters $R = \mathrm{diag}\{r_0, r_1, \ldots, r_{2k_{\max}}\}$ and describes mode-wise single-mode squeezing (cf. Sec. 1.3.1) in terms of these squeezing parameters. Without loss of generality and throughout the following, we consider the squeezing parameters r_ℓ to be ordered in descending order of strength $r_0 \geq r_1 \geq \ldots$.

We have previously seen that passive Gaussian unitary transformations can be associated with field modes [cf. (3.25)]. This allows for a convenient interpretation of the Bloch-Messiah decomposition: Consider that the columns of V and W define field modes, then

$$\hat{\boldsymbol{\xi}}^{\text{in}} = \begin{pmatrix} W & 0 \\ 0 & W^* \end{pmatrix}^\dagger \hat{\boldsymbol{\xi}}(-L/2), \qquad \hat{\boldsymbol{\xi}}^{\text{out}} = \begin{pmatrix} V & 0 \\ 0 & V^* \end{pmatrix}^\dagger \hat{\boldsymbol{\xi}}(L/2) \tag{3.34}$$

contain the associated annihilation an creation operators. Thus, we can see that the PDC process leads to a single-mode squeezing of the input field modes defined by W and transforms them to the output field modes defined by V as

$$\hat{\boldsymbol{\xi}}^{\text{out}} = \begin{pmatrix} \cosh(R) & \sinh(R) \\ \sinh(R) & \cosh(R) \end{pmatrix} \hat{\boldsymbol{\xi}}^{\text{in}} \tag{3.35}$$

Often one is solely interested in the case where the field in the ordinary polarization at the input face of the crystal is in the vacuum state. In this case the choice of field modes at the input face of the crystal is arbitrary (cf. Ref. [19]) and one may instead consider the polar decomposition

$$\mathbf{S} = \exp\left\{ \begin{pmatrix} 0 & Z \\ Z^* & 0 \end{pmatrix} \right\} \begin{pmatrix} X & 0 \\ 0 & X^* \end{pmatrix}^\dagger, \tag{3.36}$$

where $Z = VRV^T$ is complex symmetric (the resulting exponential is Hermitian) and $X = WV^\dagger$ is unitary. By the matrix/operator homomorphism (1.51) we can associate the operators

$$\exp\begin{pmatrix} 0 & Z \\ Z^* & 0 \end{pmatrix} \leftrightarrow \hat{Z}, \qquad \begin{pmatrix} X & 0 \\ 0 & X^* \end{pmatrix}^\dagger \leftrightarrow \hat{X}, \tag{3.37}$$

such that

$$\hat{\boldsymbol{\xi}}(L/2) = \hat{X}^\dagger \hat{Z}^\dagger \hat{\boldsymbol{\xi}}(-L/2)\hat{Z}\hat{X}. \tag{3.38}$$

If we consider an observable in terms of the field at the output face of the crystal $\hat{A}[\hat{\boldsymbol{\xi}}(L/2)]$ we can express it in terms of the input field as

$$\hat{A}[\hat{\boldsymbol{\xi}}(L/2)] = \hat{X}^\dagger \hat{Z}^\dagger \hat{A}[\hat{\boldsymbol{\xi}}(-L/2)]\hat{Z}\hat{X}. \tag{3.39}$$

Thus, in the case of the vacuum input

$$\langle \text{Vac.}|\hat{X}^\dagger \hat{Z}^\dagger \hat{A}[\hat{\boldsymbol{\xi}}(-L/2)]\hat{Z}\hat{X}|\text{Vac.}\rangle = \langle \text{Vac.}|\hat{Z}^\dagger \hat{A}[\hat{\boldsymbol{\xi}}(-L/2)]\hat{Z}|\text{Vac.}\rangle, \tag{3.40}$$

which is due to the fact that the unitary transform $\hat{X}$ does not affect the vacuum state [$\hat{X}|\text{Vac.}\rangle = |\text{Vac.}\rangle$]. Thus, for PDC with vacuum input we can focus on the representation in terms of the multimode squeezing operator $\hat{Z}$ [19]. This justifies the nomenclature of *squeezing eigenmodes* for the field modes defined by the unitary matrix V. The transition matrix X reveals how the input seeding eigenmodes are connected to the squeezing eigenmodes, as $W = RV$.

3.1.3 Modes and measurements

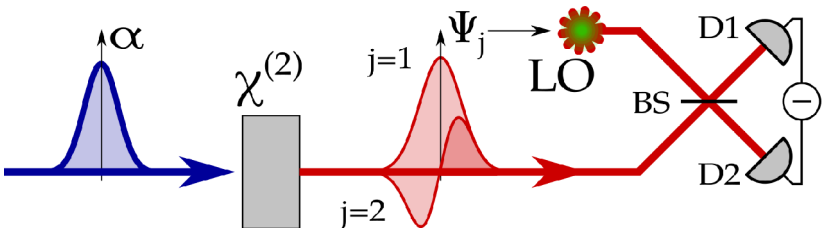

Figure 3.2: The light of a strong coherent pump (blue) enters the scheme from the left. It enters the nonlinear $\chi^{(2)}$ crystal which generates a frequency multi mode $\Psi_j(\Omega)$ pulse of squeezed modes (red). The squeezing of each of these modes can then, e.g., be accessed by shaping local oscillator (LO) pulses of a balanced homodyne detection scheme (on the right) such that its spectrum corresponds to that of the frequency multi mode squeezed modes.

In order to measure the squeezing in certain modes, the scenario of balanced homodyne detection, as depicted in Fig. 3.2, of the down-converted light may be considered. After exiting the crystal, the down converted light is entirely defined in terms of the field at the output face of the crystal

$$\hat{E}^{(+)}(t, L) = \int \frac{d\Omega}{\sqrt{2\pi}} e^{ik(\Omega)L/2} e^{-i(\omega_0+\Omega)t} \hat{b}(\Omega, L/2). \tag{3.41}$$

Note here the connection between coordinate system (where input and output lay at $z = 0, L$) where we have defined the $\hat{E}^{(+)}(t, z)$ and the coordinate system in which $\hat{b}(\Omega, z)$ is defined

(where input and output lay at $z = -L/2, L/2$). In balanced homodyne detection this field is superimposed with a strong coherent local oscillator field with envelope $\mathcal{E}$,

$$\hat{E}^{(+)}_{\mathrm{LO}}(t) = \int \frac{d\Omega}{\sqrt{2\pi}} e^{ik(\Omega)L/2} e^{-i(\omega_0+\Omega)t} \mathcal{E}(\Omega), \tag{3.42}$$

on a $50{:}50$ beam splitter,

$$\begin{pmatrix} E_1^+(t) \\ E_2^+(t) \end{pmatrix} = \frac{1}{\sqrt{2}} \begin{pmatrix} 1 & 1 \\ -1 & 1 \end{pmatrix} \begin{pmatrix} \hat{E}^{(+)}(t,L) \\ \hat{E}^{(+)}_{\mathrm{LO}}(t) \end{pmatrix}. \tag{3.43}$$

The two output beams are detected by photo current detectors of equal efficiency over a sufficiently long detection time and the difference of photo currents is considered, which reads as

$$\begin{aligned} \delta\hat{i} &= \eta \int dt \left[\hat{E}_1^{(-)}(t) \hat{E}_1^{(+)}(t) - \hat{E}_2^{(-)}(t) \hat{E}_2^{(+)}(t) \right] = \eta \int dt\, \hat{E}^{(-)}(t,L) \hat{E}^{(+)}_{\mathrm{LO}}(t) + \text{H.c.} \\ &= \eta \int d\Omega\, \hat{b}^\dagger(\Omega, L/2) \mathcal{E}(\Omega) + \text{H.c.}, \end{aligned} \tag{3.44}$$

with the quantum efficiency η. Representing the LO in terms of superpositions of squeezing eigenmodes,

$$\mathcal{E}(\Omega) = \sum_{\ell=0}^{2n} \mathcal{E}_\ell \Psi_\ell(\Omega), \tag{3.45}$$

yields

$$\delta\hat{i} = \eta \sum_{\ell=0}^{2n} \left[\hat{c}_\ell^\dagger(L/2) \mathcal{E}_\ell + \hat{c}_\ell(L/2) \mathcal{E}_\ell^* \right], \tag{3.46}$$

where (3.21) has been applied. Here $\hat{c}_\ell$ are the operators contained in $\hat{\boldsymbol{\xi}}^{\mathrm{out}}$ defined in Eq. (3.34) that correspond to the squeezing eigenmodes in V [cf. (3.25)] of the Bloch-Messiah decomposition (3.33). The input seeding modes are defined in terms of the matrix W of the Bloch-Messiah decomposition (3.33) and we denote the corresponding bosonic operators contained in $\hat{\boldsymbol{\xi}}^{\mathrm{in}}$ as $\hat{d}_\ell$. Then then (3.35) allows us to express (3.46) in terms of the bosonic operators $\hat{d}_\ell$ of the input field modes as

$$\delta\hat{i} = \eta \sum_{\ell=0}^{2n} \begin{pmatrix} \mathcal{E}_\ell \\ \mathcal{E}_\ell^* \end{pmatrix}^\dagger \begin{pmatrix} \hat{c}_\ell(L/2) \\ \hat{c}_\ell^\dagger(L/2) \end{pmatrix} = \eta \sum_{\ell=0}^{2n} \begin{pmatrix} \mathcal{E}_\ell \\ \mathcal{E}_\ell^* \end{pmatrix}^\dagger \begin{pmatrix} \cosh(r_\ell) & \sinh(r_\ell) \\ \sinh(r_\ell) & \cosh(r_\ell) \end{pmatrix} \begin{pmatrix} \hat{d}_\ell(-L/2) \\ \hat{d}_\ell^\dagger(-L/2) \end{pmatrix}. \tag{3.47}$$

The photo current variance in the case of PDC with vacuum input then has expectation value

$$\langle(\Delta\delta\hat{i})^2\rangle = \langle(\delta\hat{i})^2\rangle = 2\eta^2|\mathcal{E}_\ell|^2\sum_{\ell=0}^{2n}\left[e^{-2r_\ell}\sin^2[\arg(\mathcal{E}_\ell)] + e^{2r_\ell}\cos^2[\arg(\mathcal{E}_\ell)]\right]. \tag{3.48}$$

Thus, single-mode squeezing can be measured if the LO is exactly matched (i.e., $\mathcal{E}_\ell = \mathcal{E}\delta_{\ell,s}$ with $\mathcal{E} \in \mathbb{C}$ for some $s \in \mathbb{N}_0$) to one of the frequency modes. Alternatively $\mathcal{E}(\Omega)$ can be an arbitrary superposition of field modes Ψ_ℓ which corresponds to unitary transformations by LO shaping. In any case, a precise knowledge of the underlying field modes is desirable to facilitate interpretation of experimental results. Thus, throughout the following we will focus on the modification of squeezing eigenmodes in terms ordering effects.

3.2 Approximations in terms of the Magnus expansion

The symplectic transform $\mathbf{S}$ that solves Eq. (3.28) from $z = -L/2$ to $z = L/2$ can be represented in terms of the ME as (cf. Sec. 1.4.3)

$$\mathbf{S} = e^{-i\mathbf{M}}, \qquad -i\mathbf{M} = \sum_{n=1}^{\infty}(-ig)^n\,\mathbf{M}_n \tag{3.49}$$

In the present case, due to the complexity of the coupling matrix $\mathbf{F}$ [cf. (3.29)], an analytical expression for $\mathbf{M}$ cannot be found and we have to rely on approximations in terms of truncated ME

$$\mathbf{S}_m = \exp\left(\sum_{n=1}^{m}(-ig)^n\,\mathbf{M}_n\right) \tag{3.50}$$

up to order m. Here, as in the case of monochromatic PDC, the first oder approximation $\mathbf{S}_1$ corresponds to the negligence of ordering effects.

In view of the block anti-diagonal structure of the coupling matrix (3.29) and the fact that the Magnus terms $\mathbf{M}_n$ are defined in terms of its nested commutators, odd and even orders of ordering correction terms $\mathbf{M}_n$ have block anti-diagonal and block diagonal structure respectively. Thus, if we furthermore take into account that $\mathbf{S}_m$ is complex symplectic, we see that we can represent

$$\begin{aligned}\text{for } n \text{ odd } &: (-i)^n\mathbf{M}_n = \begin{pmatrix} 0 & -iM_n \\ iM_n^* & 0 \end{pmatrix},\\ \text{for } n \text{ even } &: (-i)^n\mathbf{M}_n = \begin{pmatrix} -iM_n & 0 \\ 0 & iM_n^* \end{pmatrix}.\end{aligned} \tag{3.51}$$

The first-order term of the ME,

$$\mathbf{M}_1 = \int_{-L/2}^{L/2} dz\, \mathbf{F}(z), \tag{3.52}$$

yields the matrix elements

$$M_1 = i\delta\Omega\beta_{p,q}\mathrm{sinc}(\theta_{p,q}), \tag{3.53}$$

where $p, q = -k_{\text{max}}, \ldots, k_{\text{max}}$. Furthermore, we have defined the phase-mismatch parameter $\theta_{p,q} = \Delta(p\delta\Omega, q\delta\Omega)L/2$ and represented the coarse grained phase modulated pump envelope as $\beta_{p,q} = \beta([p+q]\delta\Omega)$.

From the definition of the phase-mismatch function, Δ, follows that $\theta_{p,q}$ are the coefficients of a symmetric matrix. The same holds for the coefficients $\beta_{p,q}$ and thus M_1 is itself a symmetric matrix. Thus follows, that M_1 can be Takagi decomposed. However, note that in the case where the phase modulated pump envelope $\beta_{p,q}$ is entirely real(imaginary) the resulting matrix M_1 is entirely imaginary(real) and the Takagi decomposition can be reduced to the eigenvector decomposition of a real symmetric matrix (cf. Ref. [122]). The eigenvectors of a real symmetric matrix are always real and thus, squeezing eigenmodes resulting from the Takagi decomposition are either entirely real (for positive eigenvalues) or entirely imaginary (for negative eigenvalues). This is a useful case for the visualization of the impact of ordering effects on the squeezing eigenmodes, as deviations form entirely real or imaginary modes can only be due to ordering corrections.

Let us now specify more precisely the normalization of the pump $\mathcal{N}_p$. We have already stated that the pump is always normalized to a constant value such that a change in pump gain enters the process through the gain parameter g. Usually it is convenient to normalize functions to unity (i.e., $\mathcal{N}_p = 1$). However, we note that M_1 is linear with respect to the pump normalization (i.e., $M_1 \propto \mathcal{N}_p$) and consequently follows that $\|M_1\|_2 \propto \mathcal{N}_p$. In the context of our analysis of MAs we thus choose the value of normalization such that $\|M_1\|_2 = 1$. This implies, that for neglected ordering effects (i.e. $m = 1$), where the dependence of the degree of squeezing on the gain exponent g is linear, the highest degree of squeezing, $r_0^{[m=1]} = \|gM_1\|_2 = g\|M_1\|_2$, is identical to the gain parameter. This is a convenient choice of normalization as this was also the case for the scenario of PDC with a monochromatic pump as discussed in Chapter 2[1].

[1]There the degree of squeezing $r(\Omega)$ was maximal for $\Omega = 0$ and $r(0) = g$.

The second order term of the ME yields the matrix

$$(M_2)_{p,q} = \delta\Omega^2 \sum_r \alpha_{p,r}\alpha^*_{r,q} h_2(\theta_{p,r}, \theta_{r,q}), \tag{3.54}$$

where

$$\begin{aligned} h_2(x,y) &= \frac{\cos(x)\mathrm{sinc}(y) - \mathrm{sinc}(x)\cos(y)}{2(x-y)}, \\ h_2(x,x) &= \frac{\cos(x)j_1(x) - \sin(x)j_0(x)}{2}. \end{aligned} \tag{3.55}$$

Furthermore, the third order term yields the matrix

$$(M_3)_{p,q} = i\delta\Omega^3 \sum_{r,s} \alpha_{p,r}\alpha^*_{r,s}\alpha_{s,q} h_3(\theta_{p,r}, \theta_{r,s}, \theta_{s,q}), \tag{3.56}$$

where

$$\begin{aligned} h_3(x,y,z) &= \frac{(x+2y+z)\mathrm{sinc}(x)\mathrm{sinc}(y)\mathrm{sinc}(z) + 6\cos(x)h_2(y,z) + 6h_2(x,y)\cos(z)}{12(x-y+z)}, \\ h_3(x,x+z,z) &= -\frac{j_0(x)j_0(z)\sin(x+z) + 3h_2(x,x) + 3h_3(z,z)}{6(x+z)}, \\ h_3(x,0,-x) &= \frac{\cos(x)j_2(x) + \cos(x)\mathrm{sinc}(x) - \mathrm{sinc}^2(x)}{6}. \end{aligned} \tag{3.57}$$

The non-singularity of h_1 and h_2 is obvious from the present representation in terms of the holomorphic spherical Bessel functions j_0, j_1, j_2 [where $j_0(x) = \mathrm{sinc}(x)$]. The mth order expansion then correspondingly takes the block structure

$$\mathbf{S}_m = \exp\begin{pmatrix} -iH_0^{[m]} & -iH_I^{[m]} \\ i[H_I^{[m]}]^* & i[H_0^{[m]}]^* \end{pmatrix}, \tag{3.58}$$

with $(H_I^{[1]}, H_0^{[1]}) = (gM_1, 0)$, $(H_I^{[2]}, H_0^{[2]}) = (gM_1, g^2M_2)$, and $(H_I^{[3]}, H_0^{[3]}) = (gM_1 + g^3M_3, g^2M_2)$.

3.2.1 Gaussian pump

In order to illustrate the impact of ordering effects we consider a concrete scenario: A BBO crystal of length $L = 0.5\,\mathrm{mm}$ with Sellmeyer coefficients as given in Ref. [125] that is pumped by a Gaussian pump with central wavelength $\lambda_p = 397.5\,\mathrm{nm}$. The refractive index of the pump $n_p(\omega_p + \Omega)$ is determined by the birefringence relation

$$\frac{1}{n_p^2} = \frac{\sin^2(\theta)}{n_e^2} + \frac{\sin^2(\theta)}{n_0^2}, \tag{3.59}$$

where n_e and n_o are the refractive indices of the extraordinary and ordinary axis respectively and θ is the angle between the optical axis of the crystal and the normal vector of the fields. The wave vectors are then determined in terms of

$$k_p(\Omega) = (\omega_p + \Omega) n_p(\omega_p + \Omega)/c_0, \qquad k(\Omega) = (\omega_0 + \Omega) n_o(\omega_0 + \Omega)/c_0, \tag{3.60}$$

which determines the phase matching function $\Delta(\Omega, \Omega')$. For $\theta = 29.4°$ perfect phase matching is achieved at zero radio frequencies as

$$\Delta(0, 0) = 0. \tag{3.61}$$

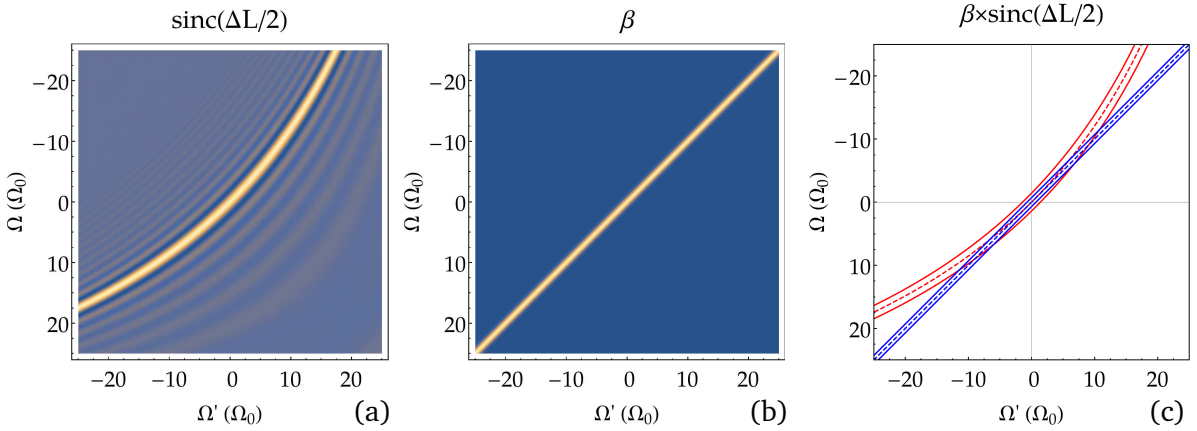

Figure 3.3: The factor $\mathrm{sinc}[\Delta(\Omega, \Omega')L/2]$ for the considered BBO scenario (a), the Gaussian pump envelope β (b). Figure (c) illustrates how the direct product of the sinc function and the pump determine the coupling: Shown are the pump maximum (blue, dashed) and its width-lines (blues, solid) as well as the sinc maximum (red, dashed) and its effective width-lines (red, solid). Effectively, coupling does only take place in the region encapsulated by the width-lines of pump and sinc.

We defined the linear frequency walk-off

$$\Omega_0 = \left. \frac{2\pi}{L \partial_\Omega \Delta(\Omega/\sqrt{2}, \Omega/\sqrt{2})} \right|_{\Omega=0} = 45.1 \times 10^{12} \frac{\mathrm{rad}}{\mathrm{s}}, \tag{3.62}$$

which we will use as frequency unit throughout the following. We consider a real Gaussian phase modulated pump envelope,

$$\beta(\Omega) = e^{-\frac{1}{2}\left(\frac{\Omega}{\Delta\Omega}\right)^2}, \tag{3.63}$$

of width $\Delta\Omega = \Omega_0/4$. Coarse graining is applied with a resolution of $\delta\Omega = \Omega_0/10$ and we consider a cutoff at $k_{\max} = 250$ (i.e., $\Omega \in [-25\Omega_0, 25\Omega_0]$). How the Gaussian pump affects the coupling in PDC is best seen from the first-order Magnus term. The shape of the first-order term is given by the direct product of the $\mathrm{sinc}[\Delta(\Omega, \Omega')L/2]$ and the Gaussian envelope

$\beta(\Omega + \Omega')$ such that coupling only takes place where both are non-zero, this is illustrated in Fig. 3.3.

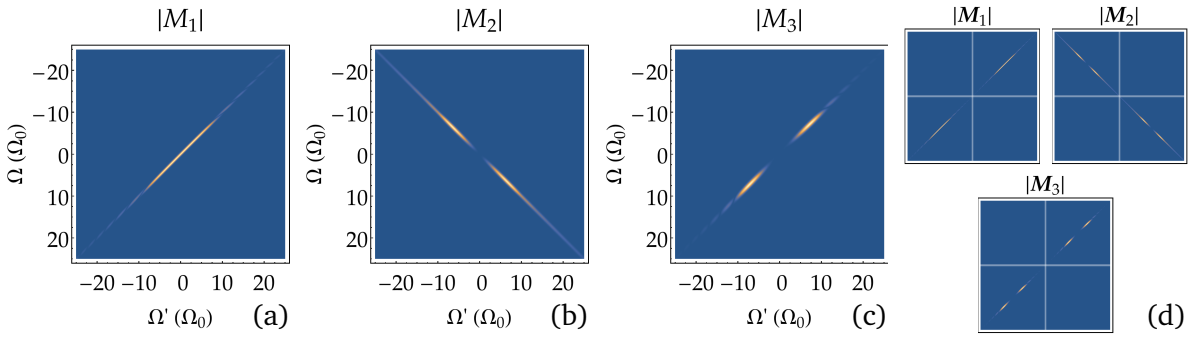

Figure 3.4: The absolute value of the first (a), second (b), and third (c) order Magnus term matrix blocks M_n as defined in (3.51). The resulting block structure of the Matrix valued Magnus terms $\mathbf{M}_n$ for the three considered orders is illustrated in (d), where blocks are separated by white lines.

The Magnus terms for this exemplary scenario are displayed in Fig. 3.4. An interesting observation from these Magnus terms is that the second and third order term go to zero in the region of phase matching $\Omega = \Omega' = 0$. Thus, these terms will supposedly yield minimal corrections of squeezing eigenmodes around the carrier frequency $\Omega = 0$.

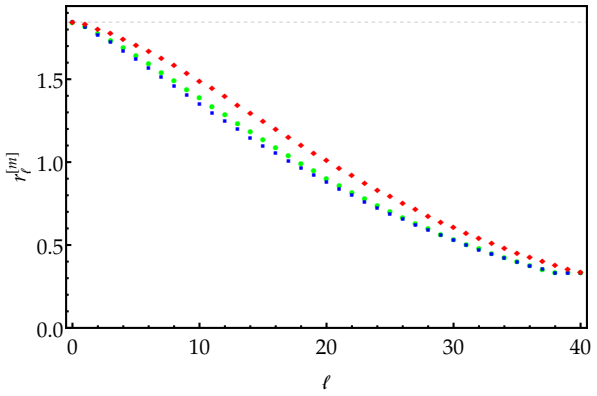

Figure 3.5: The squeezing parameters $r_\ell^{[m]}$ of the squeezing eigenmodes $\Psi_\ell^{[m]}(\Omega)$ obtained from the Bloch-Messiah decomposition in first order $m = 1$ (green, circle), second order $m = 2$ (blue, square), and third order $m = 3$ (red, diamond) MA. A horizontal gridline (dashed, gray) marks the value of gain $g = 1.84$.

As illustrated at hands of the formal solution, approximated squeezing eigenmodes, $\Psi_\ell^{[m]}$, and parameters, $r_\ell^{[m]}$, are obtained from the MA (3.58) in mth order via the Bloch-Messiah decomposition (3.33). In Figure 3.5 the squeezing parameter spectrum is given for the example of a gain of $g = 1.84$. At this regime of gain the squeezing spectrum is slightly modified for a wide range of squeezing parameters by ordering corrections. However, it is notable that the highest degree of squeezing still behaves linear with respect to the gain parameter g, i.e., $r_0^{[m]} = g$ and lays in the order of 16 dB of squeezing. Based on our observations in the case of a monochromatic pump in chapter 2 it may be hypothesized, that the third-order MA yields reliable results as long as the maximum squeezing $r_0^{[m=3]}$ increases linear with the gain

parameter g. For the considered configuration, the sufficient upper bound for gain where the ME converges [cf. (1.101)] can be obtained numerically as $g_{\max} = 2.97$. Thus, the considered gain lays well below this bound. Moreover note that, the second-order MA yields a decrease of squeezing value whilst the third order yields an increase in squeezing values.

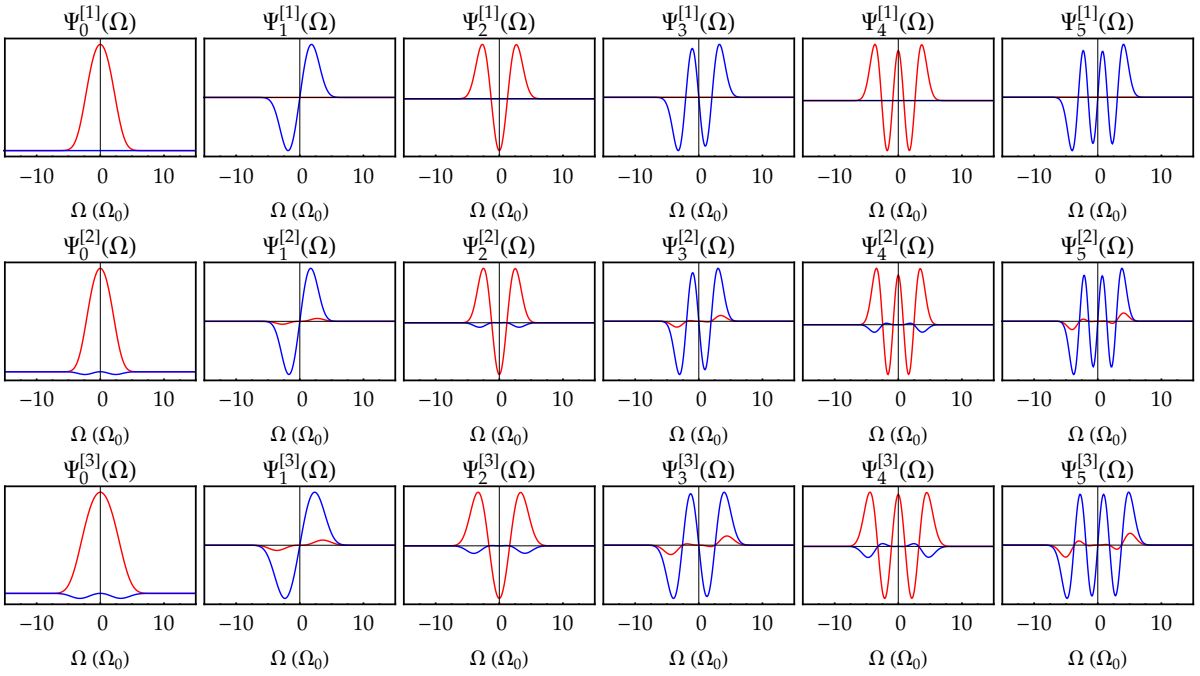

Figure 3.6: Real (red) and imaginary (blue) value of the orthonormal squeezing eigenmodes $\Psi_\ell^{[m]}(\Omega)$ corresponding to the squeezing parameter r_ℓ for $\ell = 0, 1, \ldots, 5$ as obtained in first order $m = 1$ (first row), second order $m = 2$ (second row), and third order $m = 3$ (third row) for the considered BBO scenario with a Gaussian pump at gain $g = 1.84$. Note that the plotrange is smaller than then the coarse graining cutoff $|\Omega| < 25\Omega_0$.

The squeezing eigenfunctions for the six largest squeezing parameters obtained from the first three orders of approximation are displayed in Fig. 3.6. As pointed out above, for the displayed scenario of a real Gaussian pump envelope β the eigenmodes obtained from the first-order MA are entirely real or imaginary. It can be seen, that the ordering corrections in second and third-order MA modify this behavior, as the eigenmodes obtained in these orders display both real and imaginary parts. Interestingly, corrections become minimal around the carrier frequency of the down converted light, where $\Omega = 0$, which supports the hypothesis we drew from the corresponding Magnus terms displayed in Fig. 3.4.

What might strike as obvious at first sight is the similarity of the displayed eigenmodes with Hermite Gauss functions that are defined in terms of Hermite polynomials (cf. [126]). Of course the similarity only goes so far, but we can make an important analogy: For the Hermite Gauss functions the lowest order Hermite Gauss function (simply a Gaussian) defines the weight function of the integral scalar product and thereby the orthogonal Hermite polynomials that define all higher-order Hermite Gauss functions. Thus, the width of Hermite Gauss func-

tions is determined in terms of the width of the lowest order Hermite Gauss function. With this in mind we turn our attention to the width of the squeezing eigenfunction $\Psi_0^{[m]}(\Omega)$ that defines the maximally squeezed field mode: The ordering corrections yield a decrease in width in the second-order MA and an increase in the third-order MA. Thus, it can be concluded that even and odd order ordering corrections affect the width of eigenmodes differently.

3.3 Bispectral beams

For the case of a monochromatic pump as considered in Chapter 2, we saw that coupling occurred for opposed radio frequencies Ω and $-\Omega$ and each radio frequency $|\Omega|$ could be associated with two bichromatic field modes subject to the same degree of squeezing $r(\Omega)$. Here we will consider a bispectral beam scenario, where a similar description as for monochromatic pumps can be achieved. To this end we consider the same example scenario with a BBO crystal and a real Gaussian pump as described in Sec. 3.2.1 but where the crystal is slightly turned, such that $\theta = 28.5°$. This scenario also serves as an example for an engineered output state by tailored parametric interaction (cf. [56]), as the output light will show a two-fold multiplicity in squeezing parameter values (as we will be shown below).

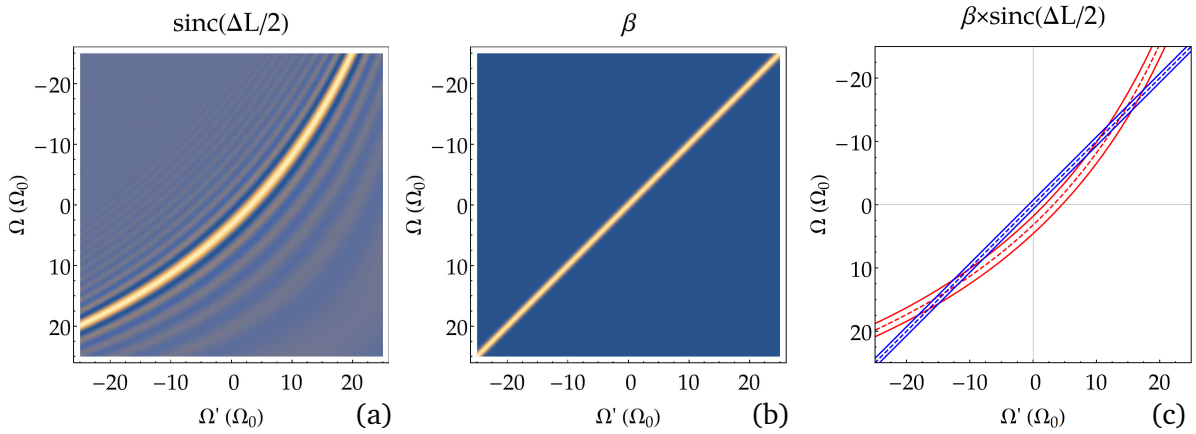

Figure 3.7: The factor $\mathrm{sinc}[\Delta(\Omega,\Omega')L/2]$ for the considered BBO scenario with modified phase-mismatch function (a), the Gaussian pump envelope β (b). Figure (c) illustrates how the direct product of the sinc function and the pump determine the coupling: Shown are the pump maximum (blue, dashed) and its width-lines (blues, solid) as well as the sinc maximum (red, dashed) and its effective width-lines (red, solid). Effectively, coupling does only take place in the region encapsulated by the width-lines of pump and sinc.

The turning of the crystal leads to a shift of the phase-mismatch function $\Delta(\Omega,\Omega')$ which modifies the frequency coupling inside the crystal as illustrated in Fig. 3.7 at hands of the factors appearing in the first-order Magnus term. Effectively, by the shift of the phase-mismatch function, the coupling is modified such that for neglected ordering effects no coupling takes place at the carrier frequency $\Omega = \Omega' = 0$ and in the regions $(\Omega,\Omega') \in [-25,0]\times[-25,0]$ and $(\Omega,\Omega') \in [0,25]\times[0,25]$. Thus, in first-order MA coupling will only take place in terms of

radio frequencies on opposite sides of the carrier frequency $\Omega = 0$. As the regions $(\Omega, \Omega') \in [-25, 0]\times[-25, 0]$ and $(\Omega, \Omega') \in [0, 25]\times[0, 25]$ in Fig. 3.7c are empty, we can establish a block structure for the first-order MA as [121][2]

$$H_I^{[1]} = \begin{pmatrix} 0 & J^{[1]} \\ (J^{[1]})^T & 0 \end{pmatrix}, \qquad H_0^{[1]} = \begin{pmatrix} 0 & 0 \\ 0 & 0 \end{pmatrix}. \tag{3.64}$$

where J is in general a complex valued matrix and does not fulfill any special symmetry.

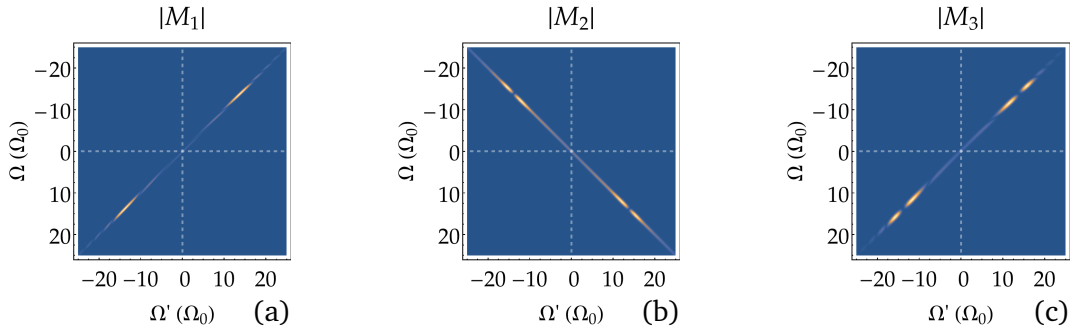

Figure 3.8: The absolute value of the first (a), second (b), and third (c) order Magnus term matrix blocks M_n as defined in (3.51). Grindlines (white, dashed) illustrate a possible block structure assignment.

In Figure 3.8, the kernels of the first three orders of approximation are displayed for the bispectral beam scenario. We can see that in each order two opposed quadrants vanish. Accordingly, up to third order, the MA can be represented in terms of the block structure

$$H_I^{[k]} = \begin{pmatrix} 0 & J^{[k]} \\ (J^{[k]})^T & 0 \end{pmatrix}, \qquad H_0^{[k]} = \begin{pmatrix} \Phi_1^{[k]} & 0 \\ 0 & \Phi_2^{[k]} \end{pmatrix}, \tag{3.65}$$

where $\Phi_1^{[k]}$ and $\Phi_2^{[k]}$ are Hermitian matrices that have no special symmetry relations to each other. Thus, the resulting symplectic transform takes the form

$$\mathbf{S}_m = \exp \begin{pmatrix} -i\Phi_1^{[m]} & 0 & 0 & -iJ^{[m]} \\ 0 & -i\Phi_2^{[m]} & -i[J^{[m]}]^T & 0 \\ 0 & i[J^{[m]}]^* & i[\Phi_1^{[m]}]^* & 0 \\ i[J^{[m]}]^\dagger & 0 & 0 & i[\Phi_2^{[m]}]^* \end{pmatrix}. \tag{3.66}$$

[2]The intervals of course graining are modified as $\mathbb{F}_k = (k\delta\Omega, [k+1]\delta\Omega]$ with $k = -k_{\max}, \ldots, k_{\max} - 1$ such that no frequency bin is allocated to the carrier frequency $\Omega = 0$. This is justified as no interaction takes place along $\Omega = 0$ and $\Omega' = 0$ and avoids to include additional superfluous nil-blocks in the block structure. The blocks are determined in terms of the indices $k = -k_{\max}, \ldots, -1$ and $k = 0, \ldots, k_{\max} - 1$.

It is then easy to show (cf. appendix. C), that the exponential $\mathbf{S}_m$ preserves the block structure of the exponent such that the input output relation can be written as

$$\begin{pmatrix} \hat{\mathbf{b}}_-(L/2) \\ \hat{\mathbf{b}}_+(L/2) \\ \hat{\mathbf{b}}_-^{\dagger T}(L/2) \\ \hat{\mathbf{b}}_+^{\dagger T}(L/2) \end{pmatrix} = \underbrace{\begin{pmatrix} A_1 & 0 & 0 & B_1 \\ 0 & A_2 & B_2 & 0 \\ 0 & B_1^* & A_1^* & 0 \\ B_2^* & 0 & 0 & A_2^* \end{pmatrix}}_{=\mathbf{S}_m} \begin{pmatrix} \hat{\mathbf{b}}_-(-L/2) \\ \hat{\mathbf{b}}_+(-L/2) \\ \hat{\mathbf{b}}_-^{\dagger T}(-L/2) \\ \hat{\mathbf{b}}_+^{\dagger T}(-L/2) \end{pmatrix}, \tag{3.67}$$

where

$$\begin{aligned} \hat{\mathbf{b}}_-(z) &= \Big(\hat{b}(-[k_{\max}-1/2]\delta\Omega), \dots, \hat{b}(-[2-1/2]\delta\Omega, z), \hat{b}(-[1-1/2]\delta\Omega, z)\Big)^T \\ \text{and } \hat{\mathbf{b}}_+(z) &= \Big(\hat{b}([1-1/2]\delta\Omega, z), \hat{b}([2-1/2]\delta\Omega, z), \dots, \hat{b}([k_{\max}-1/2]\delta\Omega, z)\Big)^T \end{aligned} \tag{3.68}$$

contain the annihilation operators of negative and positive radio frequency respectively. Thus, the transformation (3.67) can be considered as a multi-frequency generalization of the Bogoliubov transformation (2.32). Indeed, for a monochromatic pump the Blocks matrices in Eq. (3.67) become diagonal.

3.3.1 Proof of twofold multiplicity

Whilst the structure of the first-order MA (3.64) suggests a two-fold multiplicity of squeezing parameters for the modes of the generated light, it is not obvious from (3.66) that this multiplicity remains preserved when ordering effects are accounted for in terms of higher oder MAs. We can however prove this by analyzing the structure of higher oder MAs for the bispectral beam scenario. The transformations obtained by higher order MAs in this scenario have the form

$$\mathbf{S} = \begin{pmatrix} A & B \\ B^* & A^* \end{pmatrix}, \tag{3.69}$$

with the blocks

$$A = \begin{pmatrix} A_1 & 0 \\ 0 & A_2 \end{pmatrix}, \qquad B = \begin{pmatrix} 0 & B_1 \\ B_2 & 0 \end{pmatrix}. \tag{3.70}$$

As explained in Sec. 1.3.4, can the Bloch-Messiah decomposition be performed by performing the Takagi decomposition of

$$AB^T = \begin{pmatrix} 0 & A_1 B_2^T \\ A_2 B_1^T & 0 \end{pmatrix}, \tag{3.71}$$

which takes the form

$$AB^T = \frac{1}{2} V \sinh \begin{pmatrix} 2R_1 & 0 \\ 0 & 2R_2 \end{pmatrix} V^T. \tag{3.72}$$

This Takagi decomposition is sufficient to define the squeezing eigenmodes contained in V and the squeezing parameters contained in $R_1 = \mathrm{diag}\{r_0, r_2, \dots\}$ and $R_2 = \mathrm{diag}\{r_1, r_3, \dots\}$ – performing the remaining steps of the Bloch-Messiah decomposition described in Sec. 1.3.4 solely serves the purpose of determining the field modes by which the crystal input can be seeded.

From the complex symplecticity [cf. (1.52)] of (3.69) we can deduce the condition

$$A_1 B_2^T = B_1 A_2^T, \tag{3.73}$$

whereby follows, that AB^T is a symmetric matrix.

$$AB^T = \begin{pmatrix} 0 & A_1 B_2^T \\ B_1 A_2^T & 0 \end{pmatrix} = \begin{pmatrix} 0 & A_1 B_2^T \\ B_1 A_2^T & 0 \end{pmatrix}^T, \tag{3.74}$$

Using the singular value decomposition

$$A_1 B_2^T = C \Xi D^\dagger, \tag{3.75}$$

with unitary matrices C, and D and diagonal matrix Ξ we can decompose AB^T as

$$\begin{aligned} AB^T &= \begin{pmatrix} 0 & C\Xi D^\dagger \\ D^* \Xi C^T & 0 \end{pmatrix} = \begin{pmatrix} C & 0 \\ 0 & D^* \end{pmatrix} \begin{pmatrix} 0 & \Xi \\ \Xi & 0 \end{pmatrix} \begin{pmatrix} C^T & 0 \\ 0 & D^\dagger \end{pmatrix} \\ &= \begin{pmatrix} C & 0 \\ 0 & D^* \end{pmatrix} \frac{1}{\sqrt{2}} \begin{pmatrix} I & -iI \\ I & iI \end{pmatrix} \begin{pmatrix} \Xi & 0 \\ 0 & \Xi \end{pmatrix} \frac{1}{\sqrt{2}} \begin{pmatrix} I & -iI \\ I & iI \end{pmatrix}^T \begin{pmatrix} C^T & 0 \\ 0 & D^\dagger \end{pmatrix}. \end{aligned} \tag{3.76}$$

This determines the Takagi decomposition (3.72) of AB^T through

$$V = \frac{1}{\sqrt{2}} \begin{pmatrix} C & 0 \\ 0 & D^* \end{pmatrix} \begin{pmatrix} I & -iI \\ I & iI \end{pmatrix} \tag{3.77}$$

and

$$\frac{1}{2}\sinh(2R_1) = \frac{1}{2}\sinh(2R_2) = \Xi. \tag{3.78}$$

As the $\sinh$ function is uniquely invertible for all real values, we can see that the squeezing values have a multiplicity of two for any symplectic transform (3.69) with the Block structure (3.70).

3.3.2 Bispectral modes

To illustrate the effect of ordering corrections in the bispectral beam scenario, we consider a gain of $g = 1.84$. In Figure 3.9 the squeezing parameter spectrum for such a bispectral beam scenario is displayed. Note that here the maximum squeezing parameters, $r_0^{[2]}, r_1^{[2]}, r_0^{[3]}, r_1^{[3]}$, already show nonlinear dependence on gain, despite the gain, g, being the same as in Fig. 3.5, where no nonlinear dependency for the maximum squeezing value, $r_0^{[m]}$, is visible by eye (i.e., there it is similar to g). For the considered scenario the sufficient upper bound for gain reads $g_{\max} = 2.81$. Thus, for the considered gain we are a bit closer to the sufficient upper bound.

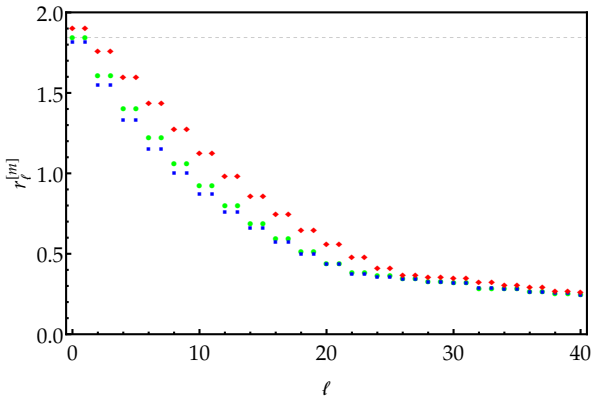

Figure 3.9: The squeezing parameters $r_\ell^{[m]}$ of the squeezing eigenmodes $\Psi_\ell^{[m]}(\Omega)$ obtained from the Bloch-Messiah decomposition in first order $m = 1$ (green, circle), second order $m = 2$ (blue, square), and third order $m = 3$ (red, diamond). A dashed horizontal gridline marks the value of gain $g = 1.84$.

The corresponding down converted phase modulated envelope modes are displayed in Fig. 3.10. We can observe that the modes have a bispectral structure, i.e., they are combinations of well separated spectral modes in the positive and negative radio frequency domain

respectively. If we analyze (3.77) with (3.25) in mind we can see that the columns of

$$\begin{pmatrix} C \\ 0 \end{pmatrix} \qquad \text{and} \qquad \begin{pmatrix} 0 \\ D^* \end{pmatrix} \tag{3.79}$$

contain modes $\Psi_{-;\ell}(\Omega)$ and $\Psi_{+;\ell}(\Omega)$, respectively, that are identical nil in the negative and positive radio frequency domain, respectively, i.e.,

$$\forall \Omega > 0 : \ \Psi_{-;\ell}(\Omega) = 0, \qquad \forall \Omega < 0 : \ \Psi_{+;\ell}(\Omega) = 0. \tag{3.80}$$

The additional passive Gaussian unitary transformation in (3.77) combines those positive and negative radio frequency field modes to the squeezing eigenmodes

$$\Psi_{2\ell}(\Omega) = \frac{1}{\sqrt{2}} \left[\Psi_{-;\ell}(\Omega) + \Psi_{+;\ell}(\Omega) \right], \qquad \Psi_{2\ell+1}(\Omega) = \frac{1}{i\sqrt{2}} \left[\Psi_{-;\ell}(\Omega) - \Psi_{+;\ell}(\Omega) \right], \tag{3.81}$$

that are squeezed by $r_{2\ell} = r_{2\ell+1}$ (for $\ell = 0, 1, \dots$), i.e., squeezing parameters have two-fold multiplicity. For all relevant modes of the considered example scenario [cf. Fig. 3.10] we can find that

$$\arg[\Psi_{2\ell+1}(\Omega)] - \arg[\Psi_{2\ell}(\Omega)] = \begin{cases} -\pi/2 & \text{for } \Omega < 0 \\ \pi/2 & \text{for } \Omega > 0 \end{cases}. \tag{3.82}$$

This explains the bispectral-mode structure we see in Fig. 3.10. With regard to different orders of ordering corrections we can see that those have quite an impact on the underlying field modes. As in the previous scenario [cf. Fig. 3.6] we see clear deviation from the entirely real or imaginary field modes for the case of neglected ordering effects $m = 1$. As discussed in Sec. 1.3.5: Two mode squeezed states may be represented in terms two single-mode-squeezed states with equal degree of squeezing and vice versa. Due to the two-fold multiplicity in the present scenario and the bispectral structure of modes (3.81), the negative $\Psi_{-;\ell}(\Omega)$ and positive $\Psi_{+;\ell}(\Omega)$ radio frequency modes can be considered entangled by two-mode squeezing [cf. (1.72)].

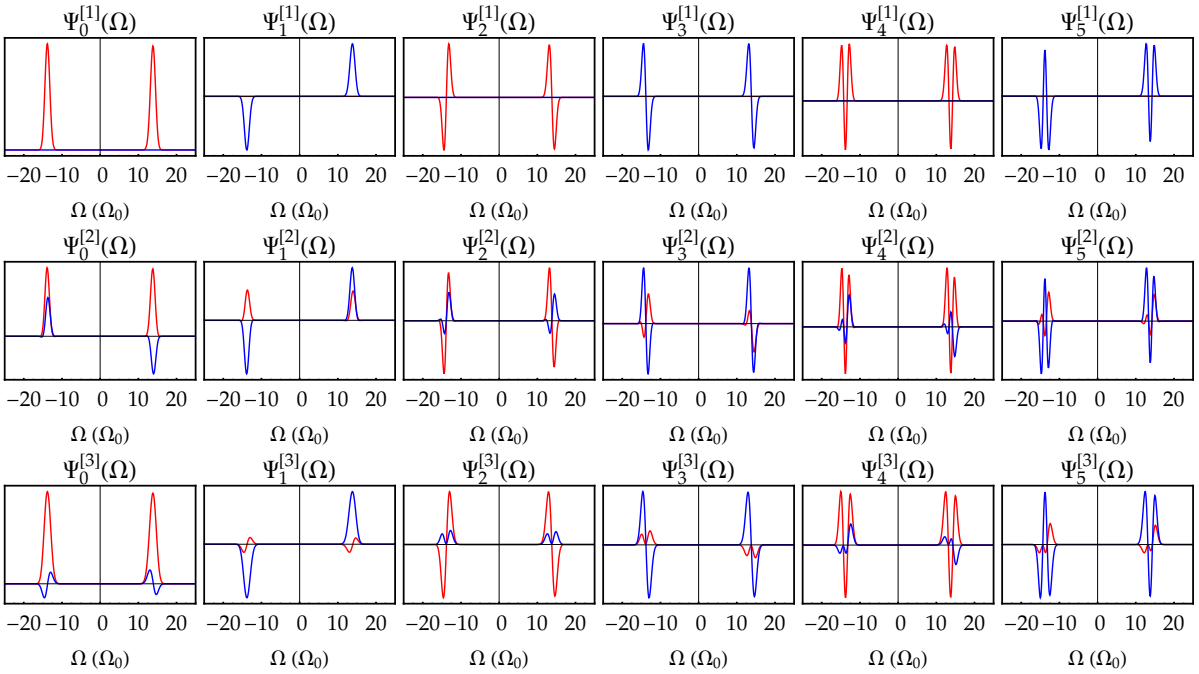

Figure 3.10: Real (red) and imaginary (blue) value of the orthonormal squeezing eigenmodes $\Psi_\ell^{[m]}(\Omega)$ corresponding to the squeezing parameter r_ℓ for $\ell = 0, 1, \ldots, 5$ as obtained in first order $m = 1$ (first row), second order $m = 2$ (second row), and third order $m = 3$ (third row) for the considered BBO scenario with a Gaussian pump at gain $g = 1.84$ and bispectral beam phase-mismatch conditions.

Chapter 4

Classically driven Jaynes-Cummings dynamics of an ion in a Paul trap

Contents

In this chapter we will consider another scenario where the methods of ME may be applied: the CJCD model. In this system another layer of complexity is added as the interaction Hamiltonian exceeds quadratic order in annihilation/creation operators for the motional degrees of freedom of the ion in the trap. To give some context, we first give a hands on derivation of the standard Jaynes-Cummings model and then of the CJCD model. Subsequently, we will introduce a spinor formalism that enables us to derive an analytical solution to this complicated time dependent problem. Then we see how the spinor formalism designed for this purpose allows us to obtain MAs and analyze time ordering effects by comparing the MAs to the derived exact solution.

4.1 The standard Jaynes-Cummings model

The Jaynes-Cummings model describes the strong interaction of two-level atoms inside cavities with single electromagnetic cavity field modes – for a comprehensive derivation see Ref. [2] or

Ref. [4]. The Hamiltonian for the electronic levels of the atom can be described in terms of its energy eigenstates

$$\hat{H}_{\mathrm{A}} = \sum_j E_j |j\rangle\langle j|. \tag{4.1}$$

Transition frequencies are necessarily given in terms of the energy differences as

$$\omega_{jk} = \frac{1}{\hbar}\left[E_j - E_k\right]. \tag{4.2}$$

When only two-levels of the atom are relevant for the interaction with the electromagnetic field, other levels than the relevant can be neglected. Without loss of generality, let us consider the levels $j = 1, 2$ such that $j = 1(j = 2)$ is the ground(excited) state. Furthermore, gauging energy to the ground level $E_1 \mapsto 0$ then yields the two-level system Hamiltonian

$$\hat{H}_{\mathrm{A}} = \hbar\omega_{21}|2\rangle\langle 2| + 0|1\rangle\langle 1| = \hbar\omega_{21}\hat{A}_{22}, \tag{4.3}$$

where we use the notation $\hat{A}_{jk} = |j\rangle\langle k|$ to denote projectors in terms of the two-level system states.

In the cavity, the quantized field is formulated in terms of

$$\hat{\mathbf{E}}(\mathbf{r}) = \sum_\gamma i\sqrt{\frac{\hbar\omega_\gamma}{2\varepsilon_0}}\mathbf{e}_\gamma \hat{b}_\gamma u_\gamma(\mathbf{r}) + \mathrm{H.c.}. \tag{4.4}$$

Here $u_\gamma(\mathbf{r})$ is the mode function of the γth cavity mode with frequency ω_γ and polarization $\mathbf{e}_\gamma$, and the $\hat{b}_\gamma(\hat{b}^\dagger_\gamma)$ denote the annihilation(creation) operators of the modes. The mode functions are normalized over the cavity volume V. We are only interested in the interaction of single mode with the two-level atom where the frequency of the mode ω_L is close to the transition frequency ω_{21} of the two-level system. In that case, and if only one polarization is considered, it is sufficient to reduce the description of the cavity field to that mode only as

$$\hat{\mathbf{E}}(\mathbf{r}) = i\sqrt{\frac{\hbar\omega_L}{2\varepsilon_0}}\mathbf{e}\,\hat{b}\,u(\mathbf{r}) + \mathrm{H.c.}. \tag{4.5}$$

The corresponding unperturbed Hamiltonian of the field then reads as

$$\hat{H}_{\mathrm{F}} = \hbar\omega_L \hat{b}^\dagger\hat{b}, \tag{4.6}$$

where we also regauge to the vacuum energy level of the field, such that the term $\hbar\omega_L/2$ does not appear.

In the Jaynes-Cummings model the interaction between the atomic two-level system and the cavity mode is described in terms of the dipole approximation. Let the atom be located at

the position $\mathbf{R}$ and $\hat{\mathbf{r}} = (\hat{x}, \hat{y}, \hat{z})^T$ be the vectorial position operator of the electron relative to the position of the nucleus. Then we can define the electronic dipole moment operator as

$$\hat{\mathbf{d}} = e\hat{\mathbf{r}}, \tag{4.7}$$

with the elementary charge e. We assume here that the atomic states carry no permanent dipole moment. Whenever $\mathbf{d}_{jk} = \langle j|\hat{\mathbf{d}}|k\rangle$ is non-zero, a dipole transition can occur. Let the atom be located at $\mathbf{R}$, then its interaction with the cavity field can be described in terms of the dipole approximation by the interaction Hamiltonian [4]

$$\hat{H}_{\text{int}} = -\hat{\mathbf{d}}\hat{\mathbf{E}}(\mathbf{R}). \tag{4.8}$$

For the two-level system the dipole operator may be expanded as

$$\hat{\mathbf{d}} = \mathbf{d}_{21}\hat{A}_{21} + \mathbf{d}_{12}\hat{A}_{12}. \tag{4.9}$$

Thus, if we move to an interaction picture as $\hat{H}_{\text{int}} \mapsto \hat{\tilde{H}}_{\text{int}}(t) = \hat{U}^\dagger(t)\hat{H}_{\text{int}}\hat{U}(t)$, in terms of $\hat{U} = \exp\left(-\frac{it}{\hbar}\left[\hat{H}_{\text{F}} + \hat{H}_{\text{A}}\right]\right)$, we obtain the interaction picture Hamiltonian

$$\begin{aligned}\hat{\tilde{H}}_{\text{int}}(t) = &- \hat{A}_{21}\mathbf{d}_{21}\left(i\sqrt{\frac{\hbar\omega_L}{2\varepsilon_0}}\mathbf{e}e^{-i\Delta\omega t}\hat{b}u(\mathbf{R}) - i\sqrt{\frac{\hbar\omega_L}{2\varepsilon_0}}\mathbf{e}e^{i(\omega_{21}+\omega_L)t}\hat{b}^\dagger u^*(\mathbf{R})\right)\\ &- \hat{A}_{12}\mathbf{d}_{12}\left(i\sqrt{\frac{\hbar\omega_L}{2\varepsilon_0}}\mathbf{e}e^{-it(\omega_{21}+\omega_L)}\hat{b}u(\mathbf{R}) - i\sqrt{\frac{\hbar\omega_L}{2\varepsilon_0}}\mathbf{e}e^{i\Delta\omega t}\hat{b}^\dagger u^*(\mathbf{R})\right),\end{aligned} \tag{4.10}$$

with $\Delta\omega = \omega_L - \omega_{21}$. As the electromagnetic field frequency ω_L is considered close to resonance with the dipole transition frequency ω_{21}, we have $\Delta\omega \ll \omega_L + \omega_{21}$. Thus, as on any considerable time scale the fast oscillations of counter propagating rotation $e^{it(\omega_L+\omega_{21})}$ cancel to zero, we can apply the rotating wave approximation and neglect these terms, i.e., $e^{it(\omega_L+\omega_{21})} \approx 0$. Subsequently moving back to the Schrödinger picture yields the interaction Hamiltonian in the dipole and rotating wave approximation

$$\hat{H}_{\text{int}} = \kappa\hat{A}_{21}\hat{b} + \kappa^*\hat{A}_{12}\hat{b}^\dagger, \tag{4.11}$$

where the coupling constant $\kappa = \left(-i\sqrt{\frac{\hbar\omega_L}{2\varepsilon_0}}\mathbf{d}_{21}\mathbf{e}u(\mathbf{R})\right)$ is defined in terms of the projection of the dipole matrix element of the transition on the electromagnetic field in the position of the atom.

Adding the unperturbed Hamiltonians and the interaction Hamiltonian then yields the Jaynes-Cummings Hamiltonian for cavity quantum electro dynamics [60]

$$\begin{aligned}\hat{H} &= \hat{H}_{\mathrm{A}} + \hat{H}_{\mathrm{F}} + \hat{H}_{\mathrm{int}} \\ &= \hbar\omega_{21}\hat{A}_{22} + \hbar\omega_L\hat{b}^\dagger\hat{b} + \kappa\hat{A}_{21}\hat{b} + \kappa^*\hat{A}_{12}\hat{b}^\dagger. \end{aligned} \tag{4.12}$$

This model is valid in a strong coupling regime (i.e., $|\kappa|$ is much bigger than the leaking rate and the spontaneous emission rate to other cavity modes). Thus, high-Q cavities are needed.

4.2 Jaynes-Cummings dynamics of an ion in a Paul trap

We now want to consider another model of Jaynes-Cummings type. If an ion is caught in a Paul trap, its motion can be described in a quantized manner, see Refs. [83–85] or Chap. 13 of Ref. [2]. The resulting states of the ion are referred to as motional or vibrational states. Via the interaction of the ion with optical radiation, e.g. a laser, the generation of a plethora of motional states became feasible [87, 89–97].

The full dynamics describing the interaction of an ion with a laser is rather complicated and can in general only be solved numerically. However, under certain but realistic approximations the interaction Hamiltonian of the system can be simplified to a nonlinear generalization of the Jaynes-Cummings Hamiltonian [86]. In the following we will give the derivation of this model. For the case of a strong coherent pump we will obtain a time dependent Hamiltonian for the CJCD. The derivations in this section follow closely those in Ref. [2] and Ref. [23].

4.2.1 Harmonic quantization of effective ion dynamics in a Paul trap

In a Paul trap [81,82] single ions can be confined by an oscillating electromagnetic quadrupole field. In the usual configuration for a three dimensional Paul trap a direct-current voltage and a radio-frequency voltage with frequency ω_{rf} are applied between a ring electrode and two end-cap electrodes. A schematic illustration of the scenario under consideration is depicted in Fig. 4.1. An ion in the trap will then be subject to a time dependent potential that can be described in terms of Mathieu type equations. If the trap is configured such that the corresponding Mathieu equations have stable solutions, one can separate the ion-motion into a fast oscillating part of frequency ω_{rf} and a slow oscillating part of frequency ν_ℓ for each of the principal axis x_ℓ with $\ell = 1, 2, 3$ of the Paul trap geometry. Under the condition that $\nu_\ell \ll \omega_{\mathrm{rf}}$ one

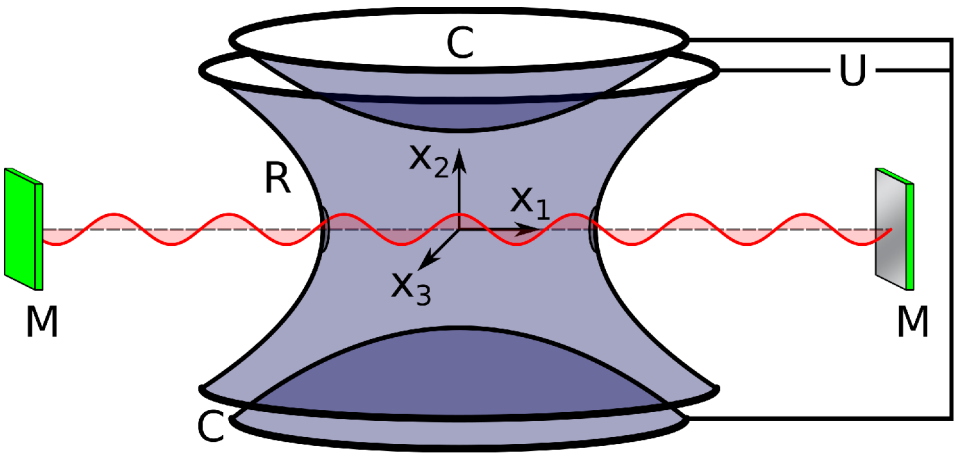

Figure 4.1: Draft scheme of a a Paul trap with a cavity. Between the end caps (C) and the ring electrode (R) an alternating current is applied. A standing wave field is present in the trap, which is confined by an external cavity that is formed by mirrors (M).

can average over the fast oscillations which then leads to the effective potential in the trap [2]

$$V(x_1, x_2, x_3) = \sum_{\ell=1}^{3} \frac{1}{2} m \nu_\ell^2 x_\ell^2. \tag{4.13}$$

As this is essentially a harmonic oscillator potential, quantization is straight forwards and one can introduce the canonical operators

$$\hat{x}_\ell = \sqrt{\frac{\hbar}{2m\nu_\ell}} \left[\hat{a}_\ell^\dagger + \hat{a}_\ell\right], \qquad \hat{p}_\ell = i\sqrt{\frac{\hbar m \nu_\ell}{2}} \left[\hat{a}_\ell^\dagger - \hat{a}_\ell\right], \tag{4.14}$$

with the annihilation(creation) operators $\hat{a}_k(\hat{a}_\ell^\dagger)$ that fulfill bosonic commutator relations

$$[\hat{a}_\ell, \hat{a}_{\ell'}^\dagger] = \delta_{\ell,\ell'}\hat{1}, \qquad [\hat{a}_\ell, \hat{a}_{\ell'}] = [\hat{a}_\ell^\dagger, \hat{a}_{\ell'}^\dagger] = 0, \tag{4.15}$$

such that

$$[\hat{x}_\ell, \hat{p}_{\ell'}] = \delta_{\ell,\ell'} i\hbar\hat{1}, \qquad [\hat{x}_\ell, \hat{x}_{\ell'}] = [\hat{p}_\ell, \hat{p}_{\ell'}] = 0. \tag{4.16}$$

The free motion Hamiltonian for the center of mass of the ion in the Paul trap then takes the form of a three dimensional harmonic oscillator [2]

$$\hat{H}_{\text{CM}} = \sum_{\ell=1}^{3} \hbar\nu_\ell \left(\hat{a}_\ell^\dagger \hat{a}_\ell + \frac{1}{2}\hat{1}\right). \tag{4.17}$$

4.2.2 Ion-standing wave interaction along a principal axis of the trap

We now consider the interaction of the ion with a standing wave optical field along one of the principal axis $k = 1, 2, 3$ of the trap. As the effective trap potential yields harmonic oscillator dynamics for the charged center of mass it can be resonantly driven by electromagnetic fields close to the trap potential frequency – usually in the radio frequency range [2]. We are not interested in this kind of interaction. Instead, as in the case of the standard Jaynes-Cummings model we are interested in the two-level dipole interactions that take place at optical frequencies. The two-level system is then again described as

$$\hat{H}_{\mathrm{A}} = \hbar\omega_{21}\hat{A}_{22} \tag{4.18}$$

and we may again describe interaction in terms of the dipole approximation

$$\hat{H}_{\mathrm{int}} = -\hat{\mathbf{d}}\hat{\mathbf{E}}(\hat{\mathbf{R}}), \tag{4.19}$$

where now however the center of mass position $\hat{R} = (\hat{x}_1, \hat{x}_2, \hat{x}_3)^T$ of the ion is also quantized. Again, we consider only one resonant mode ω_L of the electromagnetic field

$$\hat{\mathbf{E}}(\hat{\mathbf{R}}) = i\sqrt{\frac{\hbar\omega_L}{2\varepsilon_0}}\mathbf{e}\hat{b}u(\hat{\mathbf{R}}) + \mathrm{H.c.}. \tag{4.20}$$

The frequency ω_L will be specified further below. The corresponding unperturbed Hamiltonian of the field

$$\hat{H}_{\mathrm{F}} = \hbar\omega_L\hat{b}^\dagger\hat{b} \tag{4.21}$$

remains unaffected by the quantization of the atom position.

As the operator $\hat{\mathbf{R}}$ appears in the mode function $u(\hat{\mathbf{R}})$ we need to specify the mode function. For simplicity, we consider the scenario of a perfect coplanar cavity, where the mode function takes form of a standing plane wave. This can be written as

$$u(\mathbf{R}) = \sqrt{\frac{2}{V}}\cos(\mathbf{k}_L\mathbf{R} + \Delta\phi), \tag{4.22}$$

where $\Delta\phi$ accounts for offset in the position of cavity field and Paul trap potential. The wave vector is taken such that it points in direction of one of the principal axis of the trap. Without loss of generality we set $\mathbf{k}_L = k_L\mathbf{e}_1$ such that $\mathbf{k}_L\mathbf{R} = k_L\hat{x}_1$ and drop the index in the following. The interaction Hamiltonian then takes the form

$$\hat{H}_{\mathrm{int}} = -\left(\mathbf{d}_{21}\hat{A}_{21} + \mathbf{d}_{12}\hat{A}_{12}\right)\cos(\eta(\hat{a} + \hat{a}^\dagger) + \Delta\phi)\sqrt{\frac{\hbar\omega_L}{V\varepsilon_0}}\mathbf{e}i\left[\hat{b} - \hat{b}^\dagger\right], \tag{4.23}$$

with the Lamb-Dicke parameter $\eta = k_L\sqrt{\frac{\hbar}{2m\nu}}$ (cf. [2]). We also drop the corresponding indices and the vacuum contributions from the center of mass Hamiltonian, i.e.,

$$\hat{H}_{\text{CM}} = \hbar\nu\hat{a}^\dagger\hat{a}, \tag{4.24}$$

as they are not relevant to the interaction.

Naturally, the trap frequencies ν are much smaller than the optical frequencies $\nu \ll \omega_{21}$. We are interested in the scenario where vibrational bands can be resolved very well, such that we can bring the laser in quasi resonance with the kth sideband $k\nu$, i.e., such that $\omega_L = \omega_{21} - k\nu + \Delta\omega$ where the detuning $\Delta\omega$ is only small compared to the vibrational band-separation $\Delta\omega \ll \nu$. Thus, if we apply the expansion [23]

$$\cos(\eta(\hat{a}+\hat{a}^\dagger)+\Delta\phi) = \frac{1}{2}e^{-\eta^2/2}\sum_{l,m=0}^{\infty}\frac{1}{l!m!}\left[e^{i\Delta\phi}(i\eta)^{l+m} + e^{-i\Delta\phi}(-i\eta)^{m+l}\right]\hat{a}^{\dagger l}\hat{a}^m \tag{4.25}$$

to (4.23), we can apply a rotating wave approximation – for details see Appendix D – which yields

$$\hat{H}_{\text{int}} = \hbar\tilde{\kappa}\hat{f}_k(\hat{a}^\dagger\hat{a};\eta)\hat{a}^k\hat{b}\hat{A}_{21} + \text{H.c.}, \tag{4.26}$$

with the Hermitian operator [23]

$$\hat{f}_k(\hat{a}^\dagger\hat{a};\eta) = \frac{1}{2}e^{i\Delta\phi-\eta^2/2}\sum_{l=0}^{\infty}\frac{\hat{a}^{\dagger l}\hat{a}^l}{(l+k)!l!}(i\eta)^{2l+k} + \text{H.c.} \tag{4.27}$$

and the coupling constant $\tilde{\kappa} = -i\sqrt{\frac{\omega_L}{\hbar V\varepsilon_0}}\,(\mathbf{d}_{21}\mathbf{e})$.

4.2.3 Classically driven system

Above, the fully quantized Jaynes-Cummings dynamics of a trapped Ion model has been derived. We now consider the scenario of strong coherent pump, i.e., a scenario where the process is classically driven. To this purpose, we transform (4.26) to the interaction picture in terms of $\hat{U} = e^{-\frac{it}{\hbar}\left[\hat{H}_{\text{F}}+\hat{H}_{\text{A}}+\hat{H}_{\text{CM}}\right]}$ which yields

$$\hat{\tilde{H}}_{\text{int}}(t) = \hat{U}^\dagger(t)\hat{H}_{\text{int}}\hat{U}(t) = \hbar\tilde{\kappa}e^{-it\Delta\omega}\hat{f}_k(\hat{a}^\dagger\hat{a};\eta)\hat{a}^k\hat{b}\hat{A}_{21} + \text{H.c.}. \tag{4.28}$$

Considering that the pump $\hat{b}$ is in a coherent state of high amplitude allows us to replace $\hat{b}$ by the constant coherent amplitude β_{cl} in the interaction picture. This then yields the CJCD

model [23]:

$$\begin{aligned}\hat{\tilde{H}}_{\text{int}}(t) &= \hbar\tilde{\kappa}e^{-it\Delta\omega}\hat{f}_k(\hat{a}^\dagger\hat{a};\eta)\hat{a}^k\beta_{\text{cl}}\hat{A}_{21} + \text{H.c.} \\ &= \hbar|\kappa|e^{-i\Delta\omega t+i\theta}\hat{A}_{21}\hat{f}_k(\hat{a}^\dagger\hat{a};\eta)\hat{a}^k + \text{H.c.},\end{aligned} \tag{4.29}$$

where we have defined $\kappa = \tilde{\kappa}\beta_{\text{cl}}$ and $\theta = \arg(\kappa)$. The corresponding scheme is depicted in Fig. 4.2. Note, that via $\hat{f}_k(\hat{a}^\dagger\hat{a};\eta)$ a nonlinear dependence of $\hat{\tilde{H}}_{\text{int}}$ – and thereby of the dynamics – on the excitation of the vibrational mode is obtained [97][1].

The operator $\hat{f}_k(\hat{a}^\dagger\hat{a};\eta)$ can be represented in the Fock basis of motional states as [23]

$$\hat{f}_k(\hat{a}^\dagger\hat{a};\eta) = \frac{1}{2}e^{i\Delta\phi-\eta^2/2}\sum_{n=0}^{\infty}|n\rangle\langle n|\frac{(i\eta)^k n!}{(n+k)!}L_n^{(k)}(\eta^2) + \text{H.c.}, \tag{4.30}$$

with $L_n^{(k)}$ denoting the generalized Laguerre polynomials (cf. [126]). Additionally, the Hamiltonian of the free motion reads

$$\hat{H}_0 = \hbar\nu\hat{a}^\dagger\hat{a} + \hbar\omega_{21}\hat{A}_{22}. \tag{4.31}$$

Summarized, the Hamiltonian in Eq. (4.29) describes the nonlinear kth sideband coupling $|1,n\rangle \leftrightarrow |2,n-k\rangle$.

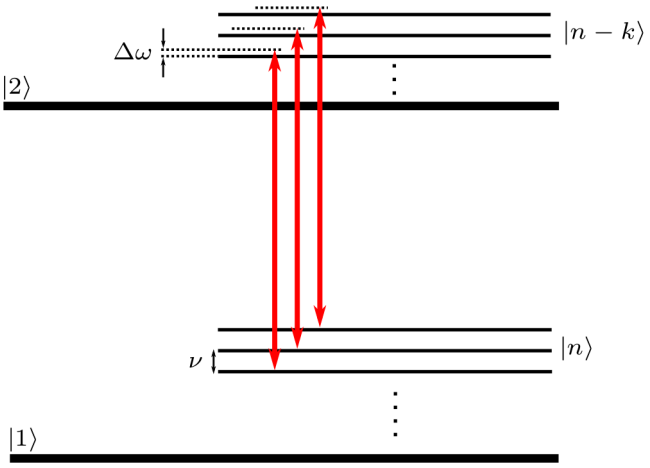

Figure 4.2: Scheme of the physical system described by the interaction Hamiltonian in Eq. (4.29). The electronic ground state, denoted with $|1\rangle$ and the corresponding excited state, labeled with $|2\rangle$, are separated by the electronic transition frequency $\omega_{21} = \omega_2 - \omega_1$. Due to the in good approximation harmonic trap potential the vibrational levels are equidistantly separated by the trap frequency ν. The frequency of the driving laser (red arrows) is detuned from the kth sideband by $\Delta\omega$. That is, $\omega_L = \omega_{21} - k\nu + \Delta\omega$. Figure by F. Krumm as presented in Ref. [59].

[1] Thus, the model is also referred to as nonlinear Jaynes-Cummings dynamics is the literature [23, 59, 86].

4.2.4 Time evolution

The time-dependent dynamics of system is governed by the evolution operator $\hat{\mathcal{U}}(t,t_0)$ which fulfills the standard Schrödinger equation

$$\frac{\partial}{\partial t}\hat{\mathcal{U}}(t,t_0) = -\frac{i}{\hbar}\hat{H}_{\text{int}}(t)\hat{\mathcal{U}}(t,t_0). \tag{4.32}$$

Note that in Eq. (4.32) the factor $1/\hbar$ always compensates the factor $\hbar$ in the Hamiltonian $\hat{H}$. To ovoid superfluous coefficients we introduce the notation

$$\hat{H}_{\text{int}}(t) = |\kappa|\hbar\hat{\mathcal{H}}(t), \tag{4.33}$$

in terms of the dimensionless Hamiltonian $\hat{\mathcal{H}}$ [cf. Eq. (4.29)] which also enables us to track the dependencies on the coupling strength $|\kappa|$ throughout the following. The reformulated evolution equation,

$$\partial_t\hat{\mathcal{U}}(t,t_0) = -i|\kappa|\hat{\mathcal{H}}(t)\hat{\mathcal{U}}(t,t_0), \tag{4.34}$$

corresponds to (1.85) with $\gamma = |\kappa|$ and thus the ME can be applied as described in Sec. 1.4.2.

4.3 Exact solution of the dynamics

In the case of type-I PDC with a monochromatic pump treated in Chapter 2, the analytical solution for the dynamics has been known for quite a while, cf. [26]. As of recently, an analytical solution for the time evolution of the nonstationary CJCD with detuning – as also considered in Ref. [23] – was not known. As part of the work leading to the present contribution I was able to derive such an analytical solution, which has been subsequently presented in Ref. [59]. In the following we demonstrate how to derive this solution to Eq. (4.34), i.e., a time integral free representation of (1.88) for the Hamiltonian (4.29) that includes all time ordering effects.

4.3.1 Decoupling the evolution equation

From the dimensionless Fock basis representation of the Hamiltonian (4.29)

$$\hat{\mathcal{H}}(t) = \sum_{n=0}^{\infty}\omega_n\left[e^{-i\Delta\omega t}e^{i\theta}|2,n\rangle\langle 1,n+k| + \text{H.c}\right],$$
$$\text{with } w_n = \cos\left(\Delta\phi + \frac{\pi}{2}k\right)\eta^k e^{-\eta^2/2}\sqrt{\frac{n!}{(n+k)!}}L_n^{(k)}(\eta^2), \tag{4.35}$$

we can see, that the interaction is entirely described in terms of projectors constructed from the states $|2,n\rangle$ and $|1,n+k\rangle$ with equal $n=0,1,\ldots$.

A compact notation for such projectors can be formulated in terms of the spinors

$$\Psi_n = \begin{pmatrix} \langle 2,n|e^{-i\theta/2} \\ \langle 1,n+k|e^{i\theta/2} \end{pmatrix} \Leftrightarrow \Psi_n^\dagger = \begin{pmatrix} e^{i\theta/2}|2,n\rangle \\ e^{-i\theta/2}|1,n+k\rangle \end{pmatrix}^T. \tag{4.36}$$

These spinors fulfill a orthogonality relation

$$\Psi_n \Psi_{n'}^\dagger = \delta_{n,n'}\mathbf{I}, \text{ with } \mathbf{I} = \begin{pmatrix} 1 & 0 \\ 0 & 1 \end{pmatrix} \tag{4.37}$$

and allow us to formulate a completeness relation as, cf. [23]

$$\hat{1} = \sum_{n=0}^{\infty} \Psi_n^\dagger \mathbf{I} \Psi_n + \sum_{q=0}^{k-1} |1,q\rangle\langle 1,q|. \tag{4.38}$$

By applying this completeness relation, the Hamiltonian (4.35) can be written in the compact form

$$\hat{\mathcal{H}}(t) = \sum_{n=0}^{\infty} \Psi_n^\dagger \mathbf{H}_n(t) \Psi_n, \tag{4.39}$$

with

$$\mathbf{H}_n(t) = \begin{pmatrix} 0 & w_n e^{-i\Delta\omega t} \\ w_n e^{i\Delta\omega t} & 0 \end{pmatrix}. \tag{4.40}$$

From the quasi-diagonal form of the Hamiltonian in the spinor basis it may be hypothesized that any evolution of the system will also be representable in this basis. Thus, a similarity ansatz for the evolution operator,

$$\hat{\mathcal{U}}(t,t_0) = \sum_{n=0}^{\infty} \Psi_n^\dagger \mathbf{U}_n(t,t_0) \Psi_n + \sum_{q=0}^{k-1} |1,q\rangle\langle 1,q|, \tag{4.41}$$

with $\mathbf{U}_n(t,t_0) \in \mathbb{C}^{2\times 2}$ and initial condition $\mathbf{U}_n(t,t_0)|_{t=t_0} = \mathbf{I}$, is suitable. Substituting (4.39) and (4.41) into (4.34) decouples the evolution equation in terms of the 2×2 matrix differential equations

$$\partial_t \mathbf{U}_n(t,t_0) = -i|\kappa|\mathbf{H}_n(t)\mathbf{U}_n(t,t_0), \tag{4.42}$$

for $n = 0, 1, \ldots$.

4.3.2 Solving the evolution equation

The time-dependent coefficient matrix (4.40) is representable as linear combination of Pauli matrices that (multiplied by the imaginary unit i) generate the Lie-group SU(2). Thus, solutions to (4.42) are always representable as

$$\mathbf{U}_n(t, t_0) = \begin{pmatrix} a_n(t, t_0) & b_n(t, t_0) \\ -b_n^*(t, t_0) & a_n^*(t, t_0) \end{pmatrix}, \tag{4.43}$$

where

$$|a_n(t, t_0)|^2 + |b_n(t, t_0)|^2 = 1. \tag{4.44}$$

Note, that in the treatment of parametric down conversion with monochromatic pumps, the solutions to matrix differential equations with parameter dependent coefficients of similar form are known [24, 26] – see also chapter 2.

To solve the matrix differential equations

$$\partial_t \mathbf{U}_n(t, t_0) = -i \begin{pmatrix} 0 & |\kappa| w_n e^{-i\Delta\omega t} \\ |\kappa| w_n e^{i\Delta\omega t} & 0 \end{pmatrix} \mathbf{U}_n(t, t_0), \tag{4.45}$$

with initial condition $\mathbf{U}_n(t, t_0)|_{t=t_0} = \mathbf{I}$ we write

$$\begin{pmatrix} 0 & |\kappa| w_n e^{-i\Delta\omega t} \\ |\kappa| w_n e^{i\Delta\omega t} & 0 \end{pmatrix} = \mathbf{S}^\dagger(t) \begin{pmatrix} 0 & |\kappa| w_n \\ |\kappa| w_n & 0 \end{pmatrix} \mathbf{S}(t), \text{ with } \mathbf{S}(t) = \begin{pmatrix} e^{i\Delta\omega t/2} & 0 \\ 0 & e^{-i\Delta\omega t/2} \end{pmatrix}, \tag{4.46}$$

such that

$$\mathbf{S}(t)\partial_t \mathbf{U}_n(t, t_0) = -i \begin{pmatrix} 0 & |\kappa| w_n \\ |\kappa| w_n & 0 \end{pmatrix} \mathbf{S}(t)\mathbf{U}_n(t, t_0). \tag{4.47}$$

Adding the term $[\partial_t \mathbf{S}(t)]\,\mathbf{U}_n(t,t_0)$ on both sides of the equation, applying the product rule on the left hand side, and executing the derivative

$$\partial_t \mathbf{S}(t) = -i \begin{pmatrix} -\Delta\omega/2 & 0 \\ 0 & \Delta\omega/2 \end{pmatrix} \mathbf{S}(t) \tag{4.48}$$

on the right hand side yields the constant parameter differential equation

$$\partial_t \left[\mathbf{S}(t)\mathbf{U}_n(t,t_0)\right] = -i \begin{pmatrix} -\Delta\omega/2 & |\kappa|w_n \\ |\kappa|w_n & \Delta\omega/2 \end{pmatrix} \left[\mathbf{S}(t)\mathbf{U}_n(t,t_0)\right], \tag{4.49}$$

with initial condition $[\mathbf{S}(t)\mathbf{U}_n(t,t_0)]|_{t=t_0} = \mathbf{S}(t_0)$. The solution is easily found as

$$[\mathbf{S}(t)\mathbf{U}_n(t,t_0)] = \exp\left\{-i(t-t_0)\begin{pmatrix} -\Delta\omega/2 & |\kappa|w_n \\ |\kappa|w_n & \Delta\omega/2 \end{pmatrix}\right\} \mathbf{S}(t_0), \tag{4.50}$$

which leads to

$$\mathbf{U}_n(t,t_0) = \mathbf{S}^\dagger(t) \exp\left\{-i(t-t_0)\begin{pmatrix} -\Delta\omega/2 & |\kappa|w_n \\ |\kappa|w_n & \Delta\omega/2 \end{pmatrix}\right\} \mathbf{S}(t_0) = \begin{pmatrix} a_n(t,t_0) & b_n(t,t_0) \\ -b_n^*(t,t_0) & a_n^*(t,t_0) \end{pmatrix}, \tag{4.51}$$

with

$$\begin{aligned} a_n(t,t_0) &= e^{-i\Delta\omega[t-t_0]/2}\left[\cos(\Gamma_n[t-t_0]) + \frac{i\Delta\omega}{2\Gamma_n}\sin(\Gamma_n[t-t_0])\right] \\ b_n(t,t_0) &= e^{-i\Delta\omega[t+t_0]/2}\frac{|\kappa|w_n}{i\Gamma_n}\sin(\Gamma_n[t-t_0]), \end{aligned} \tag{4.52}$$

for $n = 0, 1, \ldots$ and $\Gamma_n = \sqrt{\left(\frac{\Delta\omega}{2}\right)^2 + w_n^2|\kappa|^2}$. In Ref. [23] an approximated solution was found in terms of neglected time ordering – i.e., in terms of (1.94). Here, we have found an analytic expression that incorporates all time ordering corrections, i.e., an explicit representation of the time ordered exponential (1.88) for the Hamiltonian (4.29) (cf. [59]), with $\Gamma_n = \sqrt{\left(\frac{\Delta\omega}{2}\right)^2 + w_n^2|\kappa|^2}$.

These analytic expression allows us, e.g., to obtain the dynamics of the population probability of the excited electronic state,

$$\sigma_{22}(t,t_0) = \sum_{n=0}^{\infty} \langle 2,n|\hat{\mathcal{U}}(t,t_0)e^{-\frac{i}{\hbar}\hat{H}_0(t-t_0)}\hat{\rho}(t_0)e^{\frac{i}{\hbar}\hat{H}_0(t-t_0)}\hat{\mathcal{U}}^\dagger(t,t_0)|2,n\rangle, \tag{4.53}$$

and to compare it to the dynamics with neglected time ordering. This is illustrated in Fig. 4.3. Note that this is a reproduction of results that have been obtained numerically in Ref. [23]. Here however all results for the exact dynamics are based on analytical expressions. The discrepancy between the dynamics with neglected time ordering and exact dynamics was already pointed out in Ref. [23].

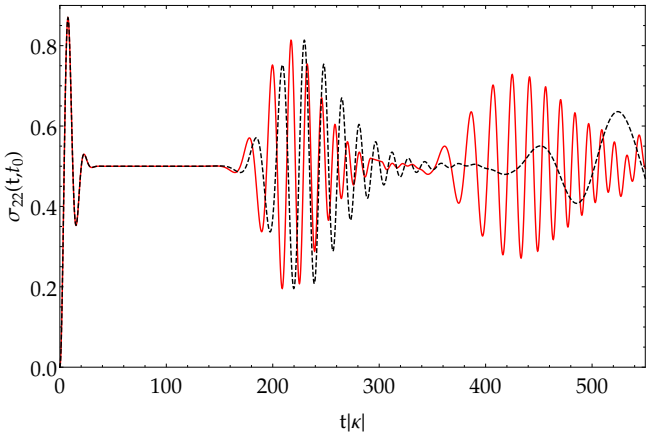

Figure 4.3: The population probability of the excited electronic state $\sigma_{22}(t,t_0)$ as given in Eq. (4.53) obtained from the exact analytical solution for $\hat{\mathcal{U}}$ (red, solid) and for neglected time ordering (black, dashed) with the initial state $\hat{\rho}^{(1)}(t_0=0)=|1,\alpha_0\rangle\langle 1,\alpha_0|$. Here, parameters have been chosen as, $\Delta\omega/|\kappa|=0.005$, $\Delta\phi=0$, $k=2$, and $\eta=0.2$. The displayed result is a reproduction (and verification) of Fig.2 in Ref. [23] – where results of the exact dynamics were obtained numerically – by means of the analytical expression (4.53). In this form it has also been presented in Ref. [59].

4.4 Time-ordering corrections

One may now be interested in how different orders of time ordering affect the temporal evolution of the system under study. Using the orthogonality (4.37) of our spinor formalism (4.36) it is easy to show that the non-equal time commutators of (4.39) fulfill

$$[\hat{\mathcal{H}}(t),\hat{\mathcal{H}}(t')]=\sum_{n=0}^{\infty}\Psi_n^{\dagger}[\mathbf{H}_n(t),\mathbf{H}_n(t')]\Psi_n. \tag{4.54}$$

Consequently, there is a one-to-one correspondence to the non-equal time commutators of the matrices $\mathbf{H}_n$. Thus it follows, that the ℓth order MA to the solution of (4.34) corresponds exactly to the result one obtains by evaluating the ℓth order MA to the solution of Eq. (4.42).

Due to the one-to-one correspondence (4.54), the Magnus terms take the same form as in the operator formulation [cf. (1.93)] such that, e.g., the first-order terms read as

$$\mathbf{M}_n^{[1]}(t,t_0)=\int_{t_0}^{t}dt_1\,\mathbf{H}_n(t_1). \tag{4.55}$$

As in the case of type-I PDC with a monochromatic pump, the anti-diagonal coupling matrix (4.40) leads to a different structure in odd and even orders of MA, i.e.,

$$\ell \text{ odd} : \mathbf{M}_n^{[\ell]}(t,t_0) = w_n^\ell [t-t_0]^\ell f_\ell\left(\frac{\Delta\omega[t-t_0]}{2}\right)\begin{pmatrix} 0 & e^{-i\Delta\omega[t+t_0]/2} \\ e^{i\Delta\omega[r+r_0]/2} & 0 \end{pmatrix},$$
$$\ell \text{ even} : \mathbf{M}_n^{[\ell]}(t,t_0) = i w_n^\ell [t-t_0]^\ell f_\ell\left(\frac{\Delta\omega[t-t_0]}{2}\right)\begin{pmatrix} 1 & 0 \\ 0 & -1 \end{pmatrix}. \tag{4.56}$$

Evaluating the first three order terms according to (1.93) yields the functions

$$f_1(z) = j_0(z), \qquad f_2(z) = \frac{1}{2}\left[j_1(z)\cos(z) - j_0(z)\sin(z)\right],$$
$$\text{and } f_3(z) = \frac{1}{6}\left[-j_0^3(z) + j_0(z) + j_2(z)\right], \tag{4.57}$$

that are defined in terms of the pole-free spherical Bessel functions $j_0(z) = \mathrm{sinc}(z)$. Additionally, the 4th order Magnus term

$$\begin{aligned} f_4(z) =& \frac{1}{12}\left[\frac{1}{2}j_0^2(z)\sin(2z) - \frac{1}{2}j_0(z)\sin(z) - \frac{1}{2}j_1^2(z)\sin(2z) - \frac{1}{2}j_2(z)\sin(z)\right. \\ & \left. - j_1(z)j_0(z)\cos(2z) + \frac{3}{10}j_1(z)\cos(z) + \frac{3}{10}j_3(z)\cos(z)\right], \end{aligned} \tag{4.58}$$

and the 5th order Magnus term

$$\begin{aligned} f_5(z) =& \frac{1}{60}\left[\frac{j_0(z)}{2} + \frac{5j_2(z)}{7} + \frac{3j_4(z)}{14} + 2j_1^2(z)j_0(z)\sin^2(z) - \frac{13}{6}j_1(z)j_0(z)\sin(z)\right. \\ & - \frac{1}{2}j_3(z)j_0(z)\sin(z) - \frac{5}{3}j_1(z)j_2(z)\sin(z) + 2j_0^3(z)\cos^2(z) - \frac{5}{2}j_0^2(z)\cos(z) \\ & \left. - \frac{5}{2}j_2(z)j_0(z)\cos(z) + 4j_1(z)j_0^2(z)\sin(z)\cos(z)\right], \end{aligned} \tag{4.59}$$

have been evaluated in terms of the corresponding expressions given in Refs. [18] and [25] respectively. Evaluating the matrix exponentials, e.g., in second order,

$$\mathbf{U}_n^{[2]}(t,t_0) = e^{-i|\kappa|\mathbf{M}_n^{[1]}(t,t_0) - |\kappa|^2\mathbf{M}_n^{[2]}(t,t_0)}, \tag{4.60}$$

yields the MAs for $a_n(t,t_0)$ and $b_n(t,t_0)$, i.e., $a_n^{[\ell]}(t,t_0)$ and $b_n^{[\ell]}(t,t_0)$.

Let us once again emphasize, that the ME series (4.64) may not always converge [18]. However, one can show that the ME (4.64) converges for [18]

$$|\kappa| \int_{t_0}^{t} d\tilde{t}\, ||\mathbf{H}_n(\tilde{t})||_2 = |\kappa w_n|[t-t_0] < \pi, \tag{4.61}$$

where $||\cdots||_2$ denotes the spectral norm [127]. In terms of the full operator (4.41) this means, we can guarantee convergence, as long as $w_{\max}|\kappa|[t-t_0] < \pi$ with $w_{\max} = \max_{n=0,1,\ldots} |w_n|$ [also cf. Eq. (4.35)].

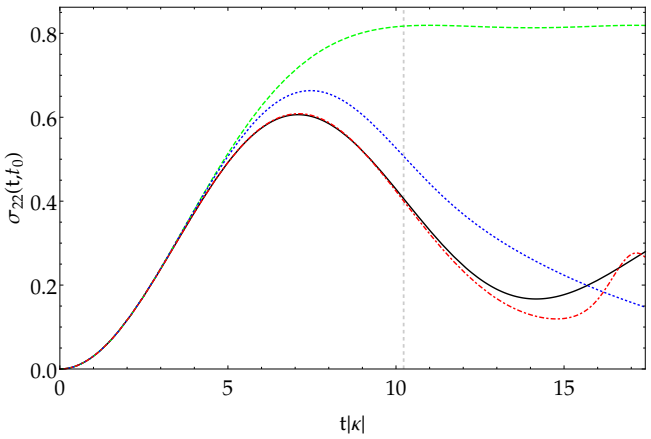

Figure 4.4: The population probability of the excited electronic state $\sigma_{22}(t,t_0)$ as given in Eq. (4.53) obtained from the exact solution for $\hat{\mathcal{U}}$ (black, solid), from the first-order approximation , i.e., neglected time ordering (green, dashed), from the second order approximation (blue, dotted), and from the fifth order approximation (red, dot-dashed) with the initial state $\hat{\rho}^{(2)}(t_0 = 0) = |2,\alpha_0\rangle\langle 2,\alpha_0|$ in the range $0 \leq t|\kappa| < 17.4$. Here, parameters have been chosen as, $\Delta\omega/|\kappa| = 0.224$, $\Delta\phi = \pi/4$, $k = 3$, and $\eta = 0.4$. This implies, that $w_{\max} = 0.307$. A vertical gridline (grey dashed) at $t|\kappa| = \pi/w_{\max}$ marks the region in which the sufficient condition [Eq. (4.61)] guarantees the convergence of the time ordering corrections. In Section 5.1 we develop criteria that allow us to state that the time ordering corrections converge in the full displayed range. Figure as presented in Ref. [59].

The upper bound (4.61) is nonetheless only a sufficient criterion for convergence. In Fig. 4.4 we give an illustrative example of convergence well above this upper bound. Here we compare the population probability of the excited electronic state (4.53) in different orders of time ordering corrections to the exact solution. The quality of approximation seemingly also improves above the bound (4.61). In Chapter 5 we will show that the ME indeed converges for all values of time displayed in this figure. Moreover the displayed timerange corresponds to the exact upper limit of convergence of time ordering corrections.

4.4.1 Generating function

The analytic solutions in Eq. (4.52) allow for the explicit formulation of the full ME. This means, we can bring (4.43) in exponential form as

$$\mathbf{U}_n(|\kappa|) = \exp\{-i\mathbf{M}_n(|\kappa|)\}\,. \tag{4.62}$$

Here and in the following we drop the time-dependence of the matrices from our notation and consider the appearing parameters as functions of the coupling parameter $|\kappa|$.

Evaluating the matrix exponential under application of the unitary condition (4.44) shows that the matrix-exponent can be chosen in the form

$$\mathbf{M}_n(|\kappa|) = \frac{\arccos(\mathrm{Re}(a_n(|\kappa|)))}{\sqrt{1-\mathrm{Re}^2(a_n(|\kappa|))}} \begin{pmatrix} -\mathrm{Im}(a_n(|\kappa|)) & ib_n(|\kappa|) \\ -ib_n^*(|\kappa|) & \mathrm{Im}(a_n(|\kappa|)) \end{pmatrix}. \tag{4.63}$$

This matrix can now serve as a generating function for the different orders of time ordering corrections, i.e., a Taylor series expansion of $\mathbf{M}_n(|\kappa|)$ in terms of $|\kappa|$ around $|\kappa| = 0$ yields the ME as

$$\mathbf{M}_n(|\kappa|) = i\sum_{\ell=1}^{\infty}(-i|\kappa|)^\ell \mathbf{M}_n^{[\ell]}, \tag{4.64}$$

where

$$\mathbf{M}_n^{[\ell]} = \frac{i^{\ell-1}}{\ell!} \left.\frac{d^\ell \mathbf{M}_n(|\kappa|)}{d|\kappa|^\ell}\right|_{|\kappa|=0}. \tag{4.65}$$

The equivalence of these expressions with those obtained from nested commutators, has been verified up to 5th order. The generating function allows us to obtain arbitrary-order time ordering corrections (in terms of arbitrary-order MAs).

Chapter 5

Convergence analysis of ordering corrections

Contents

In the preceding chapters we have analyzed (time) ordering effects in different quantum optical systems by applying the ME and MA. As pointed out at several occasions above, the ME neatly separates the part with neglected (time) ordering effects from the time ordering corrections. However, we have also noted that the application of the ME has several limitations.

In the case of PDC the spatial coordinate z took the role of the time parameter in the perturbative treatment. Consequently, the crystal length corresponds to the total evolution time. Usually the crystal length is a fixed experimental parameter Thus, sufficient criteria for the convergence of MAs for PDC where given in terms of the (maximal) gain parameter [cf. (2.54)]. A similar sufficient upper bound was formulated for the CJCD model in Chapter 4. In this case we considered the pump strength fixed and an upper bound was given in terms of the maximal time for which time ordering corrections converge.

Admittedly, for small scales – i.e., small gain or small times – the ME does always converge but significant deviations caused by the negligence of ordering effects may only arise when one moves to sufficiently large scales where divergence may occur. Thus, the exact knowledge of boundaries for the analysis of ordering effects is imperative. In the case of divergence a comparison of the cases of neglected time ordering with the case of time ordering in terms of the ME will lead to misinterpretations, i.e., unphysical results. In this context, sufficient bounds can be considered non-satisfactory, as the ME series may converge way above these bounds. However, exact upper bounds can generally only be found for cases that have been explicitly constructed to demonstrate this fact (cf. [18]).

In this chapter we will demonstrate how one can obtain exact upper bounds that exceed the sufficient bounds for the two systems considered in this contribution where analytical solutions are at hand. The main idea behind this analysis is to interpret the ME series as a Taylor series in terms of the expansion parameter. If one can associate an analytical continuation of the exponent of the analytical solution, this allows one to determine the radius of convergence of the complex Taylor series in terms of singularities of the exponent. This will first be demonstrated at hands of the Jaynes-Cummings model – this result has been published in Ref. [59]. The analysis for the PDC model will be given subsequently, as it is analogous in many steps – this result has been published in Ref. [58]. These analysis are, to my best knowledge, the first analysis of such exact limits in the context of quantum optical systems.

5.1 Classically driven Jaynes-Cummings dynamics of an ion in a Paul trap

As mentioned above; the sufficient convergence criterion (4.61) for the CJCD may underestimate the actual limits of convergence of ME approximations. As we have treated the CJCD with detuning $\Delta\omega$, one may wonder why the detuning $\Delta\omega$ makes no appearance in the sufficient upper bound criterion (4.61). Sharper bounds seem desirable in the treatment of time ordering corrections and knowing the analytic expression for the exponents (4.63) indeed allows us to perform a more sophisticated analysis.

For these purposes we may substitute $w_n \mapsto \tau_n/(|\kappa|[t-t_0])$ and $\Delta\omega \mapsto 2\Lambda/[t-t_0]$ with the dimensionless parameters τ_n and Λ into (4.63). In this manner we find expressions of the form

$$\begin{aligned} a_n(|\kappa|) &\mapsto \tilde{a}_\Lambda(\tau_n) & b_n(|\kappa|) &\mapsto \tilde{b}_\Lambda(\tau_n), \\ \mathbf{M}_n(|\kappa|) &\mapsto \tilde{\mathbf{M}}_\Lambda(\tau_n),. \end{aligned} \tag{5.1}$$

Applying the chain rule, it is now easy to show that

$$\mathbf{M}_n^{[\ell]} = \frac{\tau_n^\ell}{|\kappa|^\ell}\tilde{\mathbf{M}}_\Lambda^{[\ell]}, \tag{5.2}$$

with the partial derivatives at $\tau_n = 0$

$$\tilde{\mathbf{M}}_\Lambda^{[\ell]} = \frac{i^{\ell-1}}{\ell!}\left.\frac{\partial^\ell \tilde{\mathbf{M}}_\Lambda(\tau_n)}{\partial \tau_n^\ell}\right|_{\tau_n=0}. \tag{5.3}$$

Thus follows, that the ME series (4.64) only converges if the Maclaurin series

$$\tilde{\mathbf{M}}_\Lambda(\tau_n) = i\sum_{\ell=1}^{\infty}(-i\tau_n)^\ell \tilde{\mathbf{M}}_\Lambda^{[\ell]} \tag{5.4}$$

converges. To analyze the convergence of the series (5.4) we consider the matrix elements of $\tilde{\mathbf{M}}_\Lambda(\tau_n)$ as complex functions by replacing $\tau_n \mapsto z$. It is then possible to determine the radii of convergence, $|z| < r_\Lambda$, of these series (cf. [128]) in terms of the singularities of the analytical expressions $\tilde{\mathbf{M}}_\lambda(z)$ in the complex plane [18].

5.1.1 Analytic continuation and convergence radius

The analytic continuation of the matrix exponent to the complex plane has to be carried out with a great deal of care. The replacement $\tau_n \mapsto z$ in the matrix elements of $\tilde{\mathbf{M}}_\Lambda(\tau_n)$ [cf. (5.1)] is performed after the conjugations in (4.63), i.e., z itself is not conjugated. In this manner we get the representations as

$$\tilde{\mathbf{M}}_\Lambda(z) = \frac{\arccos(A_{R,\Lambda}(z))}{\sqrt{1-A_{R,\Lambda}^2(z)}}\begin{pmatrix} -A_{I,\Lambda}(z) & e^{-i\Delta\omega[t+t_0]/2}B_\Lambda(z) \\ e^{i\Delta\omega[t+t_0]/2}B_\Lambda(z) & A_{I,\Lambda}(z)\end{pmatrix}, \tag{5.5}$$

with

$$\begin{aligned} A_{R,\Lambda}(z) &= \cos(\Lambda)\cos(\gamma_\Lambda(z)) + \Lambda\sin(\Lambda)\operatorname{sinc}(\gamma_\Lambda(z)), \\ A_{I,\Lambda}(z) &= -\sin(\Lambda)\cos(\gamma_\Lambda(z)) + \Lambda\cos(\Lambda)\operatorname{sinc}(\gamma_\Lambda(z)), \\ \text{and } B_n(z) &= z\operatorname{sinc}(\gamma_n(z)), \end{aligned} \tag{5.6}$$

where $\gamma_\Lambda(z) = \sqrt{\Lambda^2+z^2}$. Replacing $z \mapsto \tau_n$ in (5.5) yields (4.63). Thus, (5.5) is a continuation of (4.63). It remains to be shown that this is not only any continuation but an analytical continuation.

First, let us note that there is no branching in the functions (5.6) as the square root $\gamma_\Lambda(z)$ only appears in the even $\cos$- and sinc-functions. Furthermore, let us note that with the generating function [129]

$$\frac{1}{Z}\cos\left(\sqrt{Z^2-2ZT}\right) = \sum_{p=0}^{\infty}\frac{T^p}{p!}j_{p-1}(Z) \tag{5.7}$$

of the spherical Bessel functions,

$$\begin{aligned} j_{-1}(Z) &= \frac{\cos(Z)}{Z}, \\ j_p(Z) &= (-Z)^p \left(\frac{1}{Z}\frac{d}{dZ}\right)^p \frac{\sin(Z)}{Z} \text{ for } p = 0, 1, \dots \end{aligned} \tag{5.8}$$

and its derivative in terms of T, we can find the Maclaurin series representations

$$\begin{aligned} \cos\left(\gamma_\Lambda(z)\right) &= \Lambda \sum_{p=0}^{\infty} \frac{1}{p!} \left(\frac{-z^2}{2\Lambda}\right)^p j_{p-1}(\Lambda), \\ \operatorname{sinc}\left(\gamma_\Lambda(z)\right) &= \sum_{p=0}^{\infty} \frac{1}{p!} \left(\frac{-z^2}{2\Lambda}\right)^p j_p(\Lambda), \end{aligned} \tag{5.9}$$

where we have associated $Z = \Lambda$ and $-2ZT = z^2$. We can see that the series are entirely independent of the conjugated complex variable z^*.

With help of $|j_p(Z)| \leq 1$ for $p = 0, 1, \dots$ and $Z \in [0, \infty)$ we can show absolute convergence of these series with upper bounds

$$\begin{aligned} |\cos\left(\gamma_\Lambda(z)\right)| &\leq |\cos(\Lambda)| + \Lambda \left(\exp\left[\frac{|z|^2}{2|\Lambda|}\right] - 1\right), \\ \text{and } |\operatorname{sinc}\left(\gamma(z)\right)| &\leq \exp\left[\frac{|z|^2}{2|\Lambda|}\right]. \end{aligned} \tag{5.10}$$

Thus, the functions $A_{I,\Lambda}(z)$, $A_{R,\Lambda}(z)$, and $B_\Lambda(z)$, defined in (5.6), are analytical functions in the full complex plane $z \in \mathbb{C}$. Thus, singularities of $\tilde{\mathbf{M}}_\Lambda(z)$ can only stem from the factor

$$f(A_{R,\Lambda}(z)) = \frac{\arccos(A_{R,\Lambda}(z))}{\sqrt{1 - A_{R,\Lambda}^2(z)}}. \tag{5.11}$$

Note that

$$f(z) = \frac{dF(z)}{dz}, \text{ with } F(z) = -\frac{1}{2}\arccos^2(z). \tag{5.12}$$

It can be shown that the function $F(z)$ has a branch point at $z = -1$ (but unlike $\arccos(z)$ not at $z = 1$) – a very visual introduction to the concepts of branch points and analytic many-valued functions can be found in Ref. [128]. Consequently $f(z)$ has the same branch point as $F(z)$. Thus, the function $f(A_{R,\Lambda}(z))$ has branch points wherever $A_{R,\Lambda}(z) = -1$, i.e., the branch points of $f(A_{R,\Lambda}(z))$ correspond to the zeros of the analytic function

$$g_\Lambda(z) = A_{R,\Lambda}(z) + 1. \tag{5.13}$$

As we have shown that all other functions appearing in (5.5) are analytic, $\tilde{\mathbf{M}}_\Lambda(z)$ has branch points, where, and only where, $g_\Lambda(z) = 0$. It is well known that, a Taylor expansion of a analytic function will converge to said function within the disc in the complex plane, centered at the point of expansion, whose radius is the distance from the point of expansion to the nearest singularity or branch point; see the formulation of Taylors theorem in Chapter 9, Section II.2 of Ref. [128]. Thus, a series expansion of $\tilde{\mathbf{M}}_\Lambda(z)$ around $z = 0$ will converge for $|z| < r_\Lambda$, where

$$r_\Lambda = \min_{z_0 \in \mathbb{C}: g_\Lambda(z_0)=0} |z_0|. \tag{5.14}$$

This concept is illustrated in Fig. 5.1.

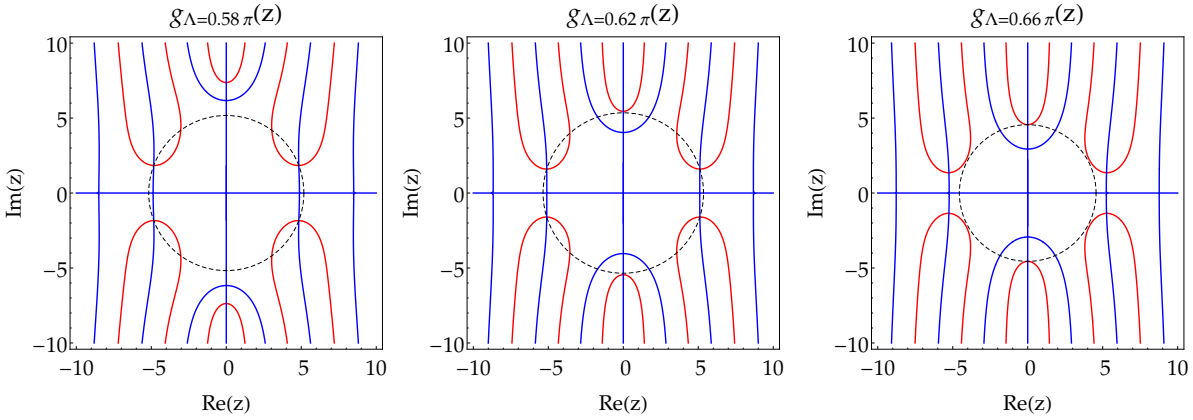

Figure 5.1: The contours $\mathrm{Re}[g_\lambda(z)] = 0$ (red) and $\mathrm{Im}[g_\lambda(z)] = 0$ (blue) for different Λ. A circle (gray, dashed) marks out the radius r_Λ as defined in (5.14) and crosses the minimal absolute value root – where the contours $\mathrm{Re}[g_\lambda(z)] = 0$ and $\mathrm{Im}[g_\lambda(z)] = 0$ intersect – of $g_\Lambda(z)$.

We have evaluated r_Λ in a range of Λ going from $\Lambda = 0.005\pi$ to $\Lambda = 200\pi$ in steps of 0.005π. This was achieved by extracting the line data from the `ContourPlot` function (Contours: $\mathrm{Re}(g_\Lambda(z)) = 0$, $\mathrm{Im}(g_\Lambda(z)) = 0$) in Mathematica to get estimates for the location of the minimal absolute value roots of $g(z)$ which where then refined by the `FindRoot` function in Mathematica.

5.1.2 Exact upper bound for the evolution operator

By determining the radii of convergence [128] r_Λ of these series $|z| < r_\Lambda$ in terms of the singularities of the analytical expressions $\tilde{\mathbf{M}}_\lambda(z)$ in the complex plane [18] we have obtained the exact criterion of convergence (cf. (5.14))

$$|\tau_n| = |\kappa w_n|[t - t_0] < r_\Lambda = r_{\Delta\omega[t-t_0]/2}, \tag{5.15}$$

in terms of time. Note that again w_n appears only as a factor here, thus for the full ME of the full operator (4.41) we may define $w_{\max} = \max_{n=0,1,\dots} |w_n|$. Then the MA for (4.41) converges for

$$0 \leq [t - t_0] < t_{\max}(\Delta\omega) = \min_{\tilde{t}\in\mathbb{R}_+ : |\kappa w_{\max}\tilde{t}| = r_{\Delta\omega\tilde{t}/2}} \tilde{t}, \tag{5.16}$$

where $t_{\max}(\Delta\omega)$ is a function of the detuning. This exact upper bound of convergence is displayed in Fig. 5.2.

Note that it may happen that the series becomes again convergent for $t > t_{\max}(\Delta\omega)$ in regions of t where Eq. (5.15) is fulfilled. However, $t_{\max}(\Delta\omega)$ is the exact upper limit of continuous convergence. Judging from the display of these regions in Fig. 5.2 they do not increase the range of convergence significantly. For large detunings the convergence time increases in a linear fashion. Note that too large detunings may undermine the validity of the model in Eq. (4.29).

Based on this analysis, the detuning $\Delta\omega$ in Fig. 4.4 has been chosen such that the maximal displayed value t corresponds to the first local maximum of $t_{\max}(\Delta\omega)$ in Fig. 5.2. Thus, we can guarantee convergence of the time ordering correction to the exact solution for all ranges of t displayed in Fig. 4.4.

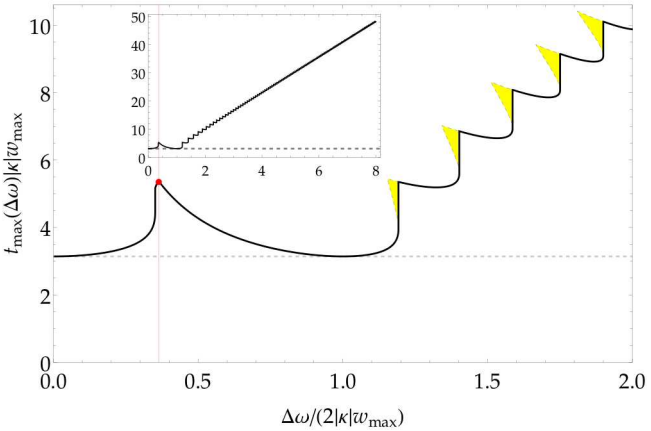

Figure 5.2: The upper bound (black) $t_{\max}(\Delta\omega)$ as a function of the phase-mismatch $\Delta\omega$ as defined in (5.16) – an inset illustrates its global behavior. The constant upper bound estimate (gray, dashed) as defined in (4.61). In the displayed regions (yellow, blue dashed boundary) the ME also converges, however the expansion will diverge in between these times $(t - t_0) > t_{\max}(\Delta\omega)$ and the initial time t_0. A vertical gridline (red) and a point (red) mark the position of the first local maximum of $t_{\max}(\Delta\omega)$. Figure as presented in Ref. [59].

5.2 Parametric down-conversion with a monochromatic pump

As for the CJCD model, we have exact analytical solutions for the evolution of light in the PDC process with a monochromatic pump. The corresponding exponential representation $\mathbf{S} =$

$\exp(-i\mathbf{M})$ of the analytic solution (2.32) reads as

$$\mathbf{M}_\theta(g) = \frac{\operatorname{arccosh}\left(\mathrm{A}_{R,\theta}(\mathrm{g})\right)}{\sqrt{A_{R,\theta}(g)-1}\sqrt{A_{R,\theta}(g)+1}} \begin{pmatrix} -A_{I,\theta}(g)I & ie^{i\theta}e^{i\arg(\sigma)}B_\theta(g)P \\ ie^{-i\theta}e^{-i\arg(\sigma)}B_\theta(g)P & A_{I,\theta}(g)I \end{pmatrix}, \quad (5.17)$$

where we denote explicitly the dependency on the gain exponent g and the phase-mismatch angle θ. The appearing functions in terms of g read as

$$\begin{aligned} A_{R,\theta}(g) &= \left[\cos(\theta)\cosh\left(\sqrt{g^2-\theta^2}\right) + \frac{\theta}{\sqrt{g^2-\theta^2}}\sin(\theta)\sinh\left(\sqrt{g^2-\theta^2}\right)\right], \\ A_{I,\theta}(g) &= \left[\sin(\theta)\cosh\left(\sqrt{g^2-\theta^2}\right) - \frac{\theta}{\sqrt{g^2-\theta^2}}\cos(\theta)\sinh\left(\sqrt{g^2-\theta^2}\right)\right], \\ B_(g) &= \frac{g}{\sqrt{g^2-\theta^2}}\sinh\left(\sqrt{g^2-\theta^2}\right). \end{aligned} \quad (5.18)$$

Note the similarity between (5.17) and (5.5). They differ as θ takes the role of Λ and g takes the role of τ_n. Moreover we have here hyperbolic functions instead of the trigonometric functions in (5.6) and a sign change in the appearing square roots.

Again, it can be shown that the Magnus terms correspond to the terms of the Maclaurin series of $\mathbf{M}_\theta(g)$ in g. Thus, the singularities of an analytical continuation $\mathbf{M}_\theta(g) \mapsto \mathbf{M}_\theta(z)$ with $z \in \mathbb{C}$, determine the radius of convergence of the Maclaurin series. Thereby we can determine the exact upper bound for g up to which the ME will converge.

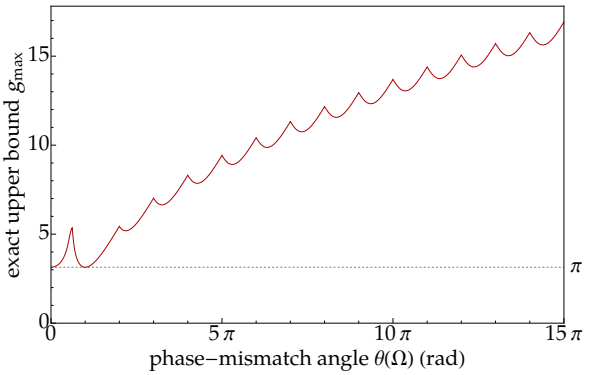

Figure 5.3: The exact upper bound $g_{\max}$ for the convergence of the MA to the exact solution as a function of the phase mismatch angle θ (dark red). A gridline (gray, dashed) illustrates the level $g_{\max} = \pi$ to which the sufficient norm criterion guarantees convergence. Figure as presented in Ref. [58].

Finding the locations of singularities of the analytic continuation $\mathbf{M}_\theta(g) \mapsto \mathbf{M}_\theta(z)$ is completely analogous to the methods discussed in the previous section for the Jaynes-Cummings dynamics. However, some modifications have to be made in the proof of holomorphicity of the functions (5.18) as they are now to be carried out in terms of hyperbolic rather then trigonometric functions. The limited radius of convergence is however again given in term of

branch points of the prefactor function $f(z) = \frac{\operatorname{arccosh}(z)}{\sqrt{z-1}\sqrt{z+1}}$ which is the derivative of $F(z) = \frac{1}{2}\operatorname{arccosh}^2(z)$ which has a branch point at $z = -1$. Thus, the radius of convergence of the ME series in the case of PDC is again given by the minimal absolute value root of the holomorphic function $g_\theta(z) = A_{R,\theta}(z) + 1$.

The exact upper bound in terms of gain obtained by this analysis is displayed in Fig. 5.3. We can see that the MA converges to the exact solution well beyond the limit $g < \pi$ for a wide range of θ. We can also observe that the limit of convergence increases with increasing phase-mismatch. Thus, this might explain the quality of approximation in this limit, cf. Fig.2.4. After all, quality of approximation by MA should improve as one moves further away from a divergent regime.

Conclusion

In summary, we have analyzed (time) ordering effects in the context of dynamic quantum optical systems. To this end, we have considered the exponential representation of time-dependent perturbation theory, i.e., the ME [17]. Truncating the ME leads to approximations of the evolution operators for dynamic systems. Increasing the orders of approximation includes increased orders of (time) ordering corrections which improve the description of the systems dynamics by the approximation. The first-order approximation corresponds to the negligence of (time) ordering corrections. Thus, this expansion allows for the clear identification of (time) ordering effects. However, (time) ordering corrections in terms of the ME may not always converge to the exact dynamics (cf. [18]) which can lead to misinterpretations and nonphysical results.

Firstly, we have applied these methods in the process of type-I PDC in a second-order nonlinear crystal with a monochromatic pump. This system is particularly suited for an analysis of ME methods in the context of quantum optical systems, as we have access to a closed form exact analytical solution to the non-stationary dynamics (cf. [26]), which served as reference for comparisons. We have applied the Bloch-Messiah decomposition to the process. Using the exact solution for the dynamics, we have evaluated the four real parameter characterizing the Bloch-Messiah decomposition and have introduced the squeezing eigenmodes which are in a single-mode squeezed state and, therefore, are statistically independent. We have shown that for the monochromatic pump wave, the eigenmodes are bichromatic and are parameterized by two angles. Next, we have applied the ME to the quantum-mechanical evolution operator of this system and obtained analytic expressions for the first three orders of the MA. We have shown that above certain degree of squeezing corrections to the first-order MA are necessary, and have introduced a boundary value of the parametric gain exponent $g = \pi$, corresponding to 12.5 dB of squeezing, as a boundary for the ultra-high-gain regime of PDC. We have demonstrated that for squeezing as high as 16 dB the third-order MA provides a very good approximation of the broadband squeezed squeezed light generated in this process. We have shown that a nonlinear dependence of the degree of squeezing $r(g)$ for non-zero phase mismatch can serve as a signature of the ultra-high-gain regime of PDC, a result which can be verified experimentally. We have also demonstrated that the photocurrent noise spectrum in the balanced homodyne detection of broadband squeezed light is very sensitive to the errors in the angle of squeezing in the respective MAs for ultra-high-gain regime. Our results confirm that the first-order MA, used in several previous publications, can be trusted for moderate

squeezing, and provides the level of squeezing for which the higher-orders corrections are necessary. We have discussed how the quality of the MA depends on the regime of gain and seen that the quality equally depends on the phase mismatch. We have furthermore seen that MAs yield the correct asymptotic behavior in terms of phase-mismatching angles for every order of approximation.

Secondly, we have considered the type-I PDC process with a broad spectral pump pulse in a single pass configuration. In this case, no closed-form analytical solution to the dynamics is available and analysis of ordering effects was carried out in terms of the MAs. The second- and third-order MA include ordering corrections, which were compared to the first-order MA, which corresponds to the case of neglected ordering. An example scenario of a BBO crystal and a pump pulse with phase-modulated Gaussian envelope function was considered, where perfect phase-matching conditions were achieved at the central carrier frequency. A sufficient upper bound was evaluated for this example and MAs up to third order were considered below this bound. The ordering corrections showed a modification of squeezing eigenmodes, both in terms of phase modulation and width. The corresponding squeezing parameters were also affected by the ordering corrections. However, for the maximally squeezed mode, the squeezing parameter showed linear dependency to the gain parameter up to $16\,\mathrm{dB}$ squeezing, and it was hypothesized that the third-order expansion may give useful descriptions of the eigenmodes of squeezing as long as this relation to the gain parameter remains valid. Additionally, a scenario of off-center phase matching was considered as an exemplary scenario scenario for an engineered source – to this end, a slight turn of the BBO crystal was considered whilst the the rest of the configuration remained unchanged. This led to the notion of bispectral beams. Here the transformation from the input to the output of the crystal have a structure that resembles that of a the type-I PDC with a monochromatic pump, i.e., instead of bichromatic squeezing eigenmodes, we have bispectral eigenmodes. We have proven the two-fold multiplicity of squeezing parameters in such bispectral beam scenarios.

Thirdly, the CJCD model was considered. We derived an exact solution for such a dynamics for the first time. The solution was formulated by applying a spinor formalism which decoupled the dynamics in terms of 2×2 matrix differential equations, which were subsequently solved. Thus, as in the case of type-I PDC with a monochromatic pump, we were able to compare MAs to the exact dynamics of the system. The decoupling in terms of the spinor formalism allowed for an efficient investigation of time-ordering effects. The latter were considered with respect to the excitation probability of the electronic state of the two-level ion. Magnus approximations up to 5th order were considered. Furthermore, based on the analytical solution, a closed form generating function for the time-ordering corrections was derived.

Lastly, we have considered the question of convergence of MAs in more detail. To this end, we first focused on the classically driven Jaynes-Cummings dynamics of an ion in a Paul trap. By extending the generating function of time-ordering corrections – obtained from the analyt-

ical solution of the Jaynes-Cummings Dynamics – to the complex plane, we could determine the exact limits of convergence of time-ordering corrections by locating the singularities of the former in the complex plane. It was shown that these exact upper bounds depend on the detuning and exceed known sufficient upper bounds over a wide range of detunings. Additionally, we have observed isolated regions of convergence above these upper bounds. Subsequently, a similar analysis was performed for the type-I PDC process with a monochromatic pump for which an analytical solution was also available. Here the sufficient upper bound in terms of the gain parameter was exceeded for a wide range of phase mismatch angles. For large phase mismatch angles, the exact upper bound increased in a quasi-linear fashion. This was taken as an explanation as to why all orders of MA show the correct asymptotic behavior in this limit. The analysis of the exact upper limits of convergence for the two systems are, to my best knowledge, the first in the context of quantum optical systems.

In conclusion, we have shown that the ME can serve as a useful tool in order to analyze (time) ordering effects in quantum optical systems. The MA, as all approximative methods, comes with a trade off and we have seen that this trade off is, e.g., the limitations in terms of (sufficient) upper bounds of convergence. What we could also see throughout our employment of MAs was that we did not need to worry about the preservation of symmetries in our treatment. The ME itself preserved all relevant symmetries. This allowed us, e.g., to adopt the notion of squeezing operators in the context of PDC instead of having to speak of two-photon generation and the-like – as one would do in a perturbative Dyson series treatment. The accuracy of low-order MAs in the context of PDC also underlies its utility as an approximative tool. We were able to show that exact upper bounds of convergence may exceed those obtained by sufficient criteria by quite a margin for a wide range of configurations, which also underlies the power of this representation of time-dependent perturbation theory.

It is my sincerest hope that the presented body of work yields useful intuitions and vocabulary to researchers, theoreticians and experimenters alike, that wish to apply methods resulting from the ME, treat non stationary systems, or discuss quantum (time) ordering effects.

Appendix A

Equivalence of Magnus expansion in operator and matrix formulation

We consider purely quadratic symmetrically ordered hermitian operators

$$\hat{f}(\mathbf{A}) = \hat{\boldsymbol{\xi}}^\dagger \mathbf{A} \hat{\boldsymbol{\xi}}, \tag{A.1}$$

with

$$\hat{\boldsymbol{\xi}} = (\hat{a}_1, \dots, \hat{a}_n, \hat{a}_1^\dagger, \dots, \hat{a}_n^\dagger)^T, \tag{A.2}$$

that are defined in terms of the Hermitian $2n \times 2n$ matrices $\mathbf{A}$ with block structure

$$\mathbf{A} = \begin{pmatrix} A_0 & A_I \\ A_I^* & A_0^* \end{pmatrix}, \tag{A.3}$$

where $A_0 \in \mathbb{C}^{n\times n}$ is Hermitian and $A_I \in \mathbb{C}^{n\times n}$ is complex symmetric. This implies, that

$$\mathbf{A}^T = \mathbf{A}^* = \mathbf{PAP} \text{ with } \mathbf{P} = \begin{pmatrix} 0 & I \\ I & 0 \end{pmatrix}. \tag{A.4}$$

Note, that this representation is linear in the Hermitian matrices

$$\hat{f}(\mathbf{A} + \mathbf{B}) = \hat{f}(\mathbf{A}) + \hat{f}(\mathbf{B}). \tag{A.5}$$

Furthermore, we write $\hat{\xi}_k = \hat{a}_k$ for $k \leq n$ and $\hat{\xi}_k = \hat{a}_{k-n}^\dagger$ for $k > n$ by which

$$\hat{f}(\mathbf{A}) = \hat{\xi}_k^\dagger \mathbf{A}_{k,l} \hat{\xi}_l, \tag{A.6}$$

where we have adopted the Einstein sum convention in the sense that repeated indices are summed over the range $1, \dots, 2n$. The bosonic commutator relations can be formulated as

$$[\hat{\xi}_p, \hat{\xi}_q^\dagger] = \mathbf{K}_{p,q} \text{ with } \mathbf{K} = \begin{pmatrix} I & 0 \\ 0 & -I \end{pmatrix}. \tag{A.7}$$

Furthermore, note that

$$\hat{\xi}_p^\dagger = \mathbf{P}_{p,q}\hat{\xi}_q, \tag{A.8}$$

by which also follows, that

$$[\hat{\xi}_p, \hat{\xi}_q] = (\mathbf{KP})_{p,q} \qquad [\hat{\xi}_p^\dagger, \hat{\xi}_q^\dagger] = (\mathbf{PK})_{p,q}. \tag{A.9}$$

We will furthermore make use of the properties $\mathbf{P}^2 = \mathbf{K}^2 = \mathbf{I}$, $(\mathbf{PK})^T = -\mathbf{PK}$, and $\mathbf{PK} = -\mathbf{KP}$. We may write

After clarifying the notation, it is straight forward to show that

$$\begin{aligned}
&[\hat{f}(\mathbf{A}), \hat{f}(\mathbf{B})] = \mathbf{A}_{k,l}\mathbf{B}_{p,q}[\hat{\xi}_k^\dagger\hat{\xi}_l, \xi_p^\dagger\hat{\xi}_q] = \mathbf{A}_{k,l}\mathbf{B}_{p,q}\hat{\xi}_k^\dagger[\hat{\xi}_l, \xi_p^\dagger\hat{\xi}_q] + \mathbf{A}_{k,l}\mathbf{B}_{p,q}[\hat{\xi}_k^\dagger, \xi_p^\dagger\hat{\xi}_q]\hat{\xi}_l \\
=&\mathbf{A}_{k,l}\mathbf{B}_{p,q}\hat{\xi}_k^\dagger\xi_p^\dagger[\hat{\xi}_l, \hat{\xi}_q] + \mathbf{A}_{k,l}\mathbf{B}_{p,q}\hat{\xi}_p^\dagger[\hat{\xi}_k^\dagger, \hat{\xi}_q]\hat{\xi}_l + \mathbf{A}_{k,l}\mathbf{B}_{p,q}\hat{\xi}_k^\dagger[\hat{\xi}_l, \hat{\xi}_p^\dagger]\hat{\xi}_q + \mathbf{A}_{k,l}\mathbf{B}_{p,q}[\hat{\xi}_k^\dagger, \hat{\xi}_p^\dagger]\hat{\xi}_q\hat{\xi}_l \\
=&\hat{\xi}_k^\dagger\mathbf{A}_{k,l}(\mathbf{KP})_{l,q}\mathbf{B}_{p,q}\hat{\xi}_p^\dagger - \hat{\xi}_p^\dagger\mathbf{B}_{p,q}\mathbf{K}_{q,k}\mathbf{A}_{k,l}\hat{\xi}_l + \hat{\xi}_k^\dagger\mathbf{A}_{k,l}\mathbf{K}_{l,p}\mathbf{B}_{p,q}\hat{\xi}_q + \hat{\xi}_q\mathbf{B}_{p,q}(\mathbf{PK})_{k,p}\mathbf{A}_{k,l}\hat{\xi}_l \\
=&\hat{\xi}_k^\dagger\mathbf{A}_{k,l}(\mathbf{KP})_{l,q}(\mathbf{PBP})_{q,p}\mathbf{P}_{p,r}\hat{\xi}_r - \hat{\xi}_p^\dagger\mathbf{B}_{p,q}\mathbf{K}_{q,k}\mathbf{A}_{k,l}\hat{\xi}_l + \hat{\xi}_k^\dagger\mathbf{A}_{k,l}\mathbf{K}_{l,p}\mathbf{B}_{p,q}\hat{\xi}_q \\
&- \hat{\xi}_r^\dagger\mathbf{P}_{r,q}(\mathbf{PBP})_{q,p}(\mathbf{PK})_{p,k}\mathbf{A}_{k,l}\hat{\xi}_l \\
=&\hat{\boldsymbol{\xi}}^\dagger\mathbf{AKPPBPP}\hat{\boldsymbol{\xi}} - \hat{\boldsymbol{\xi}}^\dagger\mathbf{BKA}\hat{\boldsymbol{\xi}} + \hat{\boldsymbol{\xi}}^\dagger\mathbf{AKB}\hat{\boldsymbol{\xi}} - \hat{\boldsymbol{\xi}}^\dagger\mathbf{PPBPPKA}\hat{\boldsymbol{\xi}} \\
=&2\hat{\boldsymbol{\xi}}^\dagger\mathbf{KKAKB}\hat{\boldsymbol{\xi}} - 2\hat{\boldsymbol{\xi}}^\dagger\mathbf{KKBKA}\hat{\boldsymbol{\xi}} \\
=&2\hat{\boldsymbol{\xi}}^\dagger\mathbf{K}[\mathbf{KA}, \mathbf{KB}]\hat{\boldsymbol{\xi}} \\
=&\hat{f}(2\mathbf{K}[\mathbf{KA}, \mathbf{KB}]).
\end{aligned} \tag{A.10}$$

Nesting is also obvious as

$$[\hat{f}(\mathbf{A}), [\hat{f}(\mathbf{B}), \hat{f}(\mathbf{C})]] = [\hat{f}(\mathbf{A}), \hat{f}(2\mathbf{K}[\mathbf{KB}, \mathbf{KC}])] = \hat{f}(4\mathbf{K}[\mathbf{KA}, [\mathbf{KB}, \mathbf{KC}]]) \tag{A.11}$$

Consider now the quadratic Hamiltonian $\hat{\mathcal{H}}(z) = \hat{f}(\mathbf{H}(z))$

$$\partial_t\hat{\mathcal{U}}(z, z_0) = -i\gamma\hat{\mathcal{H}}(z)\hat{\mathcal{U}}(z, z_0), \tag{A.12}$$

with The corresponding matrix differential equation – cf. (1.51) reads as

$$\partial_z \mathbf{S}(z, z_0) = -i\gamma \mathbf{F}(z)\mathbf{S}(z, z_0), \tag{A.13}$$

where $\mathbf{F}(z) = 2\mathbf{KH}(z)$. The one can easily see that there is a one-to one correspondence for nested commutators of unequal position Hamiltonians as

$$\begin{aligned}
\hat{\mathcal{H}}(z_1) &= \hat{\boldsymbol{\xi}}^\dagger \frac{1}{2}\mathbf{KF}(z_1)\hat{\boldsymbol{\xi}} \\
[\hat{\mathcal{H}}(z_1), \hat{\mathcal{H}}(z_2)] &= \hat{\boldsymbol{\xi}}^\dagger \frac{1}{2}\mathbf{K}[\mathbf{F}(z_1), \mathbf{F}(z_2)]\hat{\boldsymbol{\xi}} \\
[\hat{\mathcal{H}}(z_1), [\hat{\mathcal{H}}(z_2), \hat{\mathcal{H}}(z_3)]] &= \hat{\boldsymbol{\xi}}^\dagger \frac{1}{2}\mathbf{K}[\mathbf{F}(z_1), [\mathbf{F}(z_2), \mathbf{F}(z_3)]]\hat{\boldsymbol{\xi}} \\
&\vdots
\end{aligned} \tag{A.14}$$

Thus, considering that the Magnus terms correspond time ordered integrals of nested commutators, the kth order Magnus expansion approximation in operator formulation yields exactly the same transformation as the kth order Magnus expansion approximation in matrix formulation.

Appendix B

Mathematica implementation of the Bloch-Messiah decompositon

Implementations of the Bloch-Messiah decomposition have been discussed in the literature – see Refs. [113, 114]. See also the proof of a symplectic singular value decomposition in Ref. [130], for a related result that can be adapted into a decomposition algorithm. Here we give a simple Mathematica implementation of the decomposition that has been employed in this mansucript to derive Bloch-Messiah decompositions. In Ref. [115] the following Mathematica implementation of the Takagi (labled `TD`) decompostion (1.61) was given:

$$\texttt{TD}[M\_] := \left\{\#[[2]], \#[[1]].\texttt{MatrixPower}\left[\texttt{CT}[\#[[3]]].\texttt{CO}[\#[[1]]], \frac{1}{2}\right]\right\} \&@\texttt{SVD}[M];,$$

where `CO`, `CT`, and `SVD` are abbreviations for the Mathematica functions `Conjugate`, `ConjugateTranspose`, and `SingularValueDecomposition` respectivley. The returned format is $\{\Xi, P\}$, i.e., two matrices for a decomposition $M = P\Xi P^T$.

Likewise the Bloch-Messiah decompositon (1.60) can be implemented in Mathematica as

$$\begin{aligned}\texttt{BMD}[A\_, B\_] := &\left\{\#[[2]], \texttt{DM}[\#[[1]]], \texttt{CT}[A].\#[[2]].\texttt{DM}\left[\frac{1}{\texttt{Cosh}[\#[[1]]]}\right]\right\} \&@ \\ &\left\{\frac{\texttt{ArcSinh}[2\texttt{DI}[\#[[1]]]]}{2}, \#[[2]]\right\} \&@\texttt{TD}[A.\texttt{TR}[B]];,\end{aligned}$$

where `TR`, `DI`, and `DM` are abbreviations for the Mathematica functions `Transpose`, `Diagonal`, and `DiagonalMatrix` respectivley. The output format is $\{V, R, W\}$. These are the matrices of the Bloch-Messiah decomposition

$$A = V\cosh(R)W^\dagger \qquad\qquad B = V\sinh(R)W^T. \tag{B.1}$$

Appendix C

Bispectral beam exponent

For two matrices with block structure

$$\mathbf{X} = \begin{pmatrix} X_{1,1} & 0 & 0 & X_{1,4} \\ 0 & X_{2,2} & X_{2,3} & 0 \\ 0 & X_{3,2} & X_{3,3} & 0 \\ X_{4,1} & 0 & 0 & X_{4,4} \end{pmatrix} \qquad \mathbf{Y} = \begin{pmatrix} Y_{1,1} & 0 & 0 & Y_{1,4} \\ 0 & Y_{2,2} & Y_{2,3} & 0 \\ 0 & Y_{3,2} & Y_{3,3} & 0 \\ Y_{4,1} & 0 & 0 & Y_{4,4} \end{pmatrix}, \tag{C.1}$$

with arbitrary blocks $X_{p,q}$ and $Y_{p,q}$, we can see that the block structure remains preserved under matrix multiplication:

$$\mathbf{XY} = \begin{pmatrix} X_{1,1}Y_{1,1} + X_{1,4}Y_{4,1} & 0 & 0 & X_{1,1}Y_{1,4} + X_{1,4}Y_{4,4} \\ 0 & X_{2,2}Y_{2,2} + X_{2,3}Y_{3,2} & X_{2,2}Y_{2,3} + X_{2,3}Y_{3,3} & 0 \\ 0 & X_{3,2}Y_{2,2} + X_{3,3}Y_{3,2} & X_{3,2}Y_{2,3} + X_{3,3}Y_{3,3} & 0 \\ X_{4,1}Y_{1,1} + X_{4,4}Y_{4,1} & 0 & 0 & X_{4,1}Y_{1,4} + X_{4,4}Y_{4,4} \end{pmatrix}. \tag{C.2}$$

Thus, we can see that the matrix powers [cf. (3.66)]

$$\mathbf{P}^{(\ell)} = \begin{pmatrix} -i\Phi_1 & 0 & 0 & -iJ \\ 0 & -i\Phi_2 & -iJ^T & 0 \\ 0 & iJ^* & i\Phi_1^* & 0 \\ iJ^\dagger & 0 & 0 & i\Phi_2^* \end{pmatrix}^\ell \tag{C.3}$$

for $\ell = 0, 1, 2, \dots$ always have a block structure of

$$\mathbf{P}^{(\ell)} = \begin{pmatrix} P_{1,1}^{(\ell)} & 0 & 0 & P_{1,4}^{(\ell)} \\ 0 & P_{2,2}^{(\ell)} & P_{2,3}^{(\ell)} & 0 \\ 0 & P_{3,2}^{(\ell)} & P_{3,3}^{(\ell)} & 0 \\ P_{4,1}^{(\ell)} & 0 & 0 & P_{4,4}^{(\ell)} \end{pmatrix}. \tag{C.4}$$

Note that this also holds true for $\mathbf{P}^{(0)} = \mathbf{I}$. Then, for the symplectic transform $\mathbf{S} = \exp(\mathbf{P^{(1)}})$ we have

$$\mathbf{S} = \sum_{\ell=0}^{\infty} \frac{1}{\ell!} \mathbf{P}^{(\ell)} = \begin{pmatrix} \sum\limits_{\ell=0}^{\infty} \frac{1}{\ell!} P_{1,1}^{(\ell)} & 0 & 0 & \sum\limits_{\ell=0}^{\infty} \frac{1}{\ell!} P_{1,4}^{(\ell)} \\ 0 & \sum\limits_{\ell=0}^{\infty} \frac{1}{\ell!} P_{2,2}^{(\ell)} & \sum\limits_{\ell=0}^{\infty} \frac{1}{\ell!} P_{2,3}^{(\ell)} & 0 \\ 0 & \sum\limits_{\ell=0}^{\infty} \frac{1}{\ell!} P_{3,2}^{(\ell)} & \sum\limits_{\ell=0}^{\infty} \frac{1}{\ell!} P_{3,3}^{(\ell)} & 0 \\ \sum\limits_{\ell=0}^{\infty} \frac{1}{\ell!} P_{4,1}^{(\ell)} & 0 & 0 & \sum\limits_{\ell=0}^{\infty} \frac{1}{\ell!} P_{4,4}^{(\ell)} \end{pmatrix}. \tag{C.5}$$

Taking into account that $\mathbf{S}$ is symplectic, it follows that $\mathbf{S}$ preserves the strcuture of the exponent (C.3) as

$$\mathbf{S} = \begin{pmatrix} A_1 & 0 & 0 & B_1 \\ 0 & A_2 & B_1 & 0 \\ 0 & B_1^* & A_1^* & 0 \\ B_2^* & 0 & 0 & A_1^* \end{pmatrix}. \tag{C.6}$$

Appendix D

Rotating wave approximation

Here the explicit application off the rotating wave approximation in Sec. 4.2.2 is given. Applying the expansion [23]

$$\cos(\eta(\hat{a}+\hat{a}^\dagger)+\Delta\phi) = \frac{1}{2}e^{-\eta^2/2}\sum_{l,m=0}^{\infty}\frac{1}{l!m!}\left[e^{i\Delta\phi}(i\eta)^{l+m}+e^{-i\Delta\phi}(-i\eta)^{m+l}\right]\hat{a}^{\dagger l}\hat{a}^m \tag{D.1}$$

to (4.23) yields

$$\begin{aligned}
\hat{H}_{\text{int}} =& -i\sqrt{\frac{\hbar\omega_L}{V\varepsilon_0}}\,(\mathbf{d}_{21}\mathbf{e})\,\frac{1}{2}e^{-\eta^2/2}\sum_{l,m=0}^{\infty}\frac{1}{l!m!}\left[e^{i\Delta\phi}(i\eta)^{l+m}+e^{-i\Delta\phi}(-i\eta)^{m+l}\right]\hat{a}^{\dagger l}\hat{a}^m\hat{A}_{21}\hat{b}\\
&+i\sqrt{\frac{\hbar\omega_L}{V\varepsilon_0}}\,(\mathbf{d}_{21}\mathbf{e})\,\frac{1}{2}e^{-\eta^2/2}\sum_{l,m=0}^{\infty}\frac{1}{l!m!}\left[e^{i\Delta\phi}(i\eta)^{l+m}+e^{-i\Delta\phi}(-i\eta)^{m+l}\right]\hat{a}^{\dagger l}\hat{a}^m\hat{A}_{21}\hat{b}^\dagger\\
&-i\sqrt{\frac{\hbar\omega_L}{V\varepsilon_0}}\,(\mathbf{d}_{12}\mathbf{e})\,\frac{1}{2}e^{-\eta^2/2}\sum_{l,m=0}^{\infty}\frac{1}{l!m!}\left[e^{i\Delta\phi}(i\eta)^{l+m}+e^{-i\Delta\phi}(-i\eta)^{m+l}\right]\hat{a}^{\dagger l}\hat{a}^m\hat{A}_{12}\hat{b}\\
&+i\sqrt{\frac{\hbar\omega_L}{V\varepsilon_0}}\,(\mathbf{d}_{12}\mathbf{e})\,\frac{1}{2}e^{-\eta^2/2}\sum_{l,m=0}^{\infty}\frac{1}{l!m!}\left[e^{i\Delta\phi}(i\eta)^{l+m}+e^{-i\Delta\phi}(-i\eta)^{m+l}\right]\hat{a}^{\dagger l}\hat{a}^m\hat{A}_{12}\hat{b}^\dagger.
\end{aligned} \tag{D.2}$$

Moving to the interaction picture as $\hat{\tilde{H}}_{\text{int}}(t) = \hat{U}^\dagger(t)\hat{H}_I\hat{U}(t)$ in terms of $\hat{U} = e^{-\frac{it}{\hbar}[\hat{H}_F+\hat{H}_A+\hat{H}_{\text{CM}}]}$ we obtain the interaction picture Hamiltonian

$$\begin{aligned}
\hat{\tilde{H}}_{\text{int}}(t) =& -i\sqrt{\frac{\hbar\omega_L}{V\varepsilon_0}}\,(\mathbf{d}_{21}\mathbf{e})\,\frac{1}{2}e^{-\eta^2/2}\sum_{l,m=0}^{\infty}\frac{1}{l!m!}\left[e^{i\Delta\phi}(i\eta)^{l+m}+e^{-i\Delta\phi}(-i\eta)^{m+l}\right]\\
&\times\hat{a}^{\dagger l}\hat{a}^m\hat{A}_{21}\hat{b}e^{it[\omega_{21}+[l-m]\nu-\omega_L]}\\
&+i\sqrt{\frac{\hbar\omega_L}{V\varepsilon_0}}\,(\mathbf{d}_{21}\mathbf{e})\,\frac{1}{2}e^{-\eta^2/2}\sum_{l,m=0}^{\infty}\frac{1}{l!m!}\left[e^{i\Delta\phi}(i\eta)^{l+m}+e^{-i\Delta\phi}(-i\eta)^{m+l}\right]\\
&\times\hat{a}^{\dagger l}\hat{a}^m\hat{A}_{21}\hat{b}^\dagger e^{it[\omega_{21}+[l-m]\nu+\omega_L]}\\
&-i\sqrt{\frac{\hbar\omega_L}{V\varepsilon_0}}\,(\mathbf{d}_{12}\mathbf{e})\,\frac{1}{2}e^{-\eta^2/2}\sum_{l,m=0}^{\infty}\frac{1}{l!m!}\left[e^{i\Delta\phi}(i\eta)^{l+m}+e^{-i\Delta\phi}(-i\eta)^{m+l}\right]\\
&\times\hat{a}^{\dagger l}\hat{a}^m\hat{A}_{12}\hat{b}e^{it[-\omega_{21}+[l-m]\nu-\omega_L]}\\
&+i\sqrt{\frac{\hbar\omega_L}{V\varepsilon_0}}\,(\mathbf{d}_{12}\mathbf{e})\,\frac{1}{2}e^{-\eta^2/2}\sum_{l,m=0}^{\infty}\frac{1}{l!m!}\left[e^{i\Delta\phi}(i\eta)^{l+m}+e^{-i\Delta\phi}(-i\eta)^{m+l}\right]\\
&\times\hat{a}^{\dagger l}\hat{a}^m\hat{A}_{12}\hat{b}^\dagger e^{it[-\omega_{21}+[l-m]\nu+\omega_L]}.
\end{aligned}\tag{D.3}$$

Considering $\Delta\omega \ll \nu \ll \omega_{21}$ we may rewrite this in terms of $\omega_L = \omega_{21} - k\nu + \Delta\omega$ as

$$\begin{aligned}
\hat{\tilde{H}}_{\text{int}}(t) =& -i\sqrt{\frac{\hbar\omega_L}{V\varepsilon_0}}\,(\mathbf{d}_{21}\mathbf{e})\,\frac{1}{2}e^{-\eta^2/2}\sum_{l,m=0}^{\infty}\frac{1}{l!m!}\left[e^{i\Delta\phi}(i\eta)^{l+m}+e^{-i\Delta\phi}(-i\eta)^{m+l}\right]\\
&\times\hat{a}^{\dagger l}\hat{a}^m\hat{A}_{21}\hat{b}e^{-it[\Delta\omega-[(l+k)-m]\nu]}\\
&+i\sqrt{\frac{\hbar\omega_L}{V\varepsilon_0}}\,(\mathbf{d}_{21}\mathbf{e})\,\frac{1}{2}e^{-\eta^2/2}\sum_{l,m=0}^{\infty}\frac{1}{l!m!}\left[e^{i\Delta\phi}(i\eta)^{l+m}+e^{-i\Delta\phi}(-i\eta)^{m+l}\right]\\
&\times\hat{a}^{\dagger l}\hat{a}^m\hat{A}_{21}\hat{b}^\dagger e^{it[\Delta\omega+2\omega_{21}+[l-(m+k)]\nu]}\\
&-i\sqrt{\frac{\hbar\omega_L}{V\varepsilon_0}}\,(\mathbf{d}_{12}\mathbf{e})\,\frac{1}{2}e^{-\eta^2/2}\sum_{l,m=0}^{\infty}\frac{1}{l!m!}\left[e^{i\Delta\phi}(i\eta)^{l+m}+e^{-i\Delta\phi}(-i\eta)^{m+l}\right]\\
&\times\hat{a}^{\dagger l}\hat{a}^m\hat{A}_{12}\hat{b}e^{-it[\Delta\omega+2\omega_{21}-[(l+k)-m]\nu]}\\
&+i\sqrt{\frac{\hbar\omega_L}{V\varepsilon_0}}\,(\mathbf{d}_{12}\mathbf{e})\,\frac{1}{2}e^{-\eta^2/2}\sum_{l,m=0}^{\infty}\frac{1}{l!m!}\left[e^{i\Delta\phi}(i\eta)^{l+m}+e^{-i\Delta\phi}(-i\eta)^{m+l}\right]\\
&\times\hat{a}^{\dagger l}\hat{a}^m\hat{A}_{12}\hat{b}^\dagger e^{it[\Delta\omega+[l-(m+k)]\nu]}.
\end{aligned}\tag{D.4}$$

Here can apply the rotating wave approximation as

$$\begin{aligned}
e^{-it[\Delta\omega-[(l+k)-m]\nu]} &\approx \delta_{l+k,m}e^{-it\Delta\omega} & e^{it[\Delta\omega+2\omega_{21}+[l-(m+k)]\nu]} &\approx 0\\
e^{-it[\Delta\omega+2\omega_{21}-[(l+k)-m]\nu]} &\approx 0 & e^{it[\Delta\omega+[l-(m+k)]\nu]} &\approx \delta_{l,m+k}e^{it\Delta\omega},
\end{aligned}\tag{D.5}$$

which yields

$$\hat{\tilde{H}}_{\text{int}}(t) = \hbar\kappa e^{-it\Delta\omega}\hat{f}_k(\hat{a}^\dagger\hat{a};\eta)\hat{a}^k\hat{b}\hat{A}_{21} + \text{H.c.}, \tag{D.6}$$

with the Hermitian operator

$$\hat{f}_k(\hat{a}^\dagger\hat{a};\eta) = \frac{1}{2}e^{i\Delta\phi-\eta^2/2}\sum_{l=0}^{\infty}\frac{\hat{a}^{\dagger l}\hat{a}^l}{(l+k)!l!}(i\eta)^{2l+k} + \text{H.c.} \tag{D.7}$$

and the coupling constant $\kappa = -i\sqrt{\frac{\omega_L}{\hbar V\varepsilon_0}}(\mathbf{d}_{21}\mathbf{e})$. Moving back to the Schrödinger picture yields

$$\hat{H}_{\text{int}} = \hbar\kappa\hat{f}_k(\hat{a}^\dagger\hat{a};\eta)\hat{a}^k\hat{b}\hat{A}_{21} + \text{H.c.}. \tag{D.8}$$

Bibliography

[1] W. P. Schleich, *Quantum Optics in Phase Space* (Wiley-VCH, Berlin, 2001).

[2] W. Vogel and D.-G. Welsch, *Quantum Optics*, 3rd ed. (Wiley-VCH, Berlin, 2006).

[3] G. Grynberg, A. Aspect, and C. Fabre, *Introduction to Quantum Optics* (Cambridge Universit Press, Cambridge, 2010).

[4] G. S. Agarwal, *Quantum Optics* (Cambridge University Press, Cambridge, 2013).

[5] S. De Bièvre, D. B. Horoshko, G. Patera, and M. I. Kolobov, *Measuring nonclassicality of bosonic field quantum states via operator ordering sensitivity*, arXiv:1809.02047 (2018).

[6] H. J. Carmichael and D. F. Walls, *A quantum-mechanical master equation treatment of the dynamical Stark effect*, J. Phys. B **9**, 1199 (1976).

[7] H. J. Kimble and L. Mandel, *Theory of resonance fluorescence*, Phys. Rev. A **13**, 2123 (1976).

[8] H. J. Kimble, M. Dagenais, and L. Mandel, *Photon Antibunching in Resonance Fluorescence*, Phys. Rev. Lett. **39**, 691 (1977).

[9] A. Einstein, *Über einen die Erzeugung und Verwandlung des Lichtes betreffenden heuristischen Gesichtspunkt*, Ann. Phys. **322**, 132 (1905).

[10] A. Miranowicz, J. Bajer, H. Matsueda, M. R. B. Wahiddin, and R. Tanas, *Comparative study of photon antibunching of non-stationary fields*, J. Opt. B **1**, 511 (1999).

[11] W. Vogel, *Nonclassical Correlation Properties of Radiation Fields*, Phys. Rev. Lett. **100**, 013605 (2008).

[12] L. D. Landau and E. M. Lifshitz, *Quantum Mechanics*, 3rd ed. (Elsevier Science Ltd., Oxford, 1977).

[13] D. J. Griffiths, *Introduction to Quantum Mechanics* (Prentice-Hall, London, 1995).

[14] T. Fließbach, *Quantenmechanik*, 5th ed. (Spektrum Akademischer Verlag, Heidelberg, 2008).

[15] F. J. Dyson, *The Radiation Theories of Tomonaga, Schwinger, and Feynman*, Phys. Rev. **75**, 486 (1949).

[16] A. Christ, B. Brecht, W. Mauerer, and C. Silberhorn, *Theory of quantum frequency conversion and type-II parametric down-conversion in the high-gain regime*, New J. Phys. **15**, 053038 (2013).

[17] W. Magnus, *On the exponential solution of differential equations for a linear operator*,

Comm. Pure Appl. Math. **VII**, 649 (1954).

[18] S. Blanes, F. Casas, J. A. Oteo, and J. Ros, *The Magnus expansion and some of its applications*, Phys. Rep. **470**, 151 (2009).

[19] N. Quesada and J. E. Sipe, *Effects of time ordering in quantum nonlinear optics*, Phys. Rev. A **90**, 063840 (2014).

[20] N. Quesada and J. E. Sipe, *Time-Ordering Effects in the Generation of Entangled Photons Using Nonlinear Optical Processes*, Phys. Rev. Lett. **114**, 093903 (2015).

[21] N. Quesada and J. E. Sipe, *High efficiency in mode-selective frequency conversion*, Opt. Lett. **41**, 364 (2016).

[22] F. Krumm, J. Sperling, and W. Vogel, *Multitime correlation functions in nonclassical stochastic processes*, Phys. Rev. A **93**, 063843 (2016).

[23] F. Krumm and W. Vogel, *Time-dependent nonlinear Jaynes-Cummings dynamics of a trapped ion*, Phys. Rev. A **97**, 043806 (2018).

[24] T. Lipfert, D. B. Horoshko, G. Patera, and M. I. Kolobov, *Bloch-Messiah decomposition and Magnus expansion for parametric down-conversion with monochromatic pump*, Phys. Rev. A **98**, 013815 (2018).

[25] D. Prato and P. W. Lamberti, *A note on Magnus formula*, J. Chem. Phys. **106**, 4640 (1997).

[26] M. I. Kolobov, *The spatial behavior of nonclassical light*, Rev. Mod. Phys. **71**, 1539 (1999).

[27] L. Caspani, E. Brambilla, and A. Gatti, *Tailoring the spatiotemporal structure of biphoton entanglement in type-I parametric down-conversion*, Phys. Rev. A **81**, 033808 (2010).

[28] R. E. Slusher, L. W. Hollberg, B. Yurke, J. C. Mertz, and J. F. Valley, *Observation of Squeezed States Generated by Four-Wave Mixing in an Optical Cavity*, Phys. Rev. Lett. **55**, 2409 (1985).

[29] V. V. Dodonov, *'Nonclassical' states in quantum optics: a 'squeezed' review of the first 75 years*, J. Opt. B: Quantum Semiclass. Opt. **4**, R1 (2002).

[30] U. L. Andersen, T. Gehring, C. Marquardt, and G. Leuchs, *30 years of squeezed light generation*, Phys. Scr. **91**, 053001 (2016).

[31] S. S. Y. Chua, B. J. J. Slagmolen, D. A. Shaddock, and D. E. McClelland, *Quantum squeezed light in gravitational-wave detectors*, Class. Quantum Grav. **31**, 183001 (2014).

[32] R. Schnabel, *Squeezed states of light and their applications in laser interferometers*, Phys. Rep. **684**, 1 (2017).

[33] F. Wolfgramm, A. Cerè, F. A. Beduini, A. Predojević, M. Koschorreck, and M. W. Mitchell, *Squeezed-Light Optical Magnetometry*, Phys. Rev. Lett. **105**, 053601 (2010).

[34] S. L. Braunstein and P. van Loock, *Quantum information with continuous variables*, Rev. Mod. Phys. **7**, 513 (2005).

[35] C. Weedbrook, S. Pirandola, R. García-Patrón, N. J. Cerf, T. C. Ralph, J. H. Shapiro, and S. Lloyd, *Gaussian quantum information*, Rev. Mod. Phys. **84**, 621 (2012).

[36] S. Lloyd and S. L. Braunstein, *Quantum Computation over Continuous Variables*, Phys. Rev. Lett. **82**, 1784 (1999).

[37] N. C. Menicucci, S. T. Flammia, and O. Pfister, *One-way quantum computing in the optical frequency comb*, Phys. Rev. Lett. **101**, 130501 (2008).

[38] S. Yokoyama, R. Ukai, S. C. Armstrong, C. Sornphiphatphong, T. Kaji, S. Suzuki, J. Yoshikawa, H. Yonezawa, N. C. Menicucci, and A. Furusawa, *Ultra-large-scale continuous-variable cluster states multiplexed in the time domain*, Nat. Phot. **7**, 982 (2013).

[39] K. Marshall, C. S. Jacobsen, C. Schäfermeier, T. Gehring, C. Weedbrook, and U. L. Andersen, *Continuous-variable quantum computing on encrypted data*, Nat. Commun. **7**, 13795 (2016).

[40] N. C. Menicucci, P. Van Loock, M. Gu, C. Weedbrook, T. C. Ralph, and M. A. Nielsen, *Universal Quantum Computation with Continuous-Variable Cluster States*, Phys. Rev. Lett. **97**, 110501 (2006).

[41] N. C. Menicucci, *Fault-Tolerant Measurement-Based Quantum Computing with Continuous-Variable Cluster States*, Phys. Rev. Lett. **112**, 120504 (2014).

[42] H. Vahlbruch, M. Mehmet, K. Danzmann, and R. Schnabel, *Detection of 15 dB Squeezed States of Light and Their Application for the Absolute Calibration of Photoelectric Quantum Efficiency*, Phys. Rev. Lett. **117**, 110801 (2016).

[43] D. B. Horoshko and M. I. Kolobov, *Towards single-cycle squeezing in chirped quasi-phase-matched optical parametric down-conversion*, Phys. Rev. A **88**, 033806 (2013).

[44] D. B. Horoshko and M. I. Kolobov, *Generation of monocycle squeezed light in chirped quasi-phase-matched nonlinear crystals*, Phys. Rev. A **95**, 033837 (2017).

[45] M. V. Chekhova, S. Germanskiy, D. B. Horoshko, G. Kh. Kitaeva, M. I. Kolobov, G. Leuchs, C. R. Phillips, and P. A. Prudkovskii, *Broadband bright twin beams and their upconversion*, Opt. Lett. **43**, 375 (2018).

[46] B. Yurke, P. Grangier, R. E. Slusher, and M. J. Potasek, *Generating and detecting short-duration pulses of squeezed light*, Phys. Rev. A **35**, 3586 (1987).

[47] R. S. Bennink and R. W. Boyd, *Improved measurement of multimode squeezed light via an eigenmode approach*, Phys Rev. A **66**, 053815 (2002).

[48] W. Wasilewski, A. I. Lvovsky, K. Banaszek, and C. Radzewicz, *Pulsed squeezed light: Simultaneous squeezing of multiple modes*, Phys. Rev. A **73**, 063819 (2006).

[49] I. N. Agafonov, M. V. Chekhova, and G. Leuchs, *Two-color bright squeezed vacuum*, Phys. Rev. A **82**, 011801 (2010).

[50] A. Allevi, O. Jedrkiewicz, E. Brambilla, A. Gatti, J. Peřina Jr., O. Haderka, and M. Bondani, *Coherence properties of high-gain twin beams*, Phys. Rev. A **90**, 063812 (2014).

[51] A. M. Pérez, K. Yu. Spasibko, P. R. Sharapova, O. V. Tikhonova, G. Leuchs, and M. V. Chekhova, *Giant narrowband twin-beam generation along the pump-energy propagation direction*, Nat. Comm. **6**, 7707 (2015).

[52] G. J. de Valcárcel, G. Patera, N. Treps, and C. Fabre, *Multimode squeezing of frequency combs*, Phys. Rev. A **74**, 061801 (2006).

[53] G. Patera, N. Treps, C. Fabre, and G. J. de Valcarcel, *Quantum theory of synchronously pumped type I optical parametric oscillators: characterization of the squeezed supermodes*, Eur. Phys. J. D **56**, 123 (2010).

[54] S. Jiang, N. Treps, and C. Fabre, *A time/frequency quantum analysis of the light generated by synchronously pumped optical parametric oscillators*, New J. Phys. **14**, 043006 (2012).

[55] O. Pinel, P. Jian, R. M. de Araújo, J. Feng, B. Chalopin, C. Fabre, and N. Treps, *Generation and Characterization of Multimode Quantum Frequency Combs*, Phys. Rev. Lett. **108**, 083601 (2012).

[56] G. Patera, C. Navarrete-Benlloch, G. J. de Valcárcel, and C. Fabre, *Quantum coherent control of highly multipartite continuous-variable entangled states by tailoring parametric interactions*, Eur. Phys. J. D **66**, 241 (2012).

[57] F. Arzani, C. Fabre, and N. Treps, *Versatile engineering of multimode squeezed states by optimizing the pump spectralprofile in spontaneous parametric down-conversion*, Phys. Rev. A **97**, 033808 (2018).

[58] T. Lipfert, D. B. Horoshko, G. Patera, and M. I. Kolobov, *Bloch-Messiah decomposition and Magnus expansion for parametric down-conversion with monochromatic pump: role of the gain*, EPJ Web Conf. **198**, 00006 (2019).

[59] T. Lipfert, F. Krumm, M. I. Kolobov, and W. Vogel, *Time ordering in the classically driven nonlinear Jaynes-Cummings model*, Phys. Rev. A **98**, 063817 (2018).

[60] E. T. Jaynes and F. W. Cummings, *Comparison of quantum and semiclassical radiation theories with application to the beam maser*, Proc. IEEE **51**, 89 (1963).

[61] H. Paul, *Induzierte Emission bei starker Einstrahlung*, Ann. Phys. (Leipzig) **11**, 411 (1963).

[62] S. Haroche, Les Houches Lecture Notes, Session XXXVIII ed, in *New Trends in Atomic Physics*, edited by G. Grynberg and R. Stora (Elsevier, New York, 1984), pp. 195.

[63] S. Haroche and J.M. Raimond, *Radiative Properties of Rydberg States in Resonant Cavities*, Adv. At. Mol. Phys. **20**, 347 (1985).

[64] D. Meschede, H. Walther, and G. Müller, *One-Atom Maser*, Phys. Rev. Lett. **54**, 551 (1985).

[65] G. Rempe, H. Walther, and N. Klein, *Observation of Quantum Collapse and Revival in a One-Atom Maser*, Phys. Rev. Lett. **58**, 353 (1987).

[66] S. Bose, I. Fuentes-Guridi, P. L. Knight, and V. Vedral, *Subsystem Purity as an Enforcer of Entanglement*, Phys. Rev. Lett. **87**, 050401 (2001).

[67] S. Brattke, B. T. H. Varcoe, and H. Walther, *Generation of Photon Number States on Demand via Cavity Quantum Electrodynamics*, Phys. Rev. Lett. **86**, 3534 (2001).

[68] M. Brune, S. Haroche, J. M. Raimond, L. Davidovich, and N. Zagury, *Manipulation of photons in a cavity by dispersive atom-field coupling: Quantum-nondemolition measurements and generation of "Schrödinger cat" states*, Phys. Rev. A **45**, 5193 (1992).

[69] H. J. Carmichael, *Photon Antibunching and Squeezing for a Single Atom in a Resonant Cavity*, Phys. Rev. Lett. **56**, 539 (1986).

[70] F. Dubin, D. Rotter, M. Mukherjee, C. Russo, J. Eschner, and R. Blatt, *Photon Correlation versus Interference of Single-Atom Fluorescence in a Half-Cavity*, Phys. Rev. Lett. **98**, 183003 (2007).

[71] J. H. Eberly, N. B. Narozhny, and J. J. Sanchez-Mondragon, *Periodic Spontaneous Collapse and Revival in a Simple Quantum Model*, Phys. Rev. Lett. **44**, 1323 (1980).

[72] S. Furuichi and M. Ohya, *Entanglement Degree in the Time Development of the Jaynes-Cummings Model*, Lett. Math. Phys. **49**, 279 (1999).

[73] G.-C. Guo and S.-B. Zheng, *Generation of Schrödinger cat states via the Jaynes-Cummings model with large detuning*, Phys. Lett. A **223**, 332 (1996).

[74] M. Hennrich, A. Kuhn, and G. Rempe, *Transition from Antibunching to Bunching in Cavity QED*, Phys. Rev. Lett. **94**, 053604 (2005).

[75] M. Hillery, *Squeezing and photon number in the Jaynes-Cummings model*, Phys. Rev. A **39**, 1556 (1989).

[76] J. R. Kukliski and J. L. Madajczyk, *Strong squeezing in the Jaynes-Cummings model*, Phys. Rev. A **37**, 3175(R) (1988).

[77] N. B. Narozhny, J. J. Sanchez-Mondragon, and J. H. Eberly, *Coherence versus incoherence: Collapse and revival in a simple quantum model*, Phys. Rev. A **23**, 236 (1981).

[78] S. J. D. Phoenix and P. L. Knight, *Establishment of an entangled atom-field state in the Jaynes-Cummings model*, Phys. Rev. A **44**, 6023 (1991).

[79] J. J. Slosser, P. Meystre, and S. L. Braunstein, *Harmonic Oscillator Driven by a Quantum Current*, Phys. Rev. Lett. **63**, 934 (1989).

[80] M. Weidinger, B. T. H. Varcoe, R. Heerlein, and H. Walther, *Trapping States in the Micromaser*, Phys. Rev. Lett. **82**, 3795 (1999).

[81] W. Paul, *Electromagnetic traps for charged and neutral particles*, Rev. Mod. Phys. **62**, 531 (1990).

[82] W. Paul, O. Osberghaus, and E. Fischer, *Ein Ionenkäfig*, Forschungsberichte des Wirtschafts- und Verkehrsministeriums Nordrhein-Westfalen **415** (Westdeutscher Verlag, Köln und Opladen, 1958).

[83] C. A. Blockley, D. F. Walls, and H. Risken, *Quantum Collapses and Revivals in a Quantized Trap*, Europhys. Lett. **17** , 509 (1992).

[84] C. A. Blockley and D. F. Walls, *Cooling of a trapped ion in the strong-sideband regime*, Phys. Rev. A **47**, 2115 (1993).

[85] J. I. Cirac, R. Blatt, A. S. Parkins, and P. Zoller, *Quantum collapse and revival in the motion of a single trapped ion*, Phys. Rev. A **49**, 1202 (1994).

[86] W. Vogel and R. L. de Matos Filho, *Nonlinear Jaynes-Cummings dynamics of a trapped ion*, Phys. Rev. A **52**, 4214 (1995).

[87] D. M. Meekhof, C. Monroe, B. E. King, W. M. Itano, and D. J. Wineland, *Generation of Nonclassical Motional States of a Trapped Atom*, Phys. Rev. Lett. **76**, 1796 (1996).

[88] D. Leibfried, R. Blatt, C. Monroe, and D. Wineland, *Quantum dynamics of single trapped ions*, Rev. Mod. Phys. **75**, 281 (2003).

[89] R. L. de Matos Filho and W. Vogel, *Even and Odd Coherent States of the Motion of a Trapped Ion*, Phys. Rev. Lett. **76**, 608 (1996).

[90] R. L. de Matos Filho and W. Vogel, *Nonlinear Coherent States*, Phys. Rev. A **54**, 4560 (1996).

[91] J. I. Cirac, A. S. Parkins, R. Blatt, and P. Zoller, *"Dark" squeezed states of the motion of a trapped ion*, Phys. Rev. Lett. **70**, 556 (1993).

[92] S.-C. Gou, J. Steinbach, and P. L. Knight, *Dark pair coherent states of the motion of a trapped ion*, Phys. Rev. A **54**, R1014(R) (1996).

[93] S.-C. Gou, J. Steinbach, and P. L. Knight, *Vibrational pair cat states*, Phys. Rev. A **54**, 4315 (1996).

[94] C. C. Gerry, S.-C. Gou, and J. Steinbach, *Generation of motional SU(1,1) intelligent states of a trapped ion*, Phys. Rev. A **55**, 630 (1997).

[95] C. Monroe, D. M. Meekhof, B. E. King, and D. J. Wineland, *A "Schrödinger Cat" Superposition State of an Atom*, Science **272**, 1131 (1996).

[96] C. C. Gerry, *Generation of Schrödinger cats and entangled coherent states in the motion of a trapped ion by a dispersive interaction*, Phys. Rev. A **55**, 2478 (1997).

[97] S. Wallentowitz and W. Vogel, *Quantum-mechanical counterpart of nonlinear optics*, Phys. Rev. A **55**, 4438 (1997).

[98] L. Mandel and E. Wolf, *Optical Coherence and Quantum Optics* (Cambridge University Press, Cambridge, 1995).

[99] W. H. Louisell, *Quantum Statistical Properties of Radiation* (Wiley, New York, 1973).

[100] R. J. Glauber, *Coherent and Incoherent States of the Radiation Field*, Phys. Rev. **131**, 2766 (1963).

[101] E. C. G. Sudarshan, *Equivalence of Semiclassical and Quantum Mechanical Descriptions of Statistical Light Beams*, Phys. Rev. Lett. **10**, 277 (1963).

[102] A. Orłowski, *Eigenstates of squeeze operators do not exist*, Phys. Lett. A **154**, 319 (1991).

[103] N. Bogoliubov, *On the theory of superfluidity*, J. Phys.(USSR) **11**, 23 (1947).

[104] C. Fabre, *Quantum optics, from one mode to many modes* (Ecole Prédoctorale des Houches, session XXIV, Quantum Optics, September 10-21, 2007).

[105] P. Drummond and M. Hillery, *The Quantum Theory of Nonlinear Optics* (Cambridge University Press, Cambridge, 2014).

[106] D. N. Klyshko, Photons and Nonlinear Optics (Gordon and Breach, New York, 1988).

[107] B. Huttner and S. M. Barnett, *Quantization of the electromagnetic field in dielectrics*, Phys. Rev. A **46**, 4306 (1992).

[108] G. Adesso, S. Ragy, and A. R. Lee, *Continuous Variable Quantum Information: Gaussian States and Beyond*, Open Syst. & Inf. Dyn. **21**, 1440001 (2014).

[109] Arvind, B. Dutta, N Mukunda, and R. Simon, *The real symplectic groups in quantum mechanics and optics*, Pranama **45**, 471 (1995).

[110] C. Bloch and A. Messiah, *The canonical form of an antisymmetric tensor and its application to the theory of superconductivity*, Nucl. Phys. **39**, 95 (1962).

[111] R. Balain, C. De Dominicis, and C. Itzykson, *Forme canonique des transformations de Bogoliubov pour les bosons et des transformations (pseudo) orthogonales*, Nucl. Phys. **67**, 609 (1965).

[112] S. L. Braunstein, *Squeezing as an irreducible resource*, Phys. Rev. A **71**, 055801 (2005).

[113] G. Cariolaro and G. Pierobon, *Reexamination of Bloch-Messiah reduction*, Phys. Rev. A **93**, 062115 (2016).

[114] G. Cariolaro and G. Pierobon, *Bloch-Messiah reduction of Gaussian unitaries by Takagi factorization*, Phys. Rev. A **94**, 062109 (2016).

[115] A. M. Chebotarev and A. E. Teretenkov, *Singular value decomposition for the Takagi factorization of symmetric matrices*, Appl. Math. Comput. **234**, 380 (2014).

[116] X. Ma and W. Rhodes, *Multimode squeeze operators and squeezed states*, Phys. Rev. A **41**, 4625 (1990).

[117] W. McCutcheon, *Structure in Multimode Squeezing: A Generalised Bloch-Messiah Reduction*, arXiv:1809.02544 (2018).

[118] F. G. Tricomi, *Integral Equations* (Wiley, New York, 1967).

[119] R.Loudon, *The Quantum Theory of Light*, 3rd ed. (Oxford University Press, New York, 2000).

[120] R. W. Boyd, *Nonlinear Optics*, 3rd ed. (Academic Press, Cambridge MA, 2008).

[121] D. B. Horoshko, L. La Volpe, M. I. Kolobov, N. Treps, and C. Fabre, *Bloch-Messiah reduction for twin beams of light*, private communication, to be published.

[122] G. Patera, *Quantum properties of ultra-short pulses generated by SPOPOs: multi-mode squeezing and entanglement*, Ph.D. thesis, Université Pierre et Marie Curie – Paris6 &

Università dell'Insubria, 2008.

[123] M. Beck, *Quantum State Tomography with Array Detectors*, Phys. Rev. Lett. **84**, 5748 (2000).

[124] G. Ferrini, J. P. Gazeau, T. Coudreau, C. Fabre, and N. Treps, *Compact Gaussian quantum computation by multi-pixel homodyne detection* New J. Phys. **15**, 093015 (2013).

[125] K. Kato, *Second-harmonic generation to 2048 Å in* β*-*BaB_2O_4, IEEE J. Quant. Electron. **22**, 1013 (1986).

[126] J. Spanier and K. B. Oldham, *An Atlas of Functions* (Hemisphere, Washington, D.C., 1987).

[127] R. A. Horn and C. R. Johnson, *Matrix Analysis*, 2nd ed. (Cambridge University Press, New York, 1985), p. 346.

[128] T. Needham, *Visual Complex Analysis* (Oxford University Press, Oxford, 1997).

[129] M. Abramowitz and I. A. Stegun, *Handbook of Mathematical Functions*, (Dover, New York, 1974), 10.1.40.

[130] H. Xu, *An SVD-like matrix decomposition and its applications*, Linear Algebra Appl. **368**, 1 (2003).

Abstract

In quantum optics the electromagnetic field, contrary to classical optics, is described by a Hermitian operator. The quantum nature of the electromagnetic field manifests itself in operator ordering effects, nonexistent in classical optics. This thesis is devoted to a detailed study of such operator ordering effects that are due to the dynamics in physical systems. We consider two systems in particular, 1) traveling-wave parametric down-conversion in a nonlinear medium of the second order, and 2) an ion in a Paul trap driven by a classical field and described by the so-called nonlinear Jaynes-Cummings model. The ordering effects in both dynamical systems are studied via the mathematical technique of the Magnus expansion and approximations defined in terms of the latter. The first part of the thesis is devoted to parametric down-conversion. We consider two cases: (i) a monochromatic pump wave, and (ii) a spectrally broad pump wave. It is well known that in both cases this system is capable of generating spectrally broadband squeezed light. However, the detailed description of the properties of such squeezed light is still not available. For the monochromatic pump, where an exact solution of the dynamics is known, we write explicitly the Bloch-Messiah decomposition of the squeezing transformation and obtain the squeezing eigenmodes and the corresponding squeezing parameters. Next, we compare these exact results with the approximations that contain some or no ordering effects. We evaluate the degree of squeezing for which the ordering effects start to play an important role. Our predictions allow for direct experimental verification. We perform similar analysis for the non-monochromatic pump when the squeezing eigenmodes can only be evaluated numerically. For the nonlinear Jaynes-Cummings model with a classical pump we obtain explicitly an exact solution of the dynamics which has not been published in the literature before. Next, we compare this solution with the approximations that contain some or no ordering effects. Lastly, we evaluate the exact upper bounds of convergence for the Magnus expansion for the nonlinear Jaynes-Cummings model and for parametric down-conversion with the monochromatic pump. These bounds have not been known so far and exceed known sufficient upper bounds for a wide range of configurations.

Résumé

En optique quantique, contrairement à l'optique classique, le champ électromagnétique est décrit par un opérateur hermitien. La nature quantique du champ électromagnétique se manifeste dans les effets d'ordonnement d'opérateurs, inexistants dans l'optique classique. Cette thèse est consacrée à une étude détaillée de ce type d'effets d'ordonnement d'opérateurs dus à la dynamique de systèmes physiques. Nous considerons deux systemes en particulier, 1) la conversion paramétrique descendante d'une onde progressive dans un milieu non linéaire du deuxième ordre, et 2) un ion dans un piège de Paul entraîné par un champ classique et décrit par le-dit modèle de Jaynes-Cummings non linéaire. Les effets d'ordonnement sont étudiés dans les deux systèmes dynamiques via la technique mathématique du développement de Magnus et des approximations définies par ce dernier. La première partie de la thèse est consacrée à la conversion paramétrique descendante. Nous considérons deux cas: (i) une onde de pompe monochromatique et (ii) une onde de pompe spectralement large. Il est bien connu que dans les deux cas, ce système est capable de générer une lumière comprimée à large bande spectrale. Cependant, la description détaillée des propriétés d'une telle lumière comprimée n'est toujours pas disponible. Pour la pompe monochromatique, où une solution exacte de la dynamique est connue, nous écrivons explicitement la décomposition de Bloch-Messiah de la transformation de compression et obtenons les modes propres de compression et les paramètres de compression correspondants. Ensuite, nous comparons ces résultats exacts avec des approximations en incluant certains ou aucun effets d'ordonnement. Nous évaluons le degré de compression pour lequel les effets d'ordonnement commencent à jouer un rôle important. Nos prévisions permettent une vérification expérimentale directe. Nous effectuons une analyse similaire pour la pompe non monochromatique lorsque les modes propres de compression ne peuvent être évalués que numériquement. Pour le modèle de Jaynes-Cummings non linéaire avec une pompe classique, nous obtenons explicitement une solution exacte de la dynamique qui n'avait pas été publiée dans la littérature auparavant. Ensuite, nous comparons cette solution avec des approximations en incluant certains ou aucun effets d'ordonnement. Enfin, nous évaluons les limites exactes supérieures de convergence du développement de Magnus pour le modèle de Jaynes-Cummings non linéaire et pour la conversion paramétrique descendante avec la pompe monochromatique. Ces limites n'étaient pas connues à ce jour et dépassent les limites suffisantes supérieures connues pour un large éventail de configurations.